Supplemental Materials

Supplemental Methods

Aortic valve whole tissue collection

Aortic valve (AV) leaflets were obtained from AV replacement surgeries for severe AV stenosis (Brigham and Women's Hospital (BWH) IRB protocol number: 2011P001703). Non-diseased AVs were obtained from autopsy (BWH IRB 214P001505). A total 25 tricuspid AVs were analyzed for all experiments.

Aortic valve whole tissue sample preparation

First, three donor leaflets were prepared for whole tissue proteomics and three for transcriptomics. The samples were immediately transferred from the operating room in DMEM (Lonza, Switzerland) on ice and snap-frozen within 30 minutes of extraction in the operating room. Samples were then dissected into three macroscopically distinct segments per leaflet: (1) non-diseased, (2) fibrotic, and (3) calcific under the guidance of near-infrared molecular imaging (Osteosense 680EX, Perkin Elmar, USA). The samples were incubated in 200 nM Osteosense 680EX in PBS on ice for 30 minutes and imaged with an Olympus MVX10 microscope (Olympus, Japan). In total, 27 sub-samples were prepared for proteomics and 9 for transcriptomics. We pulverized the samples in liquid nitrogen and re-suspended them in RIPA buffer (Thermo Fisher Scientific, USA) with 1%-protease inhibitor cocktail (Roche, Switzerland) for protein sampling or Trizol (Fisher Scientific, USA) for RNA extraction. The protein samples were subsequently prepared for label-free proteomics as shown below.

AV tissue layer sample preparation

AVs obtained from three additional patients with severe aortic valve stenosis were used for tissue layer proteomics (donors CAVD1, CAVD2 and CAVD3). Non-diseased AV were obtained from autopsy donors (ND1 and ND2). The AV samples were handled in DMEM culture media (Lonza, Switzerland) on ice, were washed in PBS, and 1.5 mm slices covering the base and the tip of the AV were embedded in Optimal Cutting Temperature compound (OCT, Sakura Finetek, USA). The time between the extraction from the patient and the storage in a -80 °C freezer was maintained below 30 minutes. We then cut 15 µm sections and performed Verhoeff-van Gieson's stain (Richard-Allan Scientific Elastic Stain, ThermoFisher Scientific, USA) to visualize the anatomical structures of the three AV layers, fibrosa (F), spongiosa (S), and ventricularis (V). Using Verhoeff-van Gieson's stain as a template, we performed laser-capture microdissection on a Leica microscope (LMD6500 Microdissection System; LCM parameters: power: 50 mW, pulse duration: 2 ms) and pooled the extracted layer-specific tissue samples of 75 AV sections in RIPA buffer (Thermo Fisher Scientific, USA) supplemented with 1%-protease inhibitor cocktail (Roche, Switzerland). Preparations from 15 samples were sonicated (Branson Sonifier 450, USA). These samples were prepared for label-based, tandem mass tagging (TMT) proteomics.

AV in vitro migration assay and sample preparation

AV leaflets from eight additional patients with severe AV stenosis were inspected by a pathologist to distinguish macroscopically the fibrosa from the ventricularis side. Endothelial cells were removed by scratching the surface with a razor blade. Longitudinal sections covering the base and the tip of the leaflet were cut and placed in tissue culture wells of a 6-well plate (Corning, USA) with the fibrosa or the ventricularis side of the leaflets facing down. The cells

were expanded in growth media (DMEM (Lonza, Switzerland) supplemented with 10% FCS and 1% streptomycin/penicillin (Corning, USA) until they reached 90% confluency and three different cell culture media conditions were introduced after passage 3: 1) control media [CM; DMEM (Lonza, Switzerland), 5% FCS (VWR, USA)]; 2) osteogenic media [OM; 5% FCS (VWR, USA), 2 mM β-glycerophosphate (EMD millipore, USA), 10 nM dexamethasone (MP Biomedicals, USA), 50 µg/mL L-ascorbic acid (Sigma-Aldrich, USA)]; and 3) pro-calcifying media [PM; 5% FCS (VWR, USA), 2 mM NaH2PO4 (pH 7.4) (Sigma-Aldrich, USA), 50 µg/mL L-ascorbic acid (SIGMA-ALDRICH, USA)]. All cell culture media were supplemented with 1% streptomycin/penicillin. Prior to the first passage, the tissue samples were collected and histological sections generated. Van Gieson staining was performed to confirm the tissue orientation.

For the calcification assay, cell cultures were maintained for 21 days. Cells were fixed with 10% formalin for 15 minutes. Matrix calcium deposition was analyzed by Alizarin Red staining (Lifeline Cell Technology). Fixed cells were washed twice with distilled water and stained with 2% Alizarin Red for 15 minutes. Excess stain was washed twice with distilled water, and then images were scanned from the bottom side of culture plates. Alizarin Red staining was quantified by extracting the stain with 100 mmol/L cetylpyridinium chloride (Fisher Scientific, USA) for 3 hours, and the absorbance measured at 540 nm.

We collected protein samples at two time points for proteomics: 1) The ‘day 0’ cellular protein sample collection was conducted 24 hours after passage 3, and 2) ‘day 7’, seven days after the ‘day 0’ collection. The cells were washed twice in ice-cold PBS and 400µl RIPA buffer (Thermo Scientific, USA) supplemented with Protease Inhibitor Cocktail (Sigma Aldrich, USA) was added to lyse the cells. The cells were passed through a 25 G needle 10 times, and sonicated on ice (Branson Sonifier 450, USA). The samples were subsequently prepared for label-free proteomics.

Proteomics

Label-free proteomics preparation for valvular whole tissue and in vitro migration samples. Protein extraction and proteolysis were performed with the methanol-chloroform method and trypsin (Gold Grade; Promega, Wisconsin)/ RapiGest (Waters, USA) respectively, as previously published[1]. Fifteen micrograms of protein were used per sample. The tryptic peptides were desalted using Oasis Hlb 1cc (10 mg) columns (Waters, USA), and dried with a tabletop speed vacuum (SPD1010, Thermo Fisher Scientific, USA). After re-suspension in 40 µl of 5% mass spectrometry grade acetonitrile (Thermo Fisher Scientific, USA) and 5% formic acid (Sigma-Aldrich, USA) the tryptic peptide samples were analyzed by liquid chromatography-mass spectrometry.

Label-based, tandem mass tagging (TMT) for valvular laser microdissection samples. Protein extraction and proteolysis were performed with the methanol-chloroform method (as above) and proteolyzed with Lys-C (WAKO Chemicals, USA). Peptides were labeled with TMT™ reagents (Table S1, Thermo Fisher Scientific, USA). Of note, to account for inter-TMT experimental variability, donor 2 (D2) was analyzed in duplicate in two independent TMT experiments (Table S1). The labeled peptides were combined and desalted using Oasis Hlb 1cc (10 mg) columns (Waters, USA). The OFF-gel system (Agilent, USA) fractionated the peptides into 24 fractions depending on their isoelectric focusing point (pH range of 3–10). The fractions were cleaned with Oasis columns, dried with a tabletop speed vacuum and re-suspended in 40 µl of 5% acetonitrile (MS grade, Thermo Fisher Scientific, USA) and 5% formic acid (Sigma-Aldrich, USA) for subsequent analysis by liquid chromatography-mass spectrometry.

Liquid chromatography tandem mass spectrometry (LC-MS/MS)

AV whole tissue label-free proteomics. Peptide samples were analyzed with the high resolution/accuracy Q Exactive mass spectrometer fronted with a Nanospray FLEX ion source, and coupled to an Easy-nLC1000 HPLC pump (Thermo Scientific). The peptides were subjected to a dual column set-up: an Acclaim PepMap RSLC C18 trap column, 75 µm X 20 mm; and an Acclaim PepMap RSLC C18 analytical column 75 µm X 250 mm (Thermo Scientific). The analytical gradient was run at 300 nl/min from 5 to 18 % Solvent B (acetonitrile/0.1 % formic acid) for 120 minutes, followed by five minutes of 95 % Solvent B. Solvent A was 0.1 % formic acid. All reagents were HPLC-grade. The instrument was set to 140 K resolution, and the top 10 precursor ions (within a scan range of 380-2000 m/z) were subjected to higher energy collision induced dissociation (HCD, collision energy 25% (+/- 2.5%), isolation width 1.6 m/z, dynamic exclusion enabled (20 s), and resolution set to 17.5 K).

AV tissue layer TMT proteomics. Peptide samples were analyzed with the high resolution/accuracy LTQ-Orbitrap (Elite model) mass spectrometer fronted with a Nanospray FLEX ion source, and coupled to an Easy-nLC1000 HPLC pump (Thermo Scientific). The peptides were subjected to a dual column set-up: an Acclaim PepMap RSLC C18 trap column, 75 µm X 20 mm; and an analytical column which was packed with 3 µm, 100 Å pore size C18 resin (Bruker) in a 75 µm X 200 mm long piece of fused silica capillary in-house. The analytical gradient was run at 350 nl/min from 10 to 25 % Solvent B (acetonitrile/0.1 % formic acid) for 90 minutes, followed by five minutes of 95 % Solvent B. Solvent A was 0.1 % formic acid. All reagents were HPLC-grade. The instrument was set to 120 K resolution, and the top 20 precursor ions (within a scan range of 380-2000 m/z) were subjected to higher energy collision induced dissociation (HCD, collision energy 40%, isolation width 3 m/z, dynamic exclusion enabled, starting m/z fixed at 120 m/z, and resolution set to 30 K) for peptide sequencing (MS/MS).

In vitro migration label-free proteomics. Peptide samples were analyzed with the LTQ-Orbitrap Elite configuration as above. The analytical gradient was run at 350 nl/min from 10 to 28 % Solvent B (acetonitrile/0.1 % formic acid) for 120 minutes, followed by five minutes of 95 % Solvent B. Solvent A was 0.1 % formic acid. All reagents were HPLC-grade. The instrument was set at 120 K resolution, and the top 20 precursor ions (within a scan range of 380-2000 m/z) were subjected to collision induced dissociation (CID, collision energy 35%) for peptide sequencing (MS/MS). Each sample was analyzed in triplicate.

RNA extraction, generation of the cDNA libraries and Illumina RNA-Seq

RNA was purified from frozen tissue powders, using Trizol (Thermo Fisher, USA). The RNA quantity and quality was determined by an Agilent Bioanalyzer. Ribosomal RNA was removed by selecting RNAs with poly-A tails by annealing them to bead-bound poly-T oligonucleotides (Life Technologies, USA). The polyA subtypes were eluted by melting the annealed structures. Messenger RNAs were reverse transcribed using random hexamers (Invitrogen, USA). Double-stranded DNA synthesis was performed using Pol I and RNAse H (Invitrogen, USA). End-repair was performed using polymerases and exonucleases to obtain dsDNA fragments with no overhangs. RNA-seq libraries were then constructed from the dsDNA using Nextera XT DNA sample preparation kit (Illumina, USA). RNA-seq library quality control was performed using High-Sensitivity DNA Tapes (Agilent, USA) on an Agilent Tape Station. Libraries were sequenced as 50bp paired end sequences on a single lane of the Illumina HiSeq2500 (Illumina, USA) to a target depth of >20 million reads.

Proteomics data analysis

Common data processing steps - All MS/MS data were queried against the Human UniProt database (downloaded on August 01, 2014) using the HT-SEQUEST search algorithm, via the Proteome Discoverer (PD) Package (version 2.1, Thermo Scientific). Peptides were filtered based on a 1 % FDR[2, 3]. Peptides assigned to a given protein group (Master protein), and not present in any other protein group, were considered as unique and used for quantification. A minimum of two unique peptides were included for each dataset.

Specifically, valve tissue TMT raw data acquired from the four TMT experiments (Table S1) were combined to create a merged analysis report in PD 2.1. The raw files were queried using a 10 ppm tolerance window in the MS1 search space, and a 0.02 Da fragment tolerance window for HCD. N-terminal acetylation, methionine oxidation and the tandem mass tags were set as variable modifications; and carbamidomethylation of cysteine was set as a fixed modification. For subsequent quantification analysis, the PD 2.1 normalized raw mass tag reporter ion intensities were exported. Valve whole tissue raw data were processed as above but without the tandem mass tags variables. The *in vitro* migration data were queried using a 10 ppm tolerance window in the MS1 search space, and a 0.6 Da fragment tolerance window for CID. N-terminal acetylation and methionine oxidation were set as variable modifications; and carbamidomethylation of cysteine was set as a fixed modification. The area under the curve of the chromatographic peak intensity as a label-free measure of peptide abundance of up to the top three abundant peptides was used for quantification in the two label-free experiments. The 'Precursor Ions Area Detector' module in PD 2.1 was activated for this quantification method.

Normalization: Four independent TMT experiments were collected (Table S1). In order to perform inter-donor comparisons across the TMT sets, we performed the sum-normalization of the three layers' reporter ion intensities for each donor[4]. In other words, we calculated proportions of three layers within one donor. Only proteins found in all four TMT experiments were analyzed further (Table S2, Fig. S5). In order to perform inter-dataset comparisons of the

label-free experiments, we divided AUC by the median AUC of the entire MS run[5, 6]. The total number of proteins used in each study are provided in Table S2. For transcriptome analysis of the AV whole tissue, we employed empirical Bayesian normalization method provided by DESeq2[7].

Immunohistochemistry and immunofluorescence

AV samples from valve replacement surgeries were embedded perpendicularly in OCT and cut into 7 μm sections (Research Cryostat, Leica CM3050 S, Buffalo Grove, IL, USA). The sections were first dried for 20 minutes and then fixed for 5 minutes in 4% paraformaldehyde followed by a 5-minute rinse in distilled water and two 5 minute rinses in PBS. Sections were incubated for 3 minutes in a 0.3% hydrogen peroxide solution and rinsed with distilled water. Each section was then incubated in a 4% species appropriate blocking serum, prepared with PBS, for 45 minutes. This was followed with a 2-hour incubation at 37˚C with the appropriate primary antibody (Table S5), followed by incubation for 1 hour with a species appropriate secondary antibody. Streptavidin-coupled Alexa Fluor 488 and 594 antibodies (1:200, ThermoFisher Scientific, USA) were used. For double immunofluorescence labeling, samples were treated with an Avidin-biotin blocking solution (Vector Laboratories, USA), and then incubated for 45 minutes with a species appropriate 4% blocking serum for the second primary antibody. This step was followed by an overnight incubation at 4˚C of the second primary antibody, and a 1-hour incubation with a species-appropriate, fluorescently conjugated secondary antibody with a different wavelength then was used for the first primary antibody. Sections were washed in PBS, mounted with DAPI (4,6-diamidino-2-phenylindole mounting medium (Vector Laboratories, USA)), coverslipped, and examined with a Nikon Eclipse Ti Confocal microscope (Nikon, USA).

Histological stains

Human AV samples were embedded in OCT compound perpendicularly to obtain longitudinal sections, and 7µm cryosections were cut using a cryostat (Research Cryostat, Leica CM3050 S, USA). To detect AV tissue layers, Movat's Pentachrome staining was performed using the Russel-Movat's Pentachrome staining kit (American MasterTech KTRMP, USA). Sections were examined with a Nikon Eclipse 80i microscope (Nikon, Melville, NY, USA).

Proteomics and transcriptomics (RNA-seq) data visualization and statistical analysis

For all proteomics and transcriptomics statistical analyses, we used in-house scripts of R v3.1 (http://www.R-project.org/) and Python v2.7.10 and v3.4 (http://www.python.org). To draw principal component analysis (PCA) plots and heat maps, we used Qlucore (http://www.qlucore.com/). For PCAs and heat maps, we filtered out genes or proteins by their q-value of multiple group comparisons. The q-value was calculated using Qlucore and its threshold were indicated in the figure legend. The q-value is the proportion of the rejected null hypotheses which are erroneously rejected and is a type of false discovery rate[8]. Histograms were drawn using Python's numpy[9] and matplotlib[10]. In the proteomics data, we replaced missing values with zero. For transcriptomics analysis of the AV whole tissue, we normalized the raw read count data using DESeq2[7]. We excluded low abundant transcripts by the fragments per kilobase of transcript per million maps (FPKM) ≤ 1 and normalized read value ≤ 1. The Wald test of DESeq2 was used to compare the RNA abundances across the stages, and the FDR was used to adjust p-values. A density scatter plot (Fig. 2d) was drawn to compare the transcriptomics and the proteomics of the CAVD stage data. FPKM of the transcriptomics and median-normalized AUC of label free proteomics were compared using Spearman squared R (R2). Our label free proteomics and transcriptomics samples were not from the same donor, so we averaged FPKM and the normalized AUC by three stages (non-calcific, fibrotic and calcific stages). We used an in-house R script using ggplot2 to draw a histogram for a density scatter

plot. The enrichment analyses for the collagen, complement and SERPIN gene families were done using a two-sided Fisher's exact test considering the proteins detected in the proteomics experiments. The gene families were downloaded from the HUGO Gene Nomenclature Committee website (www.genenames.org).

Determination of the layer- and stage-specific proteins and genes

To resolve proteins and genes obtained from proteomic and transcriptomic measurements into various calcification stages and AV leaflet layers, we determined the over-represented proteins/genes in each respective condition by following the criteria below:

a) For CAVD Disease Stage proteomics, a protein was assigned to the non-diseased (ND), fibrotic (F), or calcific (C) stage if its normalized mean AUC fold change (FC) was greater than 1.2 with respect to the other stages (e.g. a protein is classified as calcific if C/F > 1.2 and C/ND > 1.2). Similarly, for CAVD Layer proteomics, a protein was assigned to the fibrosa (F), spongiosa (S) or ventricularis (V) layer if its average normalized TMT fold change (FC) is greater than 1.2 with respect to the other layers (e.g. a protein is classified into fibrosa if F/S > 1.2 and F/V > 1.2).

b) For CAVD Disease Stage transcriptomics, genes with an FDR < 0.05 in at least one stage were considered and a gene was assigned to a stage if its DESeq2 normalized count fold change (FC) was greater than 1.2 with respect to the other stages.

Together, these criteria ensure that a gene/protein is overrepresented in one stage/layer only, while being simultaneously underrepresented in the remaining two stages/layers. We note that the proteins and genes considered here are expressed in all stages and layers. Therefore, what is referred to as layer- and stage-specific is rather the result of the above classification, where a protein/gene is assigned to only one stage or layer, allowing for the spatiotemporal resolution of calcification in the AV.

c) For the CAVD *in vitro* cell proteomics, the expression levels of fibrosa (F) and ventricularis (V) on 'Day 0' were averaged over donors and proteins with a normalized mean AUC fold change (FC) greater than 1.5 with respect to the other layer were considered as over-represented (e.g. a protein is classified as belonging to the fibrosa layer if FC (F/V) > 1.5 and ventricularis layer if FC (F/V) < 1/1.5). For the different media conditions, the expression levels of fibrosa (F) on 'Day 7' were averaged over donors and proteins with a normalized mean AUC fold change (FC) greater than 1.2 for the given condition (pro-calcifying media (PM) or osteogenic media (OM)) with respect to normal media (NM) were considered as over-represented (e.g. a protein is classified as over-represented in PM if FC (PM/NM) > 1.2 and OM if FC (OM/NM) >1.2).

Network analysis

Pathway enrichment analysis and pathway maps.

Using ConsensusPathDB[11], the gene sets corresponding to each layer and stage were tested for enrichment by a hypergeometric test and adjusted for multiple comparisons using the Benjamini-Hochberg method for controlling false discovery rate (FDR). For the pathway enrichment analysis (pathway data retrieved from http://consensuspathdb.org/ in February 2017), the canonical pathways from KEGG, Biocarta, and Reactome were considered[12]. This resulted in 301 pathways from KEGG comprising 7,121 genes, 252 pathways from Biocarta comprising 1,408 genes, and 1,764 pathways from Reactome comprising 10,095 genes, which together defined a pathway space of 2,317 pathways consisting of 11,447 genes. Pathways with FDR adjusted p-value (q-value) < 0.05 are considered as significantly enriched. The pathway networks consist of pathways as the nodes and the shared genes between pathways as the edges. Node size corresponds to –log (q-value) and edge weight (thickness) corresponds to the gene overlap between pairs of pathways measured by the Jaccard index J, which is defined as

$$J = \frac{s_A \cap s_B}{s_A \cup s_B}$$

where s_A and s_B are the set of proteins detected in proteomics that belong to pathway *A* and pathway *B*, respectively. Edges with a Jaccard index < 0.1 were discarded in the visualization for clarity. The networks visualizations were made using Gephi v0.8.2 [2].

Stage- and layer-specific subnetworks and closeness of the calcific stage subnetwork to human diseases.

The stage- and layer-specific subnetworks were built by mapping the layer- and stage-specific proteins (from the CAVD Disease Stage proteomics and CAVD Layer proteomics data) onto the protein-protein interaction (PPI) network (described in detail below). Concretely, the subnetworks are the induced subgraphs $G_{PPI}[S_{layer}]$ and $G_{PPI}[S_{stage}]$ consisting of layer- and stage-specific nodes and all of the edges that connect them, where G_{PPI} is the PPI network, and S_{layer} and S_{stage} are the sets of layer- and stage-specific proteins.

The closeness of the calcific stage subnetwork to disease molecules was measured in terms of the average shortest distance. The average shortest distance D to disease genes in a module was measured by calculating the shortest distance between each calcific stage gene s and all disease genes t and then averaging over all calcific stage genes s such that

$$d_s = \sum_{t \in \mathbb{T}} d_{st}$$

and

$$D = \sum_{s \in \mathbb{S}} d_s,$$

where d_{st} is the shortest distance between s and t and $\mathbb{S}$ and $\mathbb{T}$ are the set of genes in the calcific stage proteins subnetwork and disease genes, respectively. In order to compare this average shortest distance value to a null model, the average shortest distance of the same number of randomly selected genes to disease genes was calculated for N=1,000 realizations. To correct for degree (i.e., the number of connections of a gene) bias, the random selection was done in a degree-preserving manner where all genes were binned according to their degree and random genes were selected uniformly at random from their corresponding degree bin. Finally, z-scores and empirical p-values were calculated by

$$z = \frac{D - \langle D_r \rangle}{\sigma_{D_r}}$$

and

$$p_{emp.} = P(D_r < D),$$

respectively, where D_r is the average shortest distance of a randomized instance, $\langle D_r \rangle$ is the mean of the average shortest distance of all randomized instances, and σ_{D_r} is their standard deviation. The disease genes were obtained from the DiseaseConnect (http://disease-connect.org)[13] (using entries with evidence from Genome-Wide Association Studies (GWAS) and Online Mendelian Inheritance in Man (OMIM) (http://www.omim.org/)) and MalaCards (http://www.malacards.org/)[14] databases, for a range of diseases (Table S6) covering a broad spectrum including cardiovascular, metabolic, malignant, and autoimmune disorders. Calcification-related diseases served as positive controls (pseudoxanthoma elasticum, $p<0.001$; calcification diseases [including vascular calcification, basal ganglia calcification, calcification of the joints and arteries, arterial calcification of infancy, and aortic valve calcification (contributing LPA)), $p<0.001$]. The underlying protein-protein interaction (PPI) network onto which the calcific stage and disease genes were mapped consists of curated physical protein-protein interactions

with experimental support, including binary interactions, protein complexes, enzyme-coupled reactions, signaling interactions, kinase-substrate pairs, regulatory interactions and manually curated interactions from literature, the details of which were described previously[15]. The PPI network was treated as undirected, due to the limited availability of unambiguous and robust information on the directionality of links in the available datasets[15]. Network measures including shortest distances and centralities were calculated using the NetworkX package[16] 1.9 in Python v2.7.10.

Supplemental Tables

	TMT channel / reporter ion					
n-plex exp.	**126**	**127**	**128**	**129**	**130**	**131**
6	CAVD1-1F	CAVD1-1S	CAVD1-1V	CAVD1-2F	CAVD1-2S	CAVD1-2V
6	CAVD2-1F	CAVD2-1S	CAVD2-1V	CAVD3F	CAVD3S	CAVD3V
6	CAVD2-2F	CAVD2-2S	CAVD2-2V	ND1F	ND1S	ND1V
3	ND2F	ND2S	ND2V			

Supplemental Table 1: *TMT channel, and donor and layer assignments. Valve replacement donors, D1, D2 and D3; autopsy donors, A1 and A2; fibrosa (F), spongiosa (S) and ventricularis (V). D2 was analyzed in two independent TMT experiments to evaluate inter-data set variability.*

Study	**≥2 unique peptides**	**Detected in all TMT experiments**
CAVD stages	**1744**	**-**
CAVD layers	**1872**	**856**
CAVD in vitro (Day0)	**2188**	**-**
CAVD in vitro (TimeSeries: Day0, Day7)	**2586**	**-**

Supplemental Table 2: Proteomics data overview

Supplemental Table 3

CAVD Disease Stage Pathways

Non-diseased CAVD stage

p-value	q-value	Pathway
6.78E-16	2.36E-13	L13a-mediated translational silencing of Ceruloplasmin expression
6.78E-16	2.36E-13	3, -UTR-mediated translational regulation
2.89E-15	5.04E-13	Cap-dependent Translation Initiation
2.89E-15	5.04E-13	Eukaryotic Translation Initiation
7.36E-15	1.01E-12	GTP hydrolysis and joining of the 60S ribosomal subunit
8.75E-15	1.01E-12	Formation of a pool of free 40S subunits
1.40E-14	1.39E-12	Neutrophil degranulation
1.73E-14	1.50E-12	Translation
2.58E-14	1.99E-12	Nonsense Mediated Decay (NMD) independent of the Exon Junction Complex (EJC)
1.35E-13	9.41E-12	Selenocysteine synthesis
1.64E-13	1.04E-11	Eukaryotic Translation Termination
2.08E-13	1.21E-11	ECM-receptor interaction (human)
2.73E-13	1.36E-11	Nonsense Mediated Decay (NMD) enhanced by the Exon Junction Complex (EJC)
2.73E-13	1.36E-11	Nonsense-Mediated Decay (NMD)
1.03E-12	4.76E-11	Peptide chain elongation
2.52E-12	1.10E-10	Eukaryotic Translation Elongation
4.96E-12	2.03E-10	SRP-dependent cotranslational protein targeting to membrane
1.21E-11	4.68E-10	Selenoamino acid metabolism
2.05E-11	7.50E-10	Translation initiation complex formation
2.56E-11	8.92E-10	Activation of the mRNA upon binding of the cap-binding complex and eIFs, and subsequent binding to 43S
3.00E-11	9.94E-10	Metabolism of proteins
1.08E-10	3.43E-09	Extracellular matrix organization
1.30E-10	3.93E-09	Focal adhesion (human)
2.11E-10	6.12E-09	Ribosomal scanning and start codon recognition
2.28E-10	6.36E-09	Platelet activation, signaling and aggregation
4.68E-10	1.25E-08	Formation of the ternary complex, and subsequently, the 43S complex
1.10E-09	2.82E-08	Metabolism of amino acids and derivatives
1.51E-09	3.76E-08	Ribosome (human)
3.66E-09	8.79E-08	Hemostasis
7.77E-09	1.80E-07	Platelet Aggregation (Plug Formation)
1.57E-08	3.53E-07	Innate Immune System
6.08E-07	1.32E-05	Platelet activation (human)
1.29E-06	2.71E-05	GP1b-IX-V activation signalling
2.79E-06	5.70E-05	Prefoldin mediated transfer of substrate to CCT/TriC

3.56E-06	7.09E-05	Molecules associated with elastic fibres
6.21E-06	0.00012002	Platelet Adhesion to exposed collagen
7.44E-06	0.00014002	Non-integrin membrane-ECM interactions
8.20E-06	0.00015016	Collagen formation
8.72E-06	0.00015307	Cooperation of Prefoldin and TriC/CCT in actin and tubulin folding
8.80E-06	0.00015307	Collagen chain trimerization
1.07E-05	0.00018143	Elastic fibre formation
1.53E-05	0.00025326	Laminin interactions
1.95E-05	0.00031555	Formation of tubulin folding intermediates by CCT/TriC
2.16E-05	0.00034129	Transport to the Golgi and subsequent modification
2.26E-05	0.00035004	Formation of Fibrin Clot (Clotting Cascade)
2.46E-05	0.00037212	Sema4D in semaphorin signaling
2.58E-05	0.00038247	Regulation of actin cytoskeleton (human)
2.89E-05	0.00041879	PI3K-Akt signaling pathway (human)
3.07E-05	0.00043627	Integrin alphaIIb beta3 signaling
3.33E-05	0.00046415	ECM proteoglycans
3.80E-05	0.00051859	MET promotes cell motility
4.58E-05	0.00061349	Platelet degranulation
4.93E-05	0.00064806	ER to Golgi Anterograde Transport
6.41E-05	0.00082599	Amoebiasis (human)
6.58E-05	0.00083316	Response to elevated platelet cytosolic Ca2+
7.93E-05	0.00098602	Signaling by MET
8.46E-05	0.00103351	Syndecan interactions
0.00010428	0.00125139	Assembly of collagen fibrils and other multimeric structures
0.00012362	0.00145825	Integrin cell surface interactions
0.00013246	0.00153651	Salmonella infection (human)
0.0001528	0.00174346	Immune System
0.00016727	0.00186479	Sema4D induced cell migration and growth-cone collapse
0.0001688	0.00186479	Collagen biosynthesis and modifying enzymes
0.00017828	0.00193876	Metabolism
0.0001881	0.00201411	Protein digestion and absorption (human)
0.00021957	0.00229011	Pathogenic Escherichia coli infection (human)
0.00022046	0.00229011	Spliceosome (human)
0.00022609	0.00231407	Proteoglycans in cancer (human)
0.00025873	0.00260976	Pathways in cancer (human)
0.00030706	0.00305306	Hematopoietic cell lineage (human)
0.00037013	0.00362829	Cell-extracellular matrix interactions
0.00039178	0.00378722	COPI-mediated anterograde transport
0.00050544	0.00481903	Influenza Virus Induced Apoptosis
0.0005482	0.00515601	Hypertrophic cardiomyopathy (HCM) (human)
0.0005878	0.00545477	mcalpain and friends in cell motility

0.0006397	0.00585833	Protein folding
0.00068664	0.00614018	Phagosome (human)
0.00068812	0.00614018	Asparagine N-linked glycosylation
0.00070846	0.00624164	Cell-Cell communication
0.00081103	0.00703498	Cell junction organization
0.00081873	0.00703498	Endocytosis (human)
0.00087408	0.00741899	Dilated cardiomyopathy (human)
0.00091776	0.0076959	MET activates PTK2 signaling
0.00098934	0.00819742	mRNA Splicing - Major Pathway
0.00115164	0.00942986	Arrhythmogenic right ventricular cardiomyopathy (ARVC) (human)
0.00120605	0.00976059	Folding of actin by CCT/TriC
0.00124973	0.00977316	Cleavage of Growing Transcript in the Termination Region
0.00124973	0.00977316	RNA Polymerase II Transcription Termination
0.00124973	0.00977316	Post-Elongation Processing of the Transcript
0.00128993	0.00997544	GPVI-mediated activation cascade
0.0013374	0.01021875	Intrinsic Pathway of Fibrin Clot Formation
0.00135075	0.01021875	RHO GTPases Activate WASPs and WAVEs
0.00142487	0.01066353	mRNA Splicing
0.00159056	0.01153155	RHO GTPases activate PAKs
0.00159056	0.01153155	how progesterone initiates the oocyte maturation
0.00159056	0.01153155	Post-chaperonin tubulin folding pathway
0.00163081	0.01170146	RHO GTPases activate KTN1
0.00186279	0.01318334	Chaperonin-mediated protein folding
0.00187522	0.01318334	proteasome complex
0.0021933	0.01526538	stathmin and breast cancer resistance to antimicrotubule agents
0.00240563	0.01657738	Binding and Uptake of Ligands by Scavenger Receptors
0.00273387	0.01865467	ERKs are inactivated
0.00281815	0.01904304	TGF-beta signaling pathway (human)
0.00293735	0.01965764	transcription factor creb and its extracellular signals
0.00312378	0.0206925	RHO GTPase Effectors
0.00315144	0.0206925	Axon guidance
0.00321866	0.02093631	Small cell lung cancer (human)
0.00335028	0.02159067	Vesicle-mediated transport
0.00357721	0.02284163	Golgi-to-ER retrograde transport
0.00383756	0.02428126	fc epsilon receptor i signaling in mast cells
0.00411714	0.02581559	Processing of Capped Intron-Containing Pre-mRNA
0.004208	0.02614972	Semaphorin interactions
0.0048321	0.02976232	N-glycan trimming and elongation in the cis-Golgi
0.00517877	0.03142586	agrin in postsynaptic differentiation
0.00519249	0.03142586	MAPK signaling pathway (human)
0.00551162	0.03306972	erk and pi-3 kinase are necessary for collagen binding in corneal epithelia

0.00557567	0.03316811	B cell receptor signaling pathway (human)
0.00608146	0.03556887	role of pi3k subunit p85 in regulation of actin organization and cell migration
0.00608146	0.03556887	TGF-beta receptor signaling in EMT (epithelial to mesenchymal transition)
0.00664216	0.03852453	mRNA Splicing - Minor Pathway
0.00714067	0.04061491	Synthesis of Lipoxins (LX)
0.00714067	0.04061491	Protein repair
0.00717764	0.04061491	Regulation of signaling by CBL
0.00775715	0.04354014	AGE-RAGE signaling pathway in diabetic complications (human)
0.00819964	0.0456556	Bacterial invasion of epithelial cells (human)
0.00838331	0.04630783	role of mal in rho-mediated activation of srf
0.00927327	0.05082047	NCAM1 interactions
0.00984898	0.05355382	Clearance of Nuclear Envelope Membranes from Chromatin
0.01041996	0.05621929	Factors involved in megakaryocyte development and platelet production
0.01113193	0.05869563	Scavenging by Class A Receptors
0.01113193	0.05869563	prion pathway
0.01113193	0.05869563	Negative regulation of MET activity
0.01191299	0.06234164	Signaling by BRAF and RAF fusions
0.01231652	0.06397235	Tight junction (human)
0.01267843	0.06488375	ERK/MAPK targets
0.01267843	0.06488375	phosphoinositides and their downstream targets
0.01293797	0.06525236	Sema4D mediated inhibition of cell attachment and migration
0.01293797	0.06525236	cell to cell adhesion signaling
0.01318791	0.06603444	Gene Expression
0.01389708	0.06894832	Insulin signaling pathway (human)
0.01434162	0.06894832	intrinsic prothrombin activation pathway
0.01437825	0.06894832	Gap junction (human)
0.01443804	0.06894832	Post-translational protein modification
0.0144633	0.06894832	Oncogenic MAPK signaling
0.0144633	0.06894832	mRNA 3,-end processing
0.0144633	0.06894832	Post-Elongation Processing of Intron-Containing pre-mRNA
0.01538572	0.07236856	Alzheimer,s disease (human)
0.01538872	0.07236856	Shigellosis (human)
0.01612253	0.0750455	ER-Phagosome pathway
0.01635289	0.0750455	Renal cell carcinoma (human)
0.01638925	0.0750455	MET activates RAP1 and RAC1
0.01638925	0.0750455	Crosslinking of collagen fibrils
0.01655477	0.07530799	Activated TLR4 signalling
0.01686963	0.07575006	Proteasome (human)
0.01686963	0.07575006	Cooperation of PDCL (PhLP1) and TRiC/CCT in G-protein beta folding
0.01735644	0.07700925	Central carbon metabolism in cancer (human)
0.01737134	0.07700925	Signaling by Rho GTPases

0.01757374	0.07741342	Fc gamma R-mediated phagocytosis (human)
0.01802197	0.07779577	EGFR downregulation
0.01802197	0.07779577	Nuclear Events (kinase and transcription factor activation)
0.01802197	0.07779577	WNT ligand biogenesis and trafficking
0.01844296	0.07779577	MyD88:Mal cascade initiated on plasma membrane
0.01844296	0.07779577	Toll Like Receptor TLR1:TLR2 Cascade
0.01844296	0.07779577	Toll Like Receptor TLR6:TLR2 Cascade
0.01844296	0.07779577	Toll Like Receptor 2 (TLR2) Cascade
0.01948405	0.08169215	Fc epsilon RI signaling pathway (human)
0.02004048	0.08312895	DARPP-32 events
0.02018505	0.08312895	Signal attenuation
0.02018505	0.08312895	SLBP independent Processing of Histone Pre-mRNAs
0.02060924	0.08437666	COPII (Coat Protein 2) Mediated Vesicle Transport
0.02143927	0.08726159	Intra-Golgi and retrograde Golgi-to-ER traffic
0.02298506	0.09300932	Adherens junction (human)
0.02407959	0.09396282	Toll-Like Receptors Cascades
0.02414109	0.09396282	Arginine and proline metabolism (human)
0.02423668	0.09396282	Chronic myeloid leukemia (human)
0.02430821	0.09396282	regulators of bone mineralization
0.02430821	0.09396282	apoptotic dna-fragmentation and tissue homeostasis
0.02430821	0.09396282	SLBP Dependent Processing of Replication-Dependent Histone Pre-mRNAs
0.02430821	0.09396282	Dermatan sulfate biosynthesis
0.02430821	0.09396282	insulin signaling pathway
0.02443573	0.09396282	COPI-independent Golgi-to-ER retrograde traffic
0.02568504	0.09822413	Toll Like Receptor 4 (TLR4) Cascade
0.02681245	0.10197521	Negative regulation of FGFR3 signaling
0.02696179	0.10198592	Diseases of signal transduction
0.02825177	0.10311627	Transport of Mature mRNA derived from an Intron-Containing Transcript
0.02867483	0.10311627	Osteoclast differentiation (human)
0.02874218	0.10311627	protein kinase a at the centrosome
0.02874218	0.10311627	rho-selective guanine exchange factor akap13 mediates stress fiber formation
0.02874218	0.10311627	CD28 dependent Vav1 pathway
0.02874218	0.10311627	PECAM1 interactions
0.02874218	0.10311627	phospholipase c-epsilon pathway
0.02874218	0.10311627	Host Interactions with Influenza Factors
0.02874218	0.10311627	how does salmonella hijack a cell
0.02874218	0.10311627	eNOS activation
0.0293082	0.104074	Ca-dependent events
0.0293082	0.104074	Asthma (human)
0.03076566	0.10869491	Huntington,s disease (human)
0.03113517	0.10944484	Apoptotic execution phase

0.03192249	0.11040658	MAPK targets/ Nuclear events mediated by MAP kinases
0.03192249	0.11040658	Negative regulation of FGFR4 signaling
0.03192249	0.11040658	beta-Alanine metabolism (human)
0.03251672	0.11040658	UCH proteinases
0.03305092	0.11040658	Glutathione metabolism (human)
0.03347096	0.11040658	RHO GTPases activate IQGAPs
0.03347096	0.11040658	Initiation of Nuclear Envelope Reformation
0.03347096	0.11040658	Nuclear Envelope Reassembly
0.03347096	0.11040658	Activation of DNA fragmentation factor
0.03347096	0.11040658	Apoptosis induced DNA fragmentation
0.03347096	0.11040658	attenuation of gpcr signaling
0.03347096	0.11040658	Advanced glycosylation endproduct receptor signaling
0.03347096	0.11040658	extrinsic prothrombin activation pathway
0.03465464	0.11377185	bcr signaling pathway
0.03561257	0.11636782	NCAM signaling for neurite out-growth
0.03636398	0.1182679	Signaling by PDGF
0.03750384	0.11864851	role of egf receptor transactivation by gpcrs in cardiac hypertrophy
0.03750384	0.11864851	phospholipids as signalling intermediaries
0.03750384	0.11864851	rho cell motility signaling pathway
0.03750384	0.11864851	bioactive peptide induced signaling pathway
0.03750384	0.11864851	Negative regulation of FGFR1 signaling
0.03750384	0.11864851	Glucagon signaling in metabolic regulation
0.03777558	0.11896745	Regulation of actin dynamics for phagocytic cup formation
0.03817935	0.11902878	Membrane Trafficking
0.03847913	0.11902878	il 2 signaling pathway
0.03847913	0.11902878	Spry regulation of FGF signaling
0.03847913	0.11902878	phosphorylation of mek1 by cdk5/p35 down regulates the map kinase pathway
0.03918576	0.12067828	COPI-dependent Golgi-to-ER retrograde traffic
0.04045014	0.12246299	Viral carcinogenesis (human)
0.04046909	0.12246299	integrin signaling pathway
0.04046909	0.12246299	Negative regulation of FGFR2 signaling
0.04046909	0.12246299	Cargo concentration in the ER
0.04093096	0.12332445	Opioid Signalling
0.04354928	0.12794644	Signaling by high-kinase activity BRAF mutants
0.04354928	0.12794644	Glucagon-like Peptide-1 (GLP1) regulates insulin secretion
0.0437518	0.12794644	InlB-mediated entry of Listeria monocytogenes into host cell
0.0437518	0.12794644	Constitutive Signaling by EGFRvIII
0.0437518	0.12794644	Signaling by EGFRvIII in Cancer
0.0437518	0.12794644	transcription regulation by methyltransferase of carm1
0.0437518	0.12794644	repression of pain sensation by the transcriptional regulator dream
0.04596624	0.13330211	rRNA modification in the nucleus and cytosol

0.04596624	0.13330211	rRNA processing in the nucleus and cytosol
0.04837757	0.1371805	G alpha (12/13) signalling events
0.04837757	0.1371805	Transport of Mature Transcript to Cytoplasm
0.04900813	0.1371805	Developmental Biology
0.0492746	0.1371805	Regulation of TLR by endogenous ligand
0.0492746	0.1371805	p130Cas linkage to MAPK signaling for integrins
0.0492746	0.1371805	GRB2:SOS provides linkage to MAPK signaling for Integrins
0.0492746	0.1371805	Constitutive Signaling by Ligand-Responsive EGFR Cancer Variants
0.0492746	0.1371805	Signaling by Ligand-Responsive EGFR Variants in Cancer
0.0492746	0.1371805	Signaling by EGFR in Cancer
0.0492746	0.1371805	PKA activation

Fibrotic CAVD stage

p-value	q-value	Pathway
2.60E-17	2.01E-14	Metabolism
9.81E-17	3.80E-14	Neutrophil degranulation
3.96E-14	1.02E-11	SRP-dependent cotranslational protein targeting to membrane
5.96E-14	1.15E-11	Translation
5.12E-13	7.92E-11	Eukaryotic Translation Termination
7.69E-13	9.92E-11	Eukaryotic Translation Elongation
2.51E-12	2.45E-10	Peptide chain elongation
3.58E-12	2.45E-10	Formation of a pool of free 40S subunits
3.74E-12	2.45E-10	Selenocysteine synthesis
3.79E-12	2.45E-10	GTP hydrolysis and joining of the 60S ribosomal subunit
3.79E-12	2.45E-10	L13a-mediated translational silencing of Ceruloplasmin expression
3.79E-12	2.45E-10	3, -UTR-mediated translational regulation
7.42E-12	4.42E-10	Selenoamino acid metabolism
8.05E-12	4.45E-10	Nonsense Mediated Decay (NMD) independent of the Exon Junction Complex (EJC)
1.04E-11	5.02E-10	Nonsense Mediated Decay (NMD) enhanced by the Exon Junction Complex (EJC)
1.04E-11	5.02E-10	Nonsense-Mediated Decay (NMD)
1.34E-11	5.76E-10	Metabolism of proteins
1.42E-11	5.76E-10	Cap-dependent Translation Initiation
1.42E-11	5.76E-10	Eukaryotic Translation Initiation
5.51E-10	2.13E-08	Citrate cycle (TCA cycle) (human)
6.59E-09	2.43E-07	Ribosome (human)
1.50E-08	5.27E-07	Metabolism of amino acids and derivatives
2.57E-08	8.66E-07	Protein processing in endoplasmic reticulum (human)
3.69E-08	1.18E-06	Citric acid cycle (TCA cycle)
3.80E-08	1.18E-06	Vesicle-mediated transport

4.72E-08	1.41E-06	Innate Immune System
1.78E-07	5.09E-06	Clathrin-mediated endocytosis
6.11E-07	1.69E-05	Pathogenic Escherichia coli infection (human)
6.63E-07	1.77E-05	Ribosomal scanning and start codon recognition
7.84E-07	2.02E-05	Translation initiation complex formation
9.00E-07	2.23E-05	Membrane Trafficking
9.23E-07	2.23E-05	Activation of the mRNA upon binding of the cap-binding complex and eIFs, and subsequent binding to 43S
1.20E-06	2.82E-05	Endocytosis (human)
1.28E-06	2.92E-05	Formation of the ternary complex, and subsequently, the 43S complex
1.61E-06	3.56E-05	Prefoldin mediated transfer of substrate to CCT/TriC
3.92E-06	7.80E-05	The citric acid (TCA) cycle and respiratory electron transport
4.03E-06	7.80E-05	Beta oxidation of hexanoyl-CoA to butanoyl-CoA
4.03E-06	7.80E-05	Beta oxidation of lauroyl-CoA to decanoyl-CoA-CoA
4.03E-06	7.80E-05	Beta oxidation of decanoyl-CoA to octanoyl-CoA-CoA
4.03E-06	7.80E-05	Beta oxidation of octanoyl-CoA to hexanoyl-CoA
5.50E-06	0.00010136	mitochondrial fatty acid beta-oxidation of saturated fatty acids
5.50E-06	0.00010136	Folding of actin by CCT/TriC
5.96E-06	0.00010722	Cooperation of Prefoldin and TriC/CCT in actin and tubulin folding
6.60E-06	0.00011617	Fatty acid elongation (human)
8.80E-06	0.00015142	Formation of tubulin folding intermediates by CCT/TriC
1.02E-05	0.0001715	Extracellular matrix organization
1.66E-05	0.00027022	Glucose metabolism
1.68E-05	0.00027022	Asparagine N-linked glycosylation
2.13E-05	0.00033641	Bacterial invasion of epithelial cells (human)
2.75E-05	0.00042587	Beta oxidation of palmitoyl-CoA to myristoyl-CoA
3.05E-05	0.00046296	Glycolysis / Gluconeogenesis (human)
3.59E-05	0.00053508	Legionellosis (human)
3.85E-05	0.00056236	Glycolysis
4.46E-05	0.00062796	Fatty acid degradation (human)
4.46E-05	0.00062796	Proteasome (human)
5.40E-05	0.00074572	ER to Golgi Anterograde Transport
5.89E-05	0.00079931	Metabolism of carbohydrates
8.42E-05	0.00110272	UCH proteinases
8.55E-05	0.00110272	Valine, leucine and isoleucine degradation (human)
8.55E-05	0.00110272	Amino sugar and nucleotide sugar metabolism (human)
9.95E-05	0.00126253	Pyruvate metabolism and Citric Acid (TCA) cycle
0.00010339	0.00129068	RHO GTPases Activate WASPs and WAVEs
0.00010924	0.00134215	Immune System
0.0001275	0.00154197	corticosteroids and cardioprotection
0.00015817	0.00185494	Recycling pathway of L1

0.00015817	0.00185494	Glyoxylate and dicarboxylate metabolism (human)
0.00017315	0.00200031	Tryptophan metabolism (human)
0.0002466	0.00280684	COPII (Coat Protein 2) Mediated Vesicle Transport
0.00033709	0.00372721	VLDLR internalisation and degradation
0.00033709	0.00372721	how does salmonella hijack a cell
0.00034348	0.00374441	Propanoate metabolism (human)
0.00042561	0.00457534	Mitochondrial Fatty Acid Beta-Oxidation
0.00047532	0.00497487	Advanced glycosylation endproduct receptor signaling
0.0004844	0.00497487	Cargo concentration in the ER
0.00048699	0.00497487	Endocrine and other factor-regulated calcium reabsorption (human)
0.00048849	0.00497487	Transport to the Golgi and subsequent modification
0.00053046	0.00533212	VLDL interactions
0.00055921	0.00554909	Cardiac muscle contraction (human)
0.0006146	0.00602153	COPI-mediated anterograde transport
0.00064965	0.00620772	Retrograde neurotrophin signalling
0.00064965	0.00620772	Synthesis of bile acids and bile salts via 24-hydroxycholesterol
0.00066667	0.00629275	Smooth Muscle Contraction
0.00073106	0.00681733	Shigellosis (human)
0.0007757	0.00713253	HSF1-dependent transactivation
0.00078329	0.00713253	Huntington,s disease (human)
0.00086486	0.00756549	WNT5A-dependent internalization of FZD4
0.00086486	0.00756549	Synthesis of bile acids and bile salts via 27-hydroxycholesterol
0.00087919	0.00756549	Nef Mediated CD8 Down-regulation
0.00087919	0.00756549	AUF1 (hnRNP D0) binds and destabilizes mRNA
0.00087971	0.00756549	Chaperonin-mediated protein folding
0.00089643	0.0076246	Integrin cell surface interactions
0.00114398	0.00962437	Glutathione metabolism (human)
0.00119943	0.00998236	Collagen biosynthesis and modifying enzymes
0.00124658	0.01024772	Biological oxidations
0.0012578	0.01024772	Parkinson,s disease (human)
0.00130628	0.01053187	Ub-specific processing proteases
0.00136824	0.01089577	Butanoate metabolism (human)
0.00137957	0.01089577	Protein folding
0.00143734	0.01112504	role of pi3k subunit p85 in regulation of actin organization and cell migration
0.00143734	0.01112504	y branching of actin filaments
0.00154138	0.01181219	Binding and Uptake of Ligands by Scavenger Receptors
0.00156154	0.0118493	Post-translational protein modification
0.00161279	0.01211944	Attenuation phase
0.00174645	0.0129976	EPHB-mediated forward signaling
0.00188798	0.01391712	Pentose phosphate pathway (human)
0.00193674	0.01414186	Lysine degradation (human)

0.00197156	0.01426154	Cooperation of PDCL (PhLP1) and TRiC/CCT in G-protein beta folding
0.00201668	0.01445287	Formation of annular gap junctions
0.00205674	0.01460473	Deubiquitination
0.00209699	0.01475517	Alzheimer,s disease (human)
0.00213672	0.01489932	MHC class II antigen presentation
0.002196	0.01504161	HSF1 activation
0.002196	0.01504161	beta-Alanine metabolism (human)
0.00235113	0.01596292	Platelet degranulation
0.00241695	0.01626711	EPH-Ephrin signaling
0.00253906	0.01694163	Gluconeogenesis
0.00268588	0.0174695	Beta oxidation of myristoyl-CoA to lauroyl-CoA
0.00268588	0.0174695	Utilization of Ketone Bodies
0.00268588	0.0174695	Formation of the active cofactor, UDP-glucuronate
0.00281666	0.0178696	Nef Mediated CD4 Down-regulation
0.00281666	0.0178696	Gap junction degradation
0.00281666	0.0178696	Glycogen synthesis
0.00313622	0.01973526	Response to elevated platelet cytosolic Ca2+
0.00326232	0.02036317	Cellular response to heat stress
0.00333921	0.02067637	N-glycan trimming in the ER and Calnexin/Calreticulin cycle
0.00344123	0.02113899	Arginine and proline metabolism (human)
0.00378657	0.02298271	The role of GTSE1 in G2/M progression after G2 checkpoint
0.00380076	0.02298271	Detoxification of Reactive Oxygen Species
0.0039203	0.02352183	cystic fibrosis transmembrane conductance regulator (cftr) and beta 2 adrenergic receptor (b2ar) pathway
0.0041337	0.02461138	TP53 Regulates Metabolic Genes
0.00430626	0.02544307	Starch and sucrose metabolism (human)
0.00436584	0.0255997	Lipoprotein metabolism
0.00463396	0.0265913	LDL-mediated lipid transport
0.00463396	0.0265913	Proximal tubule bicarbonate reclamation (human)
0.00463802	0.0265913	Respiratory electron transport, ATP synthesis by chemiosmotic coupling, and heat production by uncoupling proteins.
0.0049364	0.0274876	Ethanol oxidation
0.0049364	0.0274876	Gap junction trafficking
0.0049364	0.0274876	Lysine catabolism
0.0049364	0.0274876	eNOS activation
0.0052642	0.02859265	ahr signal transduction pathway
0.0052642	0.02859265	antisense pathway
0.00541485	0.02859265	Cilium Assembly
0.00543003	0.02859265	Histidine metabolism (human)
0.00543003	0.02859265	proteasome complex
0.00543003	0.02859265	Synthesis of bile acids and bile salts via 7alpha-hydroxycholesterol

0.00543003	0.02859265	Antigen Presentation: Folding, assembly and peptide loading of class I MHC
0.00543622	0.02859265	Phase 1 - Functionalization of compounds
0.00546733	0.02859265	Dilated cardiomyopathy (human)
0.00610838	0.03159819	Pyruvate metabolism (human)
0.00612368	0.03159819	Lipid digestion, mobilization, and transport
0.00627473	0.03216318	Dissolution of Fibrin Clot
0.00649158	0.03305582	Golgi-to-ER retrograde transport
0.00654731	0.03312168	Axon guidance
0.00681148	0.03403649	Regulation of mRNA stability by proteins that bind AU-rich elements
0.00681609	0.03403649	Phagosome (human)
0.00714103	0.0354305	Oxidative phosphorylation (human)
0.00751355	0.03704131	Metabolism of lipids and lipoproteins
0.00756893	0.03707818	Collagen formation
0.00780884	0.03777527	Gap junction trafficking and regulation
0.00780884	0.03777527	Golgi Cisternae Pericentriolar Stack Reorganization
0.00788479	0.03790578	Epstein-Barr virus infection (human)
0.0085921	0.04082929	Leukocyte transendothelial migration (human)
0.00859842	0.04082929	Beta oxidation of butanoyl-CoA to acetyl-CoA
0.00909221	0.04291078	Amoebiasis (human)
0.00932813	0.04375742	RHO GTPase Effectors
0.00959882	0.04475592	Proteoglycans in cancer (human)
0.0101913	0.0471206	Vasopressin-regulated water reabsorption (human)
0.01022773	0.0471206	Cargo recognition for clathrin-mediated endocytosis
0.01078035	0.04937274	VEGFR2 mediated vascular permeability
0.01115289	0.05077843	Hemostasis
0.01148769	0.05169461	Sema3A PAK dependent Axon repulsion
0.01148769	0.05169461	Synthesis of Prostaglandins (PG) and Thromboxanes (TX)
0.01212384	0.05403948	Respiratory electron transport
0.01264067	0.05570121	Acyl chain remodeling of CL
0.01274122	0.05570121	Hypertrophic cardiomyopathy (HCM) (human)
0.01274122	0.05570121	COPI-dependent Golgi-to-ER retrograde traffic
0.01280984	0.05570121	L1CAM interactions
0.01337642	0.05769615	ion channels and their functional role in vascular endothelium
0.01359347	0.05769615	RAB geranylgeranylation
0.01362284	0.05769615	mcalpain and friends in cell motility
0.01364134	0.05769615	Trafficking of GluR2-containing AMPA receptors
0.01364134	0.05769615	Phenylalanine metabolism (human)
0.01515678	0.06327758	Adrenergic signaling in cardiomyocytes (human)
0.01520624	0.06327758	Trafficking of AMPA receptors
0.01520624	0.06327758	Glutamate Binding, Activation of AMPA Receptors and Synaptic Plasticity
0.0158365	0.06487314	Malaria (human)

0.01584036	0.06487314	Degradation of the extracellular matrix
0.01600875	0.06487314	Deregulated CDK5 triggers multiple neurodegenerative pathways in Alzheimers disease models
0.01600875	0.06487314	Neurodegenerative Diseases
0.01600875	0.06487314	ucalpain and friends in cell spread
0.01690098	0.06813208	Keratan sulfate/keratin metabolism
0.01717246	0.06864661	PCP/CE pathway
0.017206	0.06864661	Fatty acid, triacylglycerol, and ketone body metabolism
0.01740974	0.06910327	Muscle contraction
0.01815325	0.07168681	Regulation of PLK1 Activity at G2/M Transition
0.01859199	0.07276851	Prostacyclin signalling through prostacyclin receptor
0.01870922	0.07276851	Synthesis of bile acids and bile salts
0.01870922	0.07276851	integrin signaling pathway
0.02029191	0.07813901	Loss of Nlp from mitotic centrosomes
0.02029191	0.07813901	Loss of proteins required for interphase microtubule organization from the centrosome
0.02063289	0.07866924	Tyrosine metabolism (human)
0.02063289	0.07866924	Elastic fibre formation
0.02106634	0.07992817	Fcgamma receptor (FCGR) dependent phagocytosis
0.02146977	0.08084617	G2/M Transition
0.02159234	0.08084617	Arrhythmogenic right ventricular cardiomyopathy (ARVC) (human)
0.02162165	0.08084617	Cargo trafficking to the periciliary membrane
0.02196978	0.08175295	Infectious disease
0.02266861	0.08237326	Axonal growth inhibition (RHOA activation)
0.02266861	0.08237326	InlA-mediated entry of Listeria monocytogenes into host cells
0.02266861	0.08237326	Aryl hydrocarbon receptor signalling
0.02266861	0.08237326	Vitamin C (ascorbate) metabolism
0.02266861	0.08237326	Regulation of cytoskeletal remodeling and cell spreading by IPP complex components
0.0233635	0.08450164	Mitotic G2-G2/M phases
0.02435961	0.08666752	AURKA Activation by TPX2
0.02441023	0.08666752	Scavenging by Class A Receptors
0.02441023	0.08666752	prion pathway
0.02441023	0.08666752	Hedgehog ligand biogenesis
0.02537367	0.08967681	Regulation of actin dynamics for phagocytic cup formation
0.02550697	0.08973817	Platelet activation, signaling and aggregation
0.02582822	0.09045719	Gastric acid secretion (human)
0.02676008	0.09329865	ECM proteoglycans
0.0276397	0.09510047	Beta-catenin independent WNT signaling
0.02764548	0.09510047	Nef-mediates down modulation of cell surface receptors by recruiting them to clathrin adapters

0.02764548	0.09510047	Nicotinate metabolism
0.02856916	0.09590874	Metabolism of ingested SeMet, Sec, MeSec into H2Se
0.02856916	0.09590874	Formyl peptide receptors bind formyl peptides and many other ligands
0.02856916	0.09590874	p75NTR regulates axonogenesis
0.02856916	0.09590874	Ketone body metabolism
0.02856916	0.09590874	Pentose phosphate pathway (hexose monophosphate shunt)
0.02863135	0.09590874	Golgi Associated Vesicle Biogenesis
0.0287843	0.09590874	Regulation of actin cytoskeleton (human)
0.02893943	0.09590874	Antigen processing and presentation (human)
0.02899566	0.09590874	Cellular responses to stress
0.02951315	0.09720501	Glutathione conjugation
0.03058346	0.09905038	Viral myocarditis (human)
0.03109721	0.09905038	Thromboxane signalling through TP receptor
0.03109721	0.09905038	Biosynthesis of unsaturated fatty acids (human)
0.03109721	0.09905038	Post-chaperonin tubulin folding pathway
0.03109721	0.09905038	how progesterone initiates the oocyte maturation
0.03109721	0.09905038	BBSome-mediated cargo-targeting to cilium
0.03109721	0.09905038	eNOS activation and regulation
0.03109721	0.09905038	Metabolism of nitric oxide
0.03203556	0.10120621	Glycine, serine and threonine metabolism (human)
0.03203556	0.10120621	Association of TriC/CCT with target proteins during biosynthesis
0.03476395	0.10881784	ADP signalling through P2Y purinoceptor 1
0.03500729	0.10881784	Synthesis and degradation of ketone bodies (human)
0.03500729	0.10881784	Hyaluronan uptake and degradation
0.03500729	0.10881784	regulation of spermatogenesis by crem
0.03587822	0.11063642	Recruitment of mitotic centrosome proteins and complexes
0.03587822	0.11063642	Centrosome maturation
0.03776589	0.11599524	ECM-receptor interaction (human)
0.03864369	0.11822221	Glyoxylate metabolism and glycine degradation
0.03921588	0.11950037	Arachidonic acid metabolism (human)
0.04034005	0.12244392	Bile acid and bile salt metabolism
0.04158312	0.12438929	Mitochondrial protein import
0.04158312	0.12438929	Synaptic vesicle cycle (human)
0.04194523	0.12438929	Dermatan sulfate biosynthesis
0.04194523	0.12438929	Nicotinamide salvaging
0.04194523	0.12438929	role of ran in mitotic spindle regulation
0.04194523	0.12438929	cxcr4 signaling pathway
0.04335493	0.1266291	Signaling by Retinoic Acid
0.04335493	0.1266291	Retinoid metabolism and transport
0.04335493	0.1266291	Histidine, lysine, phenylalanine, tyrosine, proline and tryptophan catabolism
0.04335493	0.1266291	Intrinsic Pathway for Apoptosis

0.04548464	0.13235004	Phase II conjugation
0.04934699	0.13990685	Hyaluronan metabolism
0.04934699	0.13990685	mechanism of protein import into the nucleus
0.04934699	0.13990685	Josephin domain DUBs
0.04934699	0.13990685	Hh mutants that don,t undergo autocatalytic processing are degraded by ERAD
0.04934699	0.13990685	Hh mutants abrogate ligand secretion
0.04934699	0.13990685	g-protein signaling through tubby proteins
0.04934699	0.13990685	Chk1/Chk2(Cds1) mediated inactivation of Cyclin B:Cdk1 complex

Calcific CAVD stage

p-value	q-value	Pathway
1.84E-53	8.14E-51	Complement and coagulation cascades (human)
3.91E-34	8.66E-32	Platelet degranulation
1.85E-33	2.74E-31	Response to elevated platelet cytosolic Ca2+
1.60E-24	1.77E-22	Formation of Fibrin Clot (Clotting Cascade)
2.68E-22	2.37E-20	Platelet activation, signaling and aggregation
8.53E-22	6.29E-20	Hemostasis
2.38E-19	1.50E-17	Intrinsic Pathway of Fibrin Clot Formation
1.24E-18	6.85E-17	Innate Immune System
2.07E-18	1.02E-16	Complement cascade
7.40E-18	3.28E-16	Staphylococcus aureus infection (human)
1.37E-17	5.50E-16	Regulation of Complement cascade
4.42E-17	1.63E-15	intrinsic prothrombin activation pathway
6.52E-15	2.22E-13	classical complement pathway
6.11E-14	1.93E-12	Immune System
7.71E-14	2.28E-12	Scavenging of heme from plasma
3.13E-13	8.68E-12	Neutrophil degranulation
8.46E-13	2.08E-11	Removal of aminoterminal propeptides from gamma-carboxylated proteins
8.46E-13	2.08E-11	Gamma-carboxylation of protein precursors
1.07E-12	2.50E-11	Systemic lupus erythematosus (human)
3.05E-12	6.76E-11	Gamma-carboxylation, transport, and amino-terminal cleavage of proteins
3.67E-12	7.74E-11	Common Pathway of Fibrin Clot Formation
2.30E-11	4.63E-10	extrinsic prothrombin activation pathway
1.16E-10	2.24E-09	alternative complement pathway
1.24E-10	2.30E-09	Extracellular matrix organization
2.18E-10	3.87E-09	Regulation of TLR by endogenous ligand
3.29E-10	5.60E-09	Binding and Uptake of Ligands by Scavenger Receptors
1.60E-09	2.62E-08	Initial triggering of complement
3.11E-09	4.85E-08	fibrinolysis pathway

3.17E-09	4.85E-08	Regulation of Insulin-like Growth Factor (IGF) transport and uptake by Insulin-like Growth Factor Binding Proteins (IGFBPs)
5.10E-09	7.54E-08	Activation of Matrix Metalloproteinases
6.78E-09	9.69E-08	Lipoprotein metabolism
2.06E-08	2.85E-07	Degradation of the extracellular matrix
2.51E-08	3.37E-07	Pertussis (human)
2.95E-08	3.84E-07	Lipid digestion, mobilization, and transport
4.46E-08	5.65E-07	lectin induced complement pathway
5.65E-08	6.95E-07	Activation of C3 and C5
3.28E-07	3.83E-06	Terminal pathway of complement
3.28E-07	3.83E-06	Erythrocytes take up oxygen and release carbon dioxide
3.62E-07	4.01E-06	p130Cas linkage to MAPK signaling for integrins
3.62E-07	4.01E-06	GRB2:SOS provides linkage to MAPK signaling for Integrins
6.51E-07	7.03E-06	Metabolism of fat-soluble vitamins
7.07E-07	7.46E-06	Gamma carboxylation, hypusine formation and arylsulfatase activation
1.64E-06	1.69E-05	HDL-mediated lipid transport
1.87E-06	1.88E-05	Retinoid metabolism and transport
3.14E-06	3.03E-05	Erythrocytes take up carbon dioxide and release oxygen
3.14E-06	3.03E-05	O2/CO2 exchange in erythrocytes
4.29E-06	4.05E-05	Prion diseases (human)
7.66E-06	7.07E-05	Platelet Aggregation (Plug Formation)
9.65E-06	8.73E-05	Phagosome (human)
1.40E-05	0.00012393	Integrin alphaIIb beta3 signaling
1.49E-05	0.00012921	Creation of C4 and C2 activators
2.93E-05	0.00024975	Alternative complement activation
4.67E-05	0.00039045	Integrin cell surface interactions
5.37E-05	0.00044072	Signaling by high-kinase activity BRAF mutants
6.30E-05	0.00050715	antigen processing and presentation
7.00E-05	0.00055354	Chylomicron-mediated lipid transport
7.22E-05	0.0005591	Extrinsic Pathway of Fibrin Clot Formation
7.45E-05	0.0005591	Allograft rejection (human)
7.45E-05	0.0005591	Signaling by RAS mutants
8.70E-05	0.00063173	Translocation of ZAP-70 to Immunological synapse
8.70E-05	0.00063173	Generation of second messenger molecules
8.96E-05	0.00063987	Dissolution of Fibrin Clot
0.00010113	0.00068926	MAP2K and MAPK activation
0.00010113	0.00068926	Signaling by moderate kinase activity BRAF mutants
0.00010113	0.00068926	Paradoxical activation of RAF signaling by kinase inactive BRAF
0.00010431	0.00070016	ECM proteoglycans
0.00012736	0.00084207	Antigen processing and presentation (human)
0.00013081	0.00085222	Viral myocarditis (human)

0.00013489	0.00086602	Graft-versus-host disease (human)
0.00014236	0.00088824	platelet amyloid precursor protein pathway
0.00014236	0.00088824	Metal sequestration by antimicrobial proteins
0.00015747	0.00096886	Phosphorylation of CD3 and TCR zeta chains
0.00016253	0.00098634	MHC class II antigen presentation
0.000177	0.00105963	Type I diabetes mellitus (human)
0.00018866	0.00111434	PD-1 signaling
0.00019833	0.00115606	ECM-receptor interaction (human)
0.00023678	0.00136227	Toll-Like Receptors Cascades
0.00026495	0.00150478	Asthma (human)
0.0003234	0.0018135	Classical antibody-mediated complement activation
0.00032834	0.00181818	Downstream TCR signaling
0.00035478	0.00194031	Metabolism of Angiotensinogen to Angiotensins
0.00036684	0.00198183	Cell surface interactions at the vascular wall
0.00038252	0.00203809	Transfer of LPS from LBP carrier to CD14
0.00038715	0.00203809	inhibition of matrix metalloproteinases
0.00039106	0.00203809	TCR signaling
0.00048535	0.00250013	African trypanosomiasis (human)
0.00051031	0.00259846	Autoimmune thyroid disease (human)
0.00058343	0.00293704	Hematopoietic cell lineage (human)
0.00087268	0.00434377	Visual phototransduction
0.0010537	0.00518653	Herpes simplex infection (human)
0.00112329	0.00546831	proteasome complex
0.00120214	0.00578856	Signaling by BRAF and RAF fusions
0.00127232	0.00606063	Metabolism of vitamins and cofactors
0.00154602	0.00728601	Oncogenic MAPK signaling
0.00161573	0.00753439	Proteasome (human)
0.00196805	0.00908175	Focal adhesion (human)
0.00217612	0.00993837	Intestinal immune network for IgA production (human)
0.00223608	0.01010799	Scavenging by Class H Receptors
0.00231755	0.01037045	Metabolism of proteins
0.00267556	0.01185274	Tuberculosis (human)
0.00274431	0.01203692	Platelet activation (human)
0.0028299	0.01229065	Leishmaniasis (human)
0.00367643	0.01537397	Antimicrobial peptides
0.00367865	0.01537397	Scavenging by Class B Receptors
0.00367865	0.01537397	VLDL biosynthesis
0.00367865	0.01537397	Ficolins bind to repetitive carbohydrate structures on the target cell surface
0.00501464	0.02076153	Vesicle-mediated transport
0.00544679	0.02234193	Lectin pathway of complement activation
0.00882124	0.03585145	Inflammatory bowel disease (IBD) (human)

0.00932689	0.03756195	Metabolism
0.00985573	0.03884032	Renin-angiotensin system (human)
0.00985573	0.03884032	LDL-mediated lipid transport
0.00990735	0.03884032	Heme degradation
0.01096446	0.042237	IRS-related events triggered by IGF1R
0.01096446	0.042237	IGF1R signaling cascade
0.01110322	0.04240283	Vitamin digestion and absorption (human)
0.01127058	0.04267408	Signaling by Type 1 Insulin-like Growth Factor 1 Receptor (IGF1R)
0.01143277	0.04292133	activation of csk by camp-dependent protein kinase inhibits signaling through the t cell receptor
0.01196543	0.04454356	Amoebiasis (human)
0.01233344	0.04553096	Non-integrin membrane-ECM interactions
0.0125745	0.04603722	SHC-related events triggered by IGF1R
0.01338968	0.04861992	PPAR signaling pathway (human)
0.01426807	0.05138824	Peptide hormone metabolism
0.01494119	0.05337859	Costimulation by the CD28 family
0.01530338	0.05361761	Antigen processing-Cross presentation
0.01530338	0.05361761	Malaria (human)
0.01537119	0.05361761	corticosteroids and cardioprotection
0.01551667	0.05370224	Nef mediated downregulation of MHC class I complex cell surface expression
0.01572801	0.05401171	HIF-1 signaling pathway (human)
0.01662188	0.05536461	RAF/MAP kinase cascade
0.01662188	0.05536461	SHC1 events in EGFR signaling
0.01662188	0.05536461	SOS-mediated signalling
0.01662188	0.05536461	GRB2 events in EGFR signaling
0.01711819	0.05659222	Epstein-Barr virus infection (human)
0.01788655	0.05869438	UCH proteinases
0.01867217	0.06010084	Signalling to p38 via RIT and RIN
0.01867217	0.06010084	ARMS-mediated activation
0.01872216	0.06010084	Purine catabolism
0.01921226	0.06123045	Frs2-mediated activation
0.01950045	0.06170499	MAPK family signaling cascades
0.01976361	0.06209418	MAPK1/MAPK3 signaling
0.02032633	0.06332508	Prolonged ERK activation events
0.02044128	0.06332508	Interaction between L1 and Ankyrins
0.02090055	0.06429822	Signaling by Leptin
0.02148639	0.06564462	Signalling to RAS
0.02208396	0.0663889	Interleukin receptor SHC signaling
0.02217959	0.0663889	Reversible hydration of carbon dioxide
0.02217959	0.0663889	g-protein signaling through tubby proteins
0.02251384	0.06693713	Cell adhesion molecules (CAMs) (human)

0.02340462	0.06912164	Hypertrophic cardiomyopathy (HCM) (human)
0.02394824	0.07025875	VEGFR2 mediated cell proliferation
0.02587794	0.07177236	activation of pkc through g-protein coupled receptors
0.02587794	0.07177236	hemoglobins chaperone
0.02587794	0.07177236	Endosomal/Vacuolar pathway
0.02587794	0.07177236	lck and fyn tyrosine kinases in initiation of tcr activation
0.02587794	0.07177236	il-10 anti-inflammatory signaling pathway
0.02587794	0.07177236	Purine salvage
0.02587794	0.07177236	Initiation of Nuclear Envelope Reformation
0.02587794	0.07177236	Nuclear Envelope Reassembly
0.0259223	0.07177236	Signalling to ERKs
0.02660523	0.07320569	Interleukin-2 signaling
0.02800913	0.07659286	RET signaling
0.02854051	0.07756717	Toxoplasmosis (human)
0.03048351	0.08141595	Rheumatoid arthritis (human)
0.03048351	0.08141595	Dilated cardiomyopathy (human)
0.03069179	0.08141595	Purine metabolism
0.03069179	0.08141595	Striated Muscle Contraction
0.03301084	0.08578001	Collagen degradation
0.03301084	0.08578001	Smooth Muscle Contraction
0.03306897	0.08578001	FCERI mediated MAPK activation
0.03311147	0.08578001	Host Interactions of HIV factors
0.03333301	0.08585189	Interleukin-3, 5 and GM-CSF signaling
0.03395498	0.0869483	il 4 signaling pathway
0.03447676	0.08777704	Th1 and Th2 cell differentiation (human)
0.03541862	0.08965972	Circadian Clock
0.03635954	0.09151861	SRP-dependent cotranslational protein targeting to membrane
0.03754029	0.09395677	NCAM signaling for neurite out-growth
0.03831325	0.09535263	the igf-1 receptor and longevity
0.04287158	0.10492879	Nitrogen metabolism (human)
0.04287158	0.10492879	Formation of Senescence-Associated Heterochromatin Foci (SAHF)
0.04287158	0.10492879	Glycogen breakdown (glycogenolysis)
0.0456092	0.11101579	Post-translational protein modification
0.04592443	0.11117225	Fat digestion and absorption (human)
0.04665138	0.11231827	Metabolism of nucleotides
0.04762054	0.11341881	Deregulated CDK5 triggers multiple neurodegenerative pathways in Alzheimers disease models
0.04762054	0.11341881	Neurodegenerative Diseases
0.04876566	0.11535635	Porphyrin and chlorophyll metabolism (human)
0.04895484	0.11535635	Proteoglycans in cancer (human)

Supplemental Table 4

CAVD Leaflet Layer Pathways

Diseased (CAVD) Fibrosa

p-value	q-value	Pathway
1.61E-28	2.43E-26	Extracellular matrix organization
3.28E-25	2.47E-23	ECM-receptor interaction - Homo sapiens (human)
1.65E-20	8.28E-19	Complement and coagulation cascades - Homo sapiens (human)
4.72E-19	1.78E-17	Classical complement pathway
2.28E-16	6.87E-15	ECM proteoglycans
3.67E-15	9.23E-14	Regulation of Complement cascade
1.19E-14	2.57E-13	Focal adhesion - Homo sapiens (human)
4.11E-14	7.76E-13	Complement cascade
4.78E-14	8.01E-13	Terminal pathway of complement
1.60E-13	2.35E-12	Protein digestion and absorption - Homo sapiens (human)
1.71E-13	2.35E-12	Collagen biosynthesis and modifying enzymes
5.81E-13	7.32E-12	Binding and Uptake of Ligands by Scavenger Receptors
1.98E-12	2.30E-11	Collagen chain trimerization
3.04E-12	3.28E-11	Integrin cell surface interactions
6.60E-12	6.64E-11	Collagen formation
3.78E-11	3.57E-10	Alternative complement pathway
9.92E-11	8.81E-10	PI3K-Akt signaling pathway - Homo sapiens (human)
1.64E-10	1.38E-09	Lectin induced complement pathway
1.92E-10	1.52E-09	Prion diseases - Homo sapiens (human)
5.87E-09	4.43E-08	Platelet degranulation
8.67E-09	6.23E-08	Response to elevated platelet cytosolic Ca2+
9.13E-09	6.26E-08	Scavenging by Class A Receptors
5.62E-08	3.54E-07	Amoebiasis - Homo sapiens (human)
5.62E-08	3.54E-07	Non-integrin membrane-ECM interactions
6.96E-08	4.20E-07	Systemic lupus erythematosus - Homo sapiens (human)
4.63E-07	2.69E-06	Syndecan interactions
1.13E-06	6.34E-06	Innate Immune System
1.20E-06	6.46E-06	Hemostasis
1.90E-06	9.90E-06	Pertussis - Homo sapiens (human)
1.97E-06	9.94E-06	Assembly of collagen fibrils and other multimeric structures
3.07E-06	1.50E-05	Molecules associated with elastic fibres
6.79E-06	3.20E-05	Elastic fibre formation
9.00E-06	4.12E-05	NCAM1 interactions
1.15E-05	5.11E-05	Platelet activation, signaling and aggregation
2.15E-05	9.27E-05	Retinoid metabolism and transport
2.67E-05	0.000112	Intrinsic prothrombin activation pathway

4.90E-05	0.0002	Metabolism of fat-soluble vitamins
6.43E-05	0.000256	Staphylococcus aureus infection - Homo sapiens (human)
9.42E-05	0.000356	Scavenging of heme from plasma
9.42E-05	0.000356	Immune System
0.000187	0.000688	Proteoglycans in cancer - Homo sapiens (human)
0.000284	0.001021	Cell surface interactions at the vascular wall
0.000347	0.00121	Glycosaminoglycan metabolism
0.000353	0.00121	Scavenging by Class H Receptors
0.000533	0.001789	Small cell lung cancer - Homo sapiens (human)
0.000549	0.001801	Malaria - Homo sapiens (human)
0.000585	0.001878	VLDL biosynthesis
0.000713	0.002242	Chylomicron-mediated lipid transport
0.000881	0.002714	Pancreatic secretion - Homo sapiens (human)
0.000915	0.002764	Laminin interactions
0.001029	0.003046	A tetrasaccharide linker sequence is required for GAG synthesis
0.001107	0.003215	AGE-RAGE signaling pathway in diabetic complications - Homo sapiens (human)
0.001157	0.003296	Visual phototransduction
0.001194	0.00334	Phagosome - Homo sapiens (human)
0.001282	0.003519	Keratan sulfate biosynthesis
0.001612	0.004348	Cross-presentation of particulate exogenous antigens (phagosomes)
0.001885	0.004993	Lipoprotein metabolism
0.002076	0.005405	Keratan sulfate/keratin metabolism
0.002565	0.006456	Gamma-carboxylation of protein precursors
0.002565	0.006456	Removal of aminoterminal propeptides from gamma-carboxylated proteins
0.00312	0.007477	Dermatan sulfate biosynthesis
0.00312	0.007477	regulators of bone mineralization
0.00312	0.007477	Gamma-carboxylation, transport, and amino-terminal cleavage of proteins
0.004039	0.00953	Signaling by PDGF
0.004799	0.011148	Classical antibody-mediated complement activation
0.006059	0.013862	Creation of C4 and C2 activators
0.006637	0.014958	Regulation of TLR by endogenous ligand
0.007167	0.015915	Chondroitin sulfate/dermatan sulfate metabolism
0.008232	0.018015	Metabolism of vitamins and cofactors
0.008395	0.01811	Heparan sulfate/heparin (HS-GAG) metabolism
0.008617	0.018325	Initial triggering of complement
0.008869	0.018601	NCAM signaling for neurite out-growth
0.009279	0.019193	Ion homeostasis
0.009503	0.019391	Degradation of the extracellular matrix
0.010214	0.020565	Ion transport by P-type ATPases
0.010446	0.020755	Lipid digestion, mobilization, and transport
0.011327	0.022212	Chondroitin sulfate biosynthesis
0.01351	0.025823	VLDL interactions

0.01351	0.025823	Proximal tubule bicarbonate reclamation - Homo sapiens (human)
0.018272	0.03383	Arrhythmogenic right ventricular cardiomyopathy (ARVC) - Homo sapiens (human)
0.018371	0.03383	Basigin interactions
0.018371	0.03383	Synthesis of PC
0.021144	0.038467	Vesicle-mediated transport
0.02243	0.04032	Amine compound SLC transporters
0.023585	0.041899	Metabolism of carbohydrates
0.026495	0.04652	Hypertrophic cardiomyopathy (HCM) - Homo sapiens (human)
0.028356	0.049215	African trypanosomiasis - Homo sapiens (human)
0.028878	0.049552	Developmental Biology
0.031686	0.05376	Dilated cardiomyopathy - Homo sapiens (human)
0.0326	0.054695	Salivary secretion - Homo sapiens (human)
0.033897	0.056247	Axon guidance
0.036535	0.057891	Aldosterone-regulated sodium reabsorption - Homo sapiens (human)
0.036535	0.057891	Formation of Fibrin Clot (Clotting Cascade)
0.036535	0.057891	Gamma carboxylation, hypusine formation and arylsulfatase activation
0.036535	0.057891	O-glycosylation of TSR domain-containing proteins
0.036805	0.057891	Neutrophil degranulation
0.040031	0.062316	Fat digestion and absorption - Homo sapiens (human)
0.049292	0.07595	Carbohydrate digestion and absorption - Homo sapiens (human)

Diseased (CAVD) Spongiosa

p-value	q-value	Pathway
7.66E-13	8.72E-11	Platelet degranulation
1.24E-12	8.72E-11	Response to elevated platelet cytosolic Ca2+
2.99E-11	1.40E-09	Complement and coagulation cascades - Homo sapiens (human)
4.07E-11	1.43E-09	Hemostasis
3.71E-10	1.05E-08	Neutrophil degranulation
9.38E-10	2.20E-08	Platelet activation, signaling and aggregation
2.11E-09	4.24E-08	Innate Immune System
5.58E-08	9.83E-07	Complement cascade
9.88E-08	1.55E-06	Formation of Fibrin Clot (Clotting Cascade)
1.55E-07	2.17E-06	Intrinsic Pathway of Fibrin Clot Formation
1.70E-07	2.17E-06	Initial triggering of complement
2.49E-07	2.92E-06	Histidine metabolism - Homo sapiens (human)
5.43E-07	5.89E-06	Scavenging of heme from plasma
7.68E-06	7.70E-05	Common Pathway of Fibrin Clot Formation
8.19E-06	7.70E-05	Immune System
1.30E-05	0.000115	Classical antibody-mediated complement activation
1.39E-05	0.000115	FCGR activation
1.84E-05	0.000141	Metabolism

1.91E-05	0.000141	Creation of C4 and C2 activators
3.98E-05	0.000281	Role of phospholipids in phagocytosis
5.48E-05	0.000368	Dissolution of Fibrin Clot
0.000107	0.000688	Binding and Uptake of Ligands by Scavenger Receptors
0.00017	0.001044	Regulation of actin dynamics for phagocytic cup formation
0.000197	0.001157	Arginine and proline metabolism - Homo sapiens (human)
0.000206	0.001164	Alternative complement activation
0.000288	0.001559	Glutathione metabolism - Homo sapiens (human)
0.000325	0.001659	intrinsic prothrombin activation pathway
0.000329	0.001659	Fcgamma receptor (FCGR) dependent phagocytosis
0.000512	0.002401	Metal sequestration by antimicrobial proteins
0.000528	0.002401	Regulation of Complement cascade
0.000528	0.002401	Corticosteroids and cardioprotection
0.000714	0.003091	Activation of C3 and C5
0.000724	0.003091	Pentose phosphate pathway - Homo sapiens (human)
0.000798	0.003308	Beta-Alanine metabolism - Homo sapiens (human)
0.001142	0.0046	Detoxification of Reactive Oxygen Species
0.001215	0.004628	Erythrocytes take up oxygen and release carbon dioxide
0.001215	0.004628	Pentose phosphate pathway (hexose monophosphate shunt)
0.001495	0.005468	Metabolism of carbohydrates
0.001512	0.005468	Hyaluronan uptake and degradation
0.001687	0.005948	Tryptophan metabolism - Homo sapiens (human)
0.002201	0.007218	Ethanol oxidation
0.002201	0.007218	Hyaluronan metabolism
0.002201	0.007218	G-protein signaling through tubby proteins
0.002591	0.007943	Activation of pkc through g-protein coupled receptors
0.002591	0.007943	Erythrocytes take up carbon dioxide and release oxygen
0.002591	0.007943	O2/CO2 exchange in erythrocytes
0.002689	0.008066	Ion channels and their functional role in vascular endothelium
0.003941	0.011577	Regulation of TLR by endogenous ligand
0.004091	0.011771	Lipid digestion, mobilization, and transport
0.004205	0.011859	Staphylococcus aureus infection - Homo sapiens (human)
0.00445	0.012302	Glycogen breakdown (glycogenolysis)
0.004987	0.013521	Metabolism of Angiotensinogen to Angiotensins
0.006145	0.016046	HDL-mediated lipid transport
0.006145	0.016046	Hormone-sensitive lipase (HSL)-mediated triacylglycerol hydrolysis
0.007299	0.018668	Glycolysis / Gluconeogenesis - Homo sapiens (human)
0.007414	0.018668	Cystic fibrosis transmembrane conductance regulator (cftr) and beta 2 adrenergic receptor (b2ar) pathway
0.00809	0.020011	Renin-angiotensin system - Homo sapiens (human)
0.008898	0.021632	PPAR signaling pathway - Homo sapiens (human)
0.009423	0.02252	Cell surface interactions at the vascular wall
0.010329	0.024272	Biological oxidations

0.011053	0.025549	Ascorbate and aldarate metabolism - Homo sapiens (human)
0.012688	0.028855	Peroxisomal lipid metabolism
0.014422	0.031772	Activation of camp-dependent protein kinase pka
0.015325	0.033243	Role of -arrestins in the activation and targeting of map kinases
0.017201	0.036749	African trypanosomiasis - Homo sapiens (human)
0.019171	0.039752	Roles of arrestin dependent recruitment of src kinases in gpcr signaling
0.019171	0.039752	Starch and sucrose metabolism - Homo sapiens (human)
0.02019	0.041257	Steroid hormones
0.022293	0.044273	Pyruvate metabolism - Homo sapiens (human)
0.022293	0.044273	Glutathione conjugation
0.025611	0.050154	Chrebp regulation by carbohydrates and camp
0.026196	0.050483	Phase 1 - Functionalization of compounds
0.027088	0.050483	Peptide ligand-binding receptors
0.027202	0.050483	Metabolism of lipids and lipoproteins
0.027927	0.050483	Signaling by Retinoic Acid
0.027927	0.050483	Fatty acid degradation - Homo sapiens (human)
0.027927	0.050483	Histidine, lysine, phenylalanine, tyrosine, proline and tryptophan catabolism
0.029115	0.051966	Activation of csk by camp-dependent protein kinase inhibits signaling through the t cell receptor
0.0328	0.0564	Valine, leucine and isoleucine degradation - Homo sapiens (human)
0.0328	0.0564	Peptide hormone metabolism
0.0328	0.0564	Amino sugar and nucleotide sugar metabolism - Homo sapiens (human)
0.03798	0.06452	Metabolism of fat-soluble vitamins
0.042056	0.070594	Legionellosis - Homo sapiens (human)
0.047732	0.078259	Glycerolipid metabolism - Homo sapiens (human)
0.047732	0.078259	Lysine degradation - Homo sapiens (human)

Diseased (CAVD) Ventricularis

p-value	q-value	Pathway
7.89E-15	2.04E-12	Smooth Muscle Contraction
5.69E-12	7.37E-10	Erk and pi-3 kinase are necessary for collagen binding in corneal epithelia
2.09E-11	1.80E-09	Focal adhesion - Homo sapiens (human)
3.77E-11	2.44E-09	Cell-extracellular matrix interactions
4.38E-10	2.27E-08	Integrin signaling pathway
5.60E-10	2.42E-08	Regulation of actin cytoskeleton - Homo sapiens (human)
7.68E-10	2.84E-08	RHO GTPases activate PAKs
7.67E-09	2.48E-07	Semaphorin interactions
6.48E-08	1.87E-06	Laminin interactions
7.68E-08	1.99E-06	Cell junction organization
1.73E-07	4.08E-06	Muscle contraction
2.15E-07	4.36E-06	Cell-Cell communication
2.19E-07	4.36E-06	Arrhythmogenic right ventricular cardiomyopathy (ARVC) - Homo sapiens (human)

2.82E-07	5.22E-06	RHO GTPases Activate ROCKs
3.83E-07	5.91E-06	Rho cell motility signaling pathway
3.88E-07	5.91E-06	Ucalpain and friends in cell spread
3.88E-07	5.91E-06	Apoptotic execution phase
5.23E-07	7.52E-06	Citric acid cycle (TCA cycle)
6.65E-07	9.06E-06	Hypertrophic cardiomyopathy (HCM) - Homo sapiens (human)
1.14E-06	1.48E-05	Dilated cardiomyopathy - Homo sapiens (human)
2.63E-06	3.16E-05	Platelet degranulation
2.68E-06	3.16E-05	Localization of the PINCH-ILK-PARVIN complex to focal adhesions
3.43E-06	3.62E-05	Sema4D in semaphorin signaling
3.56E-06	3.62E-05	Response to elevated platelet cytosolic Ca2+
3.91E-06	3.62E-05	Activation of DNA fragmentation factor
3.91E-06	3.62E-05	Apoptosis induced DNA fragmentation
3.91E-06	3.62E-05	Initiation of Nuclear Envelope Reformation
3.91E-06	3.62E-05	Nuclear Envelope Reassembly
5.26E-06	4.70E-05	Axon guidance
5.45E-06	4.70E-05	mRNA Splicing - Major Pathway
7.93E-06	6.62E-05	mRNA Splicing
1.22E-05	9.37E-05	Apoptosis
1.26E-05	9.37E-05	RHO GTPase Effectors
1.27E-05	9.37E-05	Formation of Senescence-Associated Heterochromatin Foci (SAHF)
1.27E-05	9.37E-05	RHO GTPases activate CIT
1.46E-05	0.000105	Programmed Cell Death
2.48E-05	0.000174	Signaling by Rho GTPases
5.10E-05	0.000347	Non-integrin membrane-ECM interactions
5.39E-05	0.000358	Sema4D induced cell migration and growth-cone collapse
6.43E-05	0.000416	EPH-Ephrin signaling
6.84E-05	0.000428	Processing of Capped Intron-Containing Pre-mRNA
6.94E-05	0.000428	Pyruvate metabolism and Citric Acid (TCA) cycle
7.66E-05	0.000461	agrin in postsynaptic differentiation
0.000101	0.000595	DNA Damage/Telomere Stress Induced Senescence
0.000111	0.00064	Salmonella infection - Homo sapiens (human)
0.000119	0.00067	SRP-dependent cotranslational protein targeting to membrane
0.000133	0.000735	Citrate cycle (TCA cycle) - Homo sapiens (human)
0.000152	0.000821	mcalpain and friends in cell motility
0.00016	0.000844	Translation
0.000184	0.000951	Spliceosome - Homo sapiens (human)
0.000193	0.000978	RHO GTPases activate PKNs
0.00021	0.001048	Tight junction - Homo sapiens (human)
0.000216	0.001054	Amoebiasis - Homo sapiens (human)
0.00022	0.001054	EPHA-mediated growth cone collapse
0.000232	0.00109	Breakdown of the nuclear lamina
0.000275	0.001273	Extracellular matrix organization

0.000368	0.00167	Eukaryotic Translation Elongation
0.000433	0.001935	Adherens junction - Homo sapiens (human)
0.00046	0.002021	Antisense pathway
0.000627	0.002706	Bacterial invasion of epithelial cells - Homo sapiens (human)
0.000689	0.002927	MET activates PTK2 signaling
0.000788	0.003292	ECM-receptor interaction - Homo sapiens (human)
0.000837	0.003441	Developmental Biology
0.000906	0.003667	Platelet activation, signaling and aggregation
0.00105	0.004139	Caspase cascade in apoptosis
0.001055	0.004139	Nuclear Envelope Breakdown
0.001499	0.005777	ECM proteoglycans
0.001584	0.005777	AUF1 (hnRNP D0) binds and destabilizes mRNA
0.001584	0.005777	TFAP2A acts as a transcriptional repressor during retinoic acid induced cell differentiation
0.001584	0.005777	2-LTR circle formation
0.001584	0.005777	Clearance of Nuclear Envelope Membranes from Chromatin
0.001882	0.006769	Glyoxylate and dicarboxylate metabolism - Homo sapiens (human)
0.002085	0.00725	MET promotes cell motility
0.002092	0.00725	Peptide chain elongation
0.002099	0.00725	Regulation of cytoskeletal remodeling and cell spreading by IPP complex components
0.002278	0.00767	Selenocysteine synthesis
0.00228	0.00767	Proteoglycans in cancer - Homo sapiens (human)
0.002375	0.007886	Eukaryotic Translation Termination
0.002599	0.008522	Shigellosis - Homo sapiens (human)
0.002684	0.008585	CHL1 interactions
0.002685	0.008585	Nonsense Mediated Decay (NMD) independent of the Exon Junction Complex (EJC)
0.003335	0.010534	Integration of provirus
0.003521	0.010987	Formation of a pool of free 40S subunits
0.003594	0.011082	Striated Muscle Contraction
0.003654	0.011134	Leukocyte transendothelial migration - Homo sapiens (human)
0.003896	0.011733	Rac1 cell motility signaling pathway
0.003984	0.011794	The citric acid (TCA) cycle and respiratory electron transport
0.004053	0.011794	apoptotic dna-fragmentation and tissue homeostasis
0.004053	0.011794	Depolymerisation of the Nuclear Lamina
0.004374	0.012315	Vascular smooth muscle contraction - Homo sapiens (human)
0.004374	0.012315	Nonsense Mediated Decay (NMD) enhanced by the Exon Junction Complex (EJC)
0.004374	0.012315	Nonsense-Mediated Decay (NMD)
0.00453	0.012615	Platelet activation - Homo sapiens (human)
0.004649	0.012808	Gene Expression
0.004716	0.012857	Axon guidance - Homo sapiens (human)
0.004892	0.013198	Apoptotic cleavage of cellular proteins
0.005366	0.014039	GTP hydrolysis and joining of the 60S ribosomal subunit
0.005366	0.014039	L13a-mediated translational silencing of Ceruloplasmin expression

0.005366	0.014039	3, -UTR-mediated translational regulation
0.005682	0.01457	B cell survival pathway
0.005682	0.01457	Platelet Adhesion to exposed collagen
0.00611	0.015514	Selenoamino acid metabolism
0.006923	0.017241	Cap-dependent Translation Initiation
0.006923	0.017241	Eukaryotic Translation Initiation
0.007561	0.018301	Pten dependent cell cycle arrest and apoptosis
0.007561	0.018301	SEMA3A-Plexin repulsion signaling by inhibiting Integrin adhesion
0.007561	0.018301	Early Phase of HIV Life Cycle
0.008056	0.01932	Hemostasis
0.009681	0.023003	Tnfr1 signaling pathway
0.010828	0.025266	Deregulated CDK5 triggers multiple neurodegenerative pathways in Alzheimers disease models
0.010828	0.025266	Neurodegenerative Diseases
0.011469	0.026431	Hiv-1 nef: negative effector of fas and tnf
0.011532	0.026431	Ribosome - Homo sapiens (human)
0.012033	0.027338	Other semaphorin interactions
0.012682	0.028561	Pathogenic Escherichia coli infection - Homo sapiens (human)
0.013148	0.029357	L1CAM interactions
0.014608	0.03185	Syndecan interactions
0.014608	0.03185	Prion pathway
0.014634	0.03185	Viral myocarditis - Homo sapiens (human)
0.01532	0.033066	Formation of the ternary complex, and subsequently, the 43S complex
0.016747	0.035847	Signaling by BRAF and RAF fusions
0.017399	0.036636	Nephrin interactions
0.017399	0.036636	Protein export - Homo sapiens (human)
0.018246	0.038111	Signaling by MET
0.019023	0.039415	Oncogenic MAPK signaling
0.021461	0.043767	Integrin cell surface interactions
0.021461	0.043767	Ribosomal scanning and start codon recognition
0.02231	0.045143	Translation initiation complex formation
0.023177	0.046535	Activation of the mRNA upon binding of the cap-binding complex and eIFs, and subsequent binding to 43S
0.023592	0.047002	Basigin interactions
0.026979	0.05334	The information processing pathway at the ifn beta enhancer
0.028741	0.056394	Molecules associated with elastic fibres
0.029756	0.057946	Pertussis - Homo sapiens (human)
0.031804	0.061472	Mitotic Anaphase
0.0324	0.061539	Propanoate metabolism - Homo sapiens (human)
0.0324	0.061539	Signaling by Robo receptor
0.032551	0.061539	Mitotic Metaphase and Anaphase
0.034295	0.064365	Base excision repair - Homo sapiens (human)
0.037252	0.069413	Mitotic Prophase

0.03821	0.070186	Elastic fibre formation
0.03821	0.070186	Signaling by high-kinase activity BRAF mutants
0.040026	0.073006	Rap1 signaling pathway - Homo sapiens (human)
0.04068	0.07368	Small cell lung cancer - Homo sapiens (human)
0.042286	0.076056	Signaling by RAS mutants
0.046518	0.081406	Pyruvate metabolism - Homo sapiens (human)
0.046518	0.081406	Signaling by moderate kinase activity BRAF mutants
0.046518	0.081406	Paradoxical activation of RAF signaling by kinase inactive BRAF
0.046518	0.081406	MAP2K and MAPK activation
0.048689	0.084634	Regulation of mRNA stability by proteins that bind AU-rich elements

Antibody	Supplier	Concentration
Vimentin (mouse)	Abcam, UK	1:200
Vimentin (rabbit)	Abcam, UK	1:200
AHSG (goat)	R&D Systems, USA	1:100
ALPL (rabbit)	Abcam, UK	1:50
APOB (goat)	Abcam, UK	1:400
AZGP1 (rabbit)	Abcam, UK	1:100
BGN (goat)	R&D Systems, USA	1:100
CATB (rabbit)	Cell Signaling Technologies, USA	1:100
CD14 (rabbit)	Abcam, UK	1:100
CD9 (mouse)	Biolegend, USA	1:100
CNN1 (rabbit)	Abcam, UK	1:100
COL1A1 (mouse)	Abcam, UK	1:500
CRTAC1(mouse)	R&D Systems, USA	1:100
CSRP1 (rabbit)	Abcam, UK	1:100
DCN (goat)	R&D Systems, USA	1:100
ELN (mouse)	Novus Biologicals, USA	1:100
Emilin1 (rabbit)	Novus Biologicals, USA	1:100
FLNA (rabbit)	Abcam, UK	1:100
FN1 (rabbit)	Abcam, UK	1:400
GFAP (mouse)	EMD Millipore, USA	1:100
HP (mouse)	Abcam, UK	1:100
IGF1 (goat)	R&D Systems, USA	1:100
LPA (goat)	Abcam, UK	1:100
LRP1 (mouse)	Invitrogen, USA	1:100
MGP (rabbit)	Abcam, UK	1:50
OGN (goat)	R&D Systems, USA	1:100
PCOLCE2 (rabbit)	Thermo Fisher Scientific, USA	1:100
PRDX2 (goat)	R&D Systems, USA	1:100
PRELP (mouse)	R&D Systems, USA	1:100
S100A9 (rabbit)	Abcam, UK	1:100
SOD3 (goat)	R&D Systems, USA	1:100
SPARC (goat)	R&D Systems, USA	1:100
SULF1 (rabbit)	Thermo Fisher Scientific, USA	1:50
TAGLN2 (rabbit)	Novus Biologicals, USA	1:100
TNFRSF11B (goat)	R&D Systems, USA	1:100

Supplemental Table 5: Primary antibodies

Alzheimer disease	Obesity
Atherosclerosis	Osteoporosis
Atrial fibrillation	Pancreatic cancer
Bladder cancer	Parkinson's disease
Bronchiolitis obliterans	Peripheral arterial disease

Calcification diseases (includes vascular calcification, basal ganglia calcification, calcification of the joints and arteries, arterial calcification of infancy, and aortic valve calcification (provides LPA))	Prostate cancer
Colon cancer	Pseudoxanthoma elasticum
Crohn disease	Pulmonary embolism
Dermatomyositis	Pulmonary fibrosis
Esophageal cancer	Pulmonary hypertension
Gastric cancer	Rheumatoid arthritis
Hypercholesterolemia	Scleroderma
Intracerebral hemorrhage	Sjogren's syndrome
Liver cancer	Systemic lupus erythematosus
Lung cancer	Takayasu disease
Mixed connective tissue disease	Type I diabetes
Multiple sclerosis	Type II diabetes
Myocardial infarction	Ulcerative colitis
Non-alcoholic fatty liver disease	Vasculitis syndrome
Supplemental Table 6: OMIM and MalaCards database diseases	

Supplemental Fig. 1

CAVD Disease Stages Transcriptomics

Non-disease stage

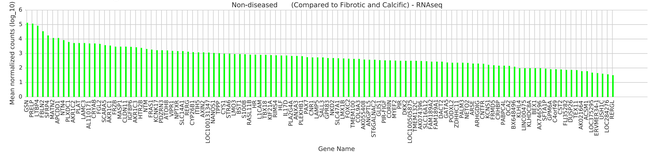

Fibrotic stage

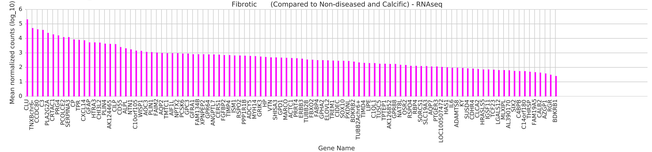

Calcific stage

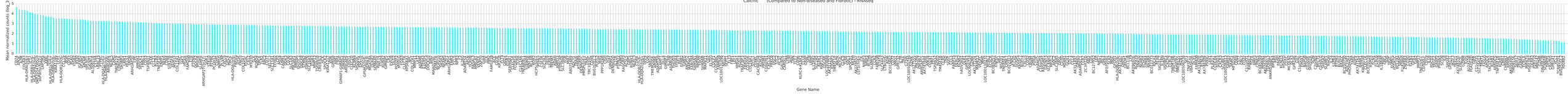

Supplemental Figure 1: CAVD Disease-associated Stages Transcriptomics (CAVD Disease Stages)

Disease “stage-specific” RNA ranked according to the logarithm of their normalized mean DESeq2 counts for the three stages from transcriptomics data (n=3 AV donors per group).

Supplemental Fig. 2

CAVD Disease Stages Proteomics

Non-disease stage

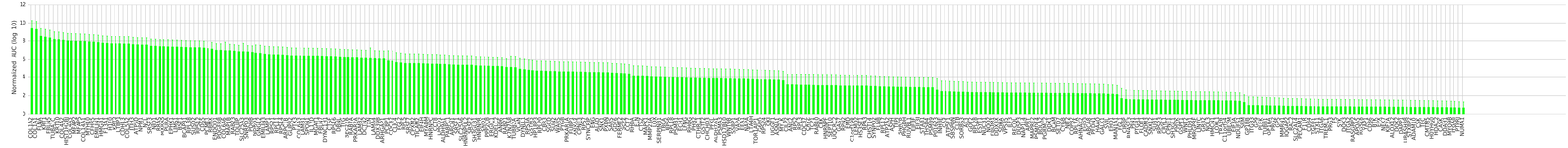

Fibrotic stage

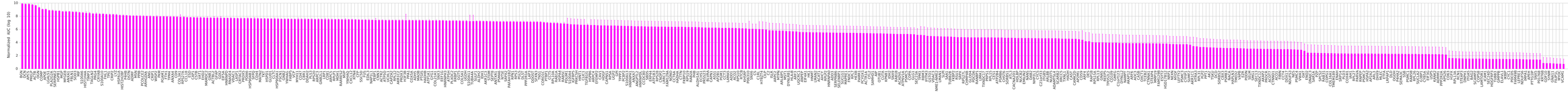

Calcific stage

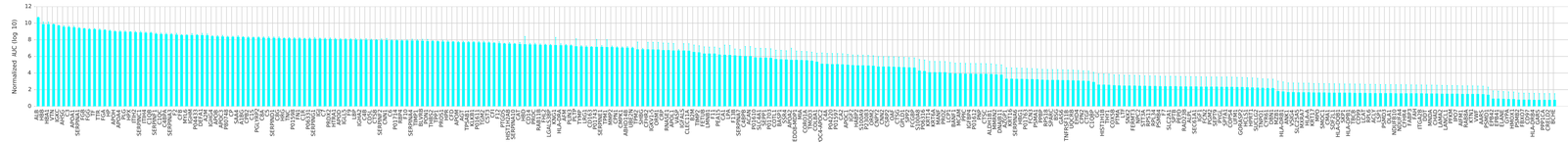

Calcific stage (serum proteins excluded)

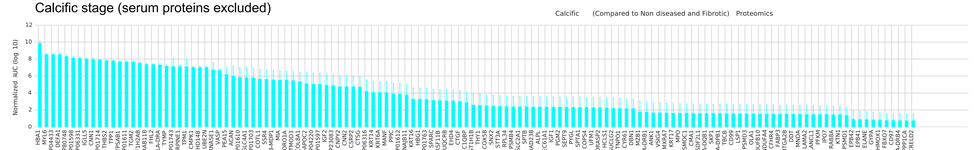

Supplemental Figure 2: CAVD Disease-associated Stages Proteomics (CAVD Disease Stages)

Disease “stage-specific” proteins ranked according to the logarithm of their normalized mean AUCs for the three stages from the proteomics data (n=9 AV donors per group). Lower panel: Calcific stage proteome with plasma proteins excluded.

Supplemental Fig. 3

a

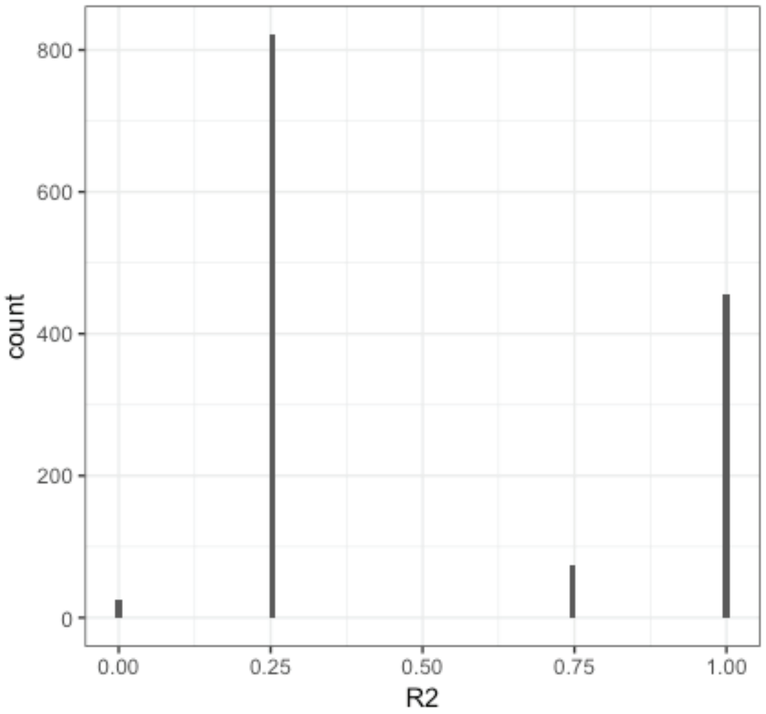

b

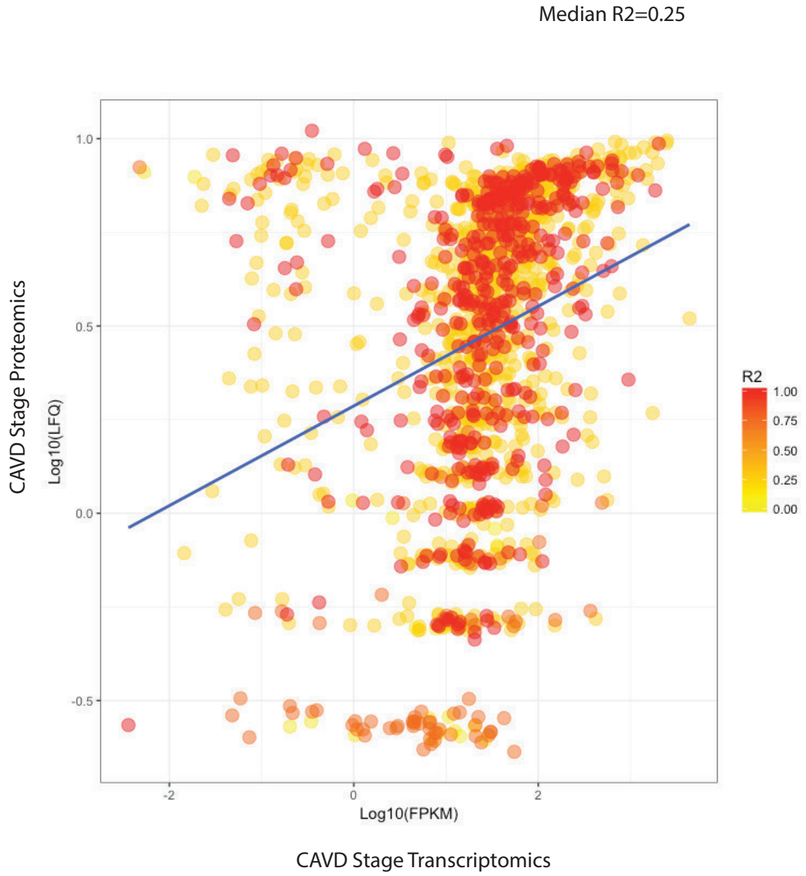

c

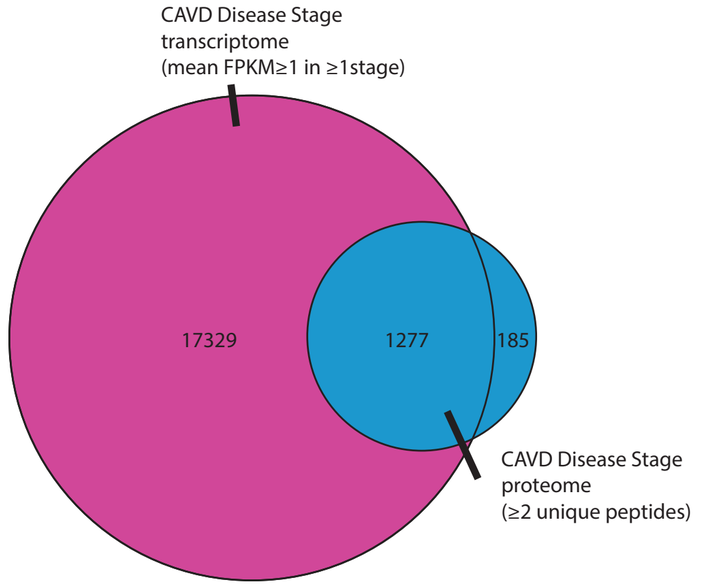

Supplemental Figure 3: Correlation Analyses CAVD Stage Transcriptomics and CAVD Stage Proteomics

a./b. FPKM of transcriptomics and median-normalized AUC of label free proteomics (LFQ) were compared using squared absolute values of Spearman correlation coefficient. The LFQ and transcriptomics samples were not from the same donor, and the FPKM and the normalized AUC in the three stages were averaged (non-diseased, fibrotic and calcific stages). We used an in-house R script using ggplot2 to draw a histogram and a density scatter plot.

c. Venn diagram of the overlap between CAVD disease stage transcriptomics (FPKM ≥1 in at least one stage), CAVD disease stage proteomics (≥2 unique peptides)

Supplemental Fig. 4

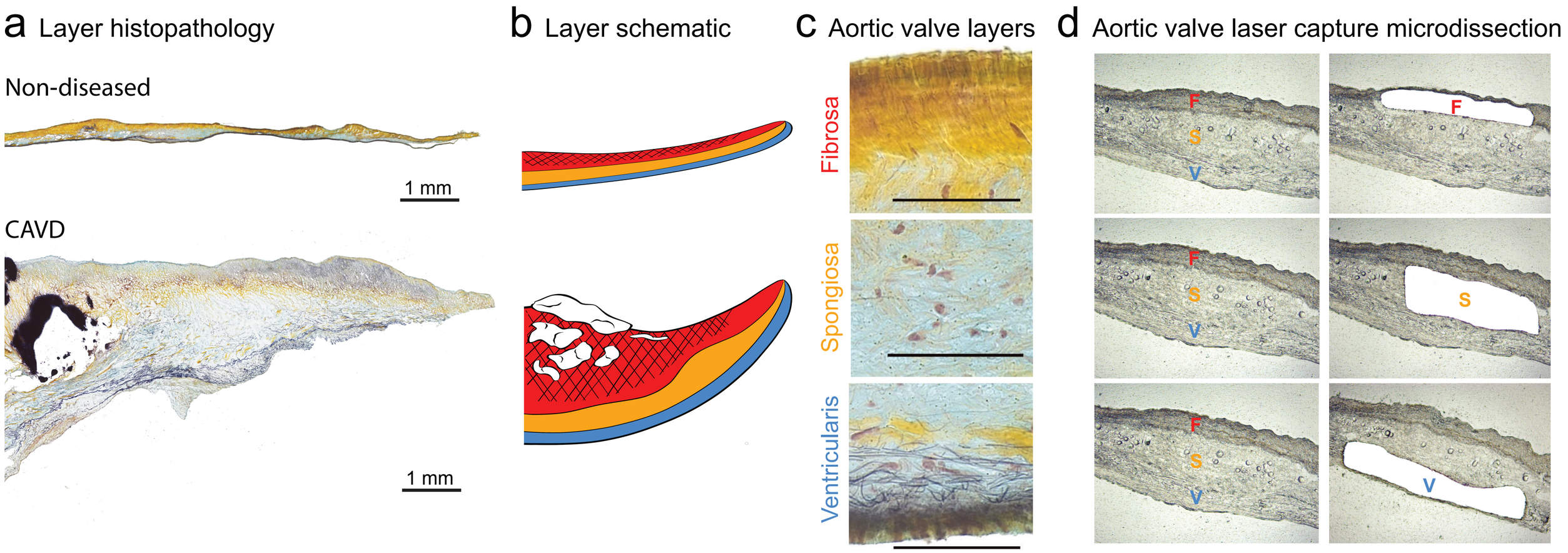

Supplemental Figure 4: CAVD Layers Overview and Methodology

a. Layer histopathology of non-diseased and CAVD human AV samples (Movat pentachrome staining).

b. Schematic of the AV layer anatomy in non-diseased and CAVD (red – fibrosa, yellow – spongiosa, blue – ventricularis).

c. Movat pentachrome staining (collagen - yellow, proteoglycans/glycosaminoglycans - blue, elastin - black) of non-diseased human AV samples. Scale bar = 100μm.

d. Layer-specific laser capture microdissection of the fibrosa, spongiosa and ventricularis.

Supplemental Fig. 5

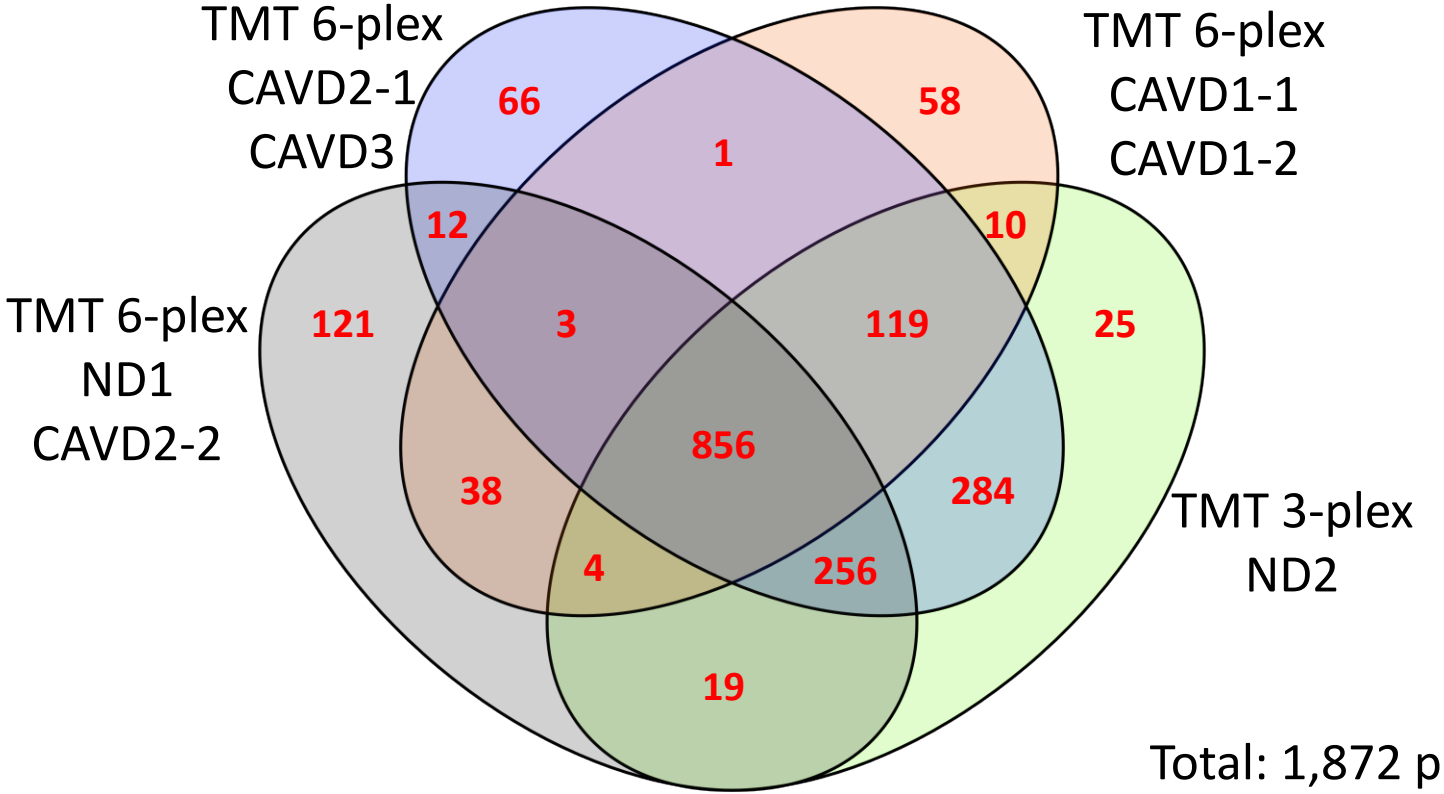

Total: 1,872 proteins
(# of unique peptide >= 2)

Supplemental Figure 5: Venn diagram of the proteins retrieved from the individual TMT experiments of the leaflet layer proteomics

ND1/2: control samples from autopsy, CAVD 1-3: CAVD samples, CAVD1 and 2 were analyzed in duplicates

Supplemental Fig. 6

Combined Leaflet Layer Proteomics

Fibrosa layer

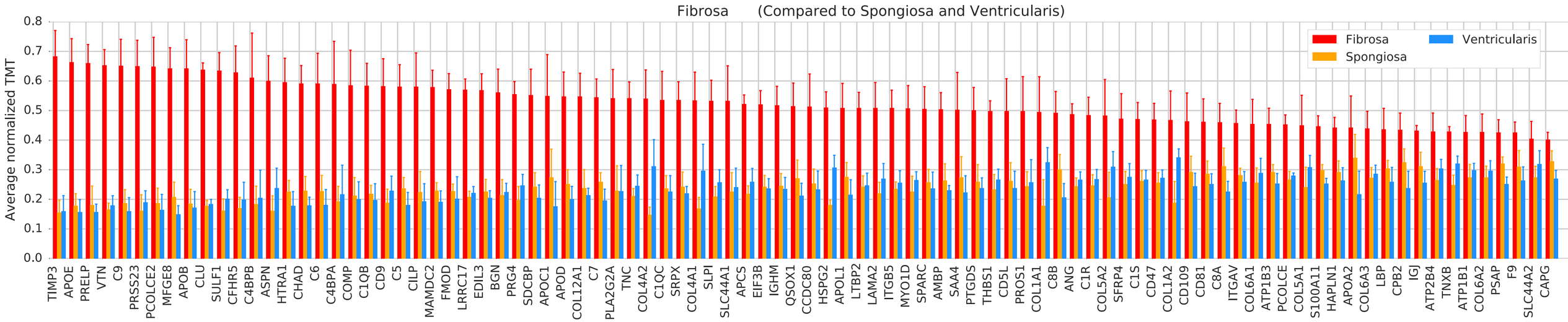

Spongiosa layer

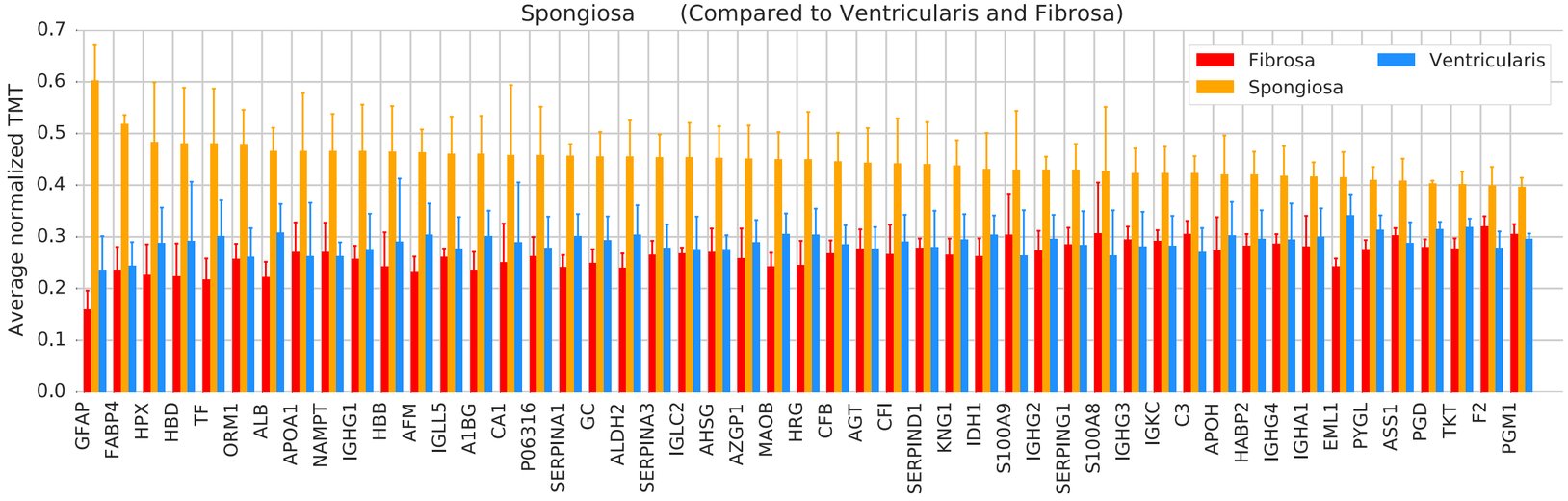

Ventricularis layer

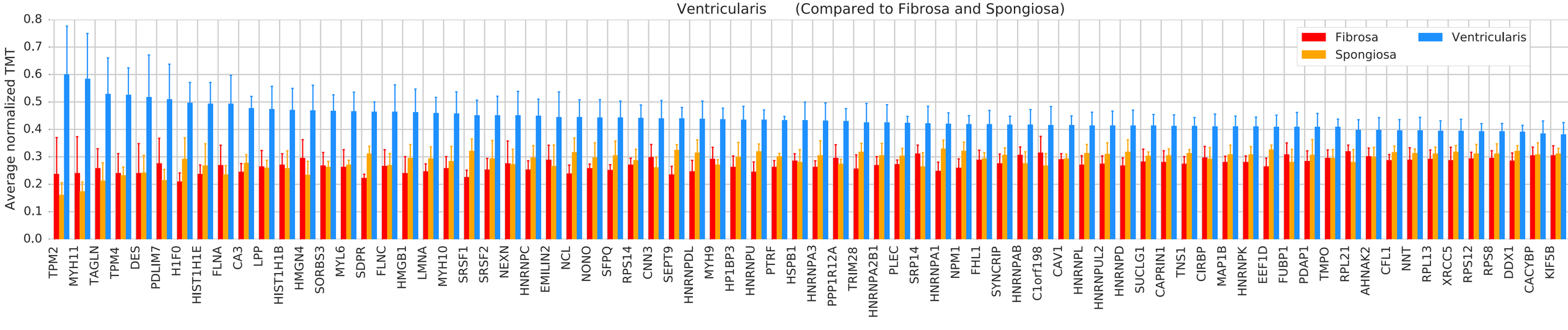

Supplemental Figure 6: Leaflet Layer ‘All’ Donors Proteomics (CAVD Layers)

CAVD AV “Layer-specific” proteins ranked according to their average normalized TMT in all three layers as a consistent signal regardless of the disease state (n=5). Error bars indicate standard deviation (SD).

Supplemental Fig. 7

Non-diseased Leaflet Layer Proteomics

Fibrosa layer

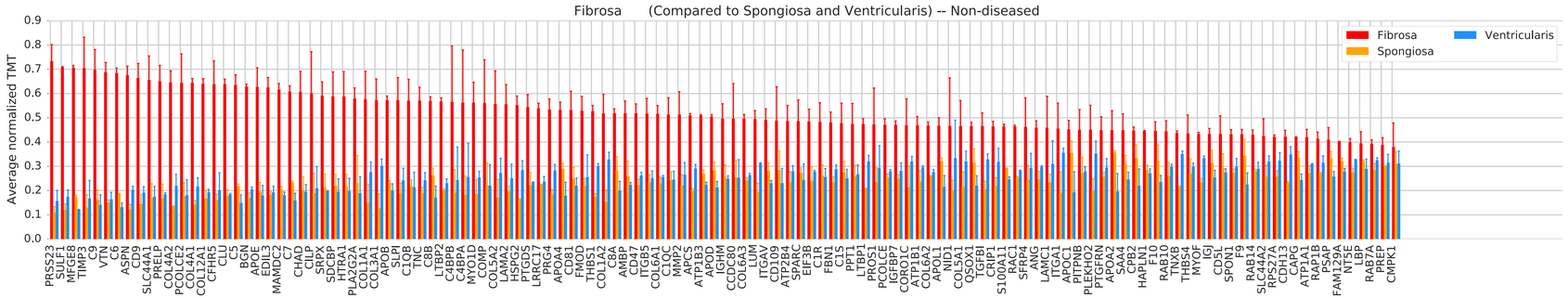

Spongiosa layer

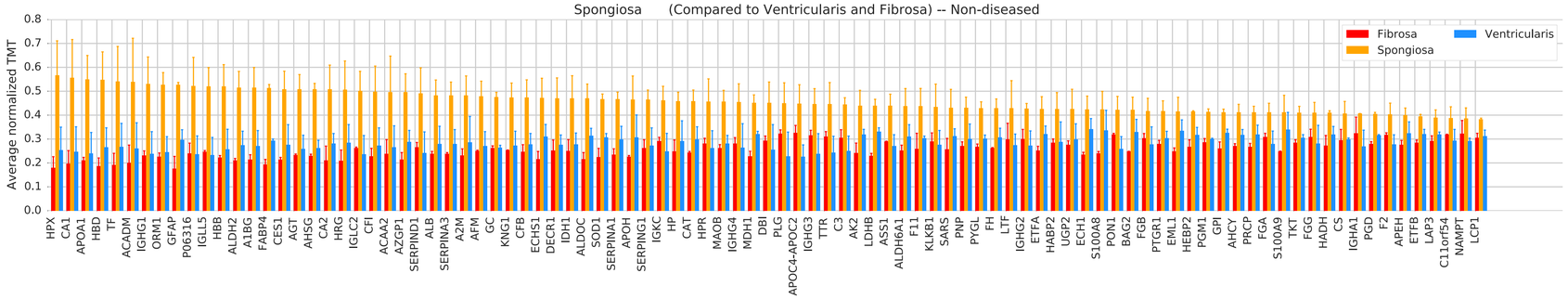

Ventricularis layer

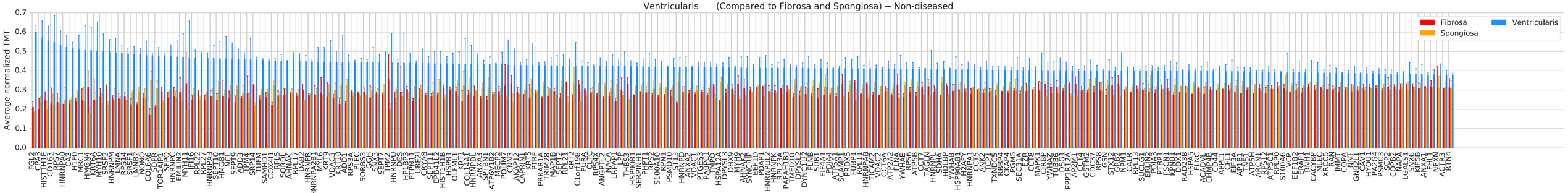

Supplemental Figure 7: Leaflet Microlayer Non-diseased Donors Proteomics (CAVD Layers)

Non-disease AV “layer-specific” proteins ranked according to their average normalized TMT in all three layers for non-diseased tissues (n=2).

Supplemental Fig. 8

CAVD Leaflet Layer Proteomics

Fibrosa layer

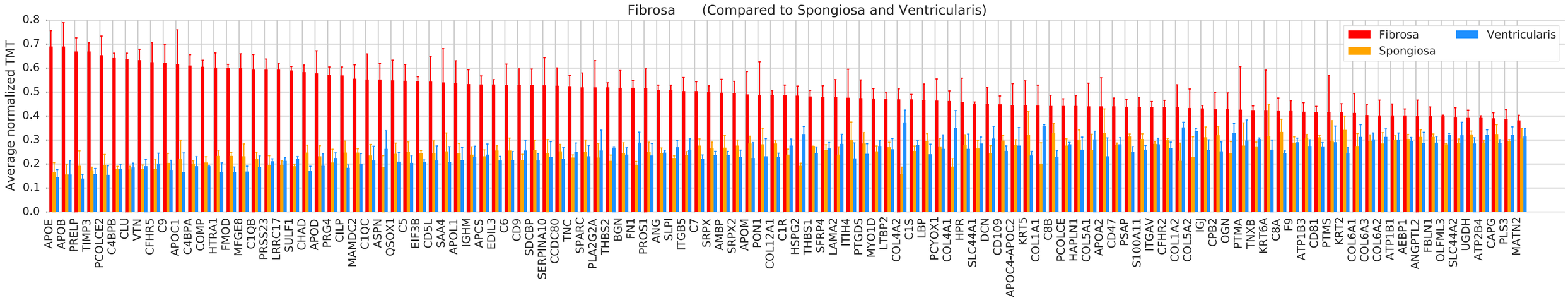

Spongiosa layer

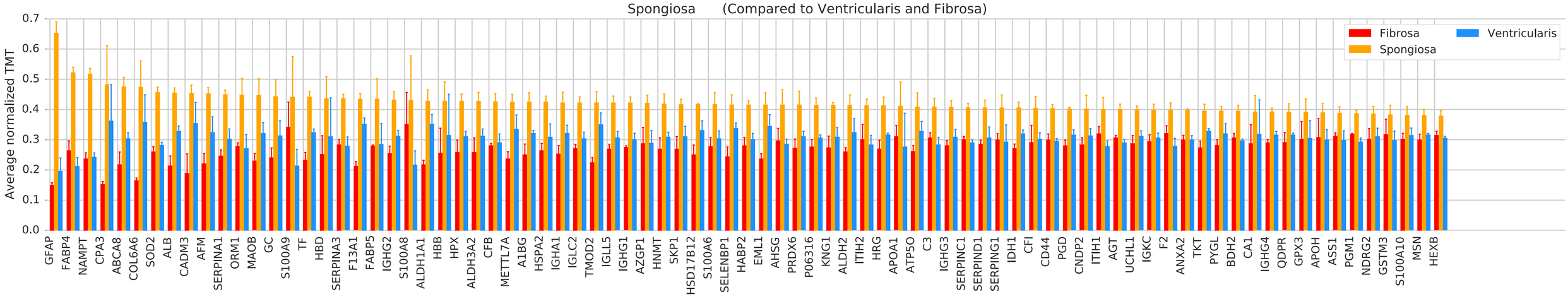

Ventricularis layer

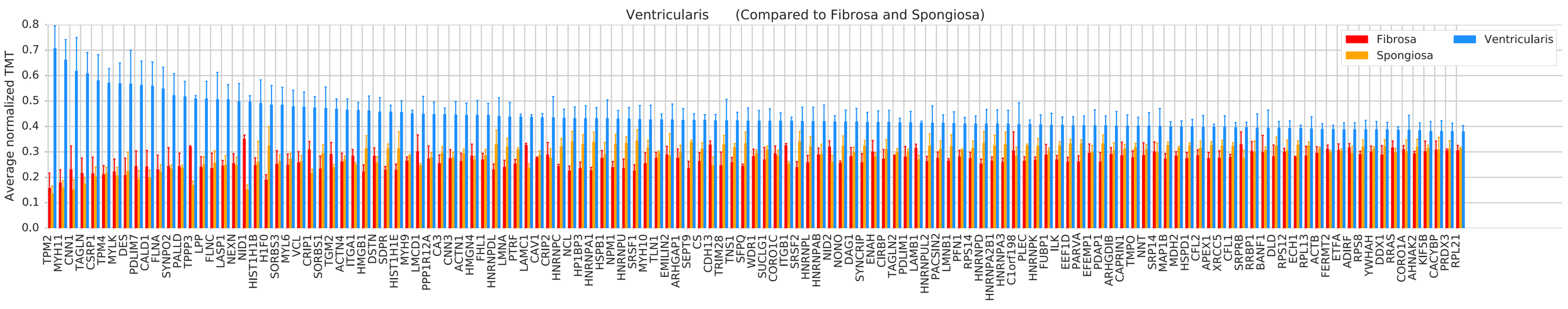

Supplemental Figure 8: Leaflet Microlayer CAVD Donors Proteomics

AV “layer-specific” proteins ranked according to their average normalized TMT in all three layers for CAVD tissues (n=3).

Supplemental Fig. 9

LDL-mediated lipid transport
Proteasome - Homo sapiens (human)
MHC class II antigen presentation
Lipoprotein metabolism
Dissolution of Fibrin Clot
Lipid digestion, mobilization, and transport
PPAR signaling pathway - Homo sapiens (human)
SHC-related events triggered by IGF1R
Vitamin digestion and absorption - Homo sapiens (human)
IGF1R signaling cascade
IRS-related events triggered by IGF1R
Signaling by Type 1 Insulin-like Growth Factor 1 Receptor (IGF1R)
activation of csk by camp-dependent protein kinase inhibits signaling through the t cell receptor
Inflammatory bowel disease (IBD) - Homo sapiens (human)
Heme degradation
Renin-angiotensin system - Homo sapiens (human)
African trypanosomiasis - Homo sapiens (human)
Autoimmune thyroid disease - Homo sapiens (human)
Asthma - Homo sapiens (human)
Toll-Like Receptors Cascades
Classical antibody-mediated complement activation
Downstream TCR signaling
TCR signaling
Transfer of LPS from LBP carrier to CD14
inhibition of matrix metalloproteinases
Cell surface interactions at the vascular wall
Metabolism of Angiotensinogen to Angiotensins
Activation of C3 and C5
lectin induced complement pathway
extrinsic prothrombin activation pathway
Common Pathway of Fibrin Clot Formation
Gamma-carboxylation, transport, and amino-terminal cleavage of proteins
Scavenging of heme from plasma
classical complement pathway
intrinsic prothrombin activation pathway
Complement and coagulation cascades - Homo sapiens (human)
Complement cascade
Regulation of Complement cascade
Staphylococcus aureus infection - Homo sapiens (human)
Systemic lupus erythematosus - Homo sapiens (human)
Gamma-carboxylation of protein precursors
Removal of aminoterminal propeptides from gamma-carboxylated proteins
Regulation of TLR by endogenous ligand
alternative complement pathway
Activation of Matrix Metalloproteinases
Initial triggering of complement
Regulation of Insulin-like Growth Factor (IGF) transport and uptake by Insulin-like Growth Factor Binding Proteins (IGFBPs)
fibrinolysis pathway
Degradation of the extracellular matrix
Pertussis - Homo sapiens (human)
GRB2:SOS provides linkage to MAPK signaling for Integrins
p130Cas linkage to MAPK signaling for Integrins
Erythrocytes take up oxygen and release carbon dioxide
Terminal pathway of complement
Gamma carboxylation, hypusine formation and arylsulfatase activation
Metabolism of fat-soluble vitamins
HDL-mediated lipid transport
Retinoid metabolism and transport
Prion diseases - Homo sapiens (human)
Erythrocytes take up carbon dioxide and release oxygen
O2/CO2 exchange in erythrocytes
Alternative complement activation
Creation of C4 and C2 activators
MAPK6 and MAPK4 activation
Paradoxical activation of RAF signaling by kinase inactive BRAF
Signaling by moderate kinase activity BRAF mutants
Generation of second messenger molecules
Translocation of ZAP-70 to Immunological synapse
Signaling by high-kinase activity BRAF mutants
antigen processing and presentation
Chylomicron-mediated lipid transport
Allograft rejection - Homo sapiens (human)
Extrinsic Pathway of Fibrin Clot Formation
Signaling by RAS mutants
PD-1 signaling
Type I diabetes mellitus - Homo sapiens (human)
Phosphorylation of CD3 and TCR zeta chains
Metal sequestration by antimicrobial proteins
platelet amyloid precursor protein pathway
Graft-versus-host disease - Homo sapiens (human)
Antigen processing and presentation - Homo sapiens (human)
Viral myocarditis - Homo sapiens (human)
Oncogenic MAPK signaling
Visual phototransduction
Herpes simplex infection - Homo sapiens (human)
Metabolism of vitamins and cofactors
Signaling by BRAF and RAF fusions
Lectin pathway of complement activation
Antimicrobial peptides
Ficolins bind to repetitive carbohydrate structures on the target cell surface
Scavenging by Class B Receptors
VLDL biosynthesis
Intestinal immune network for IgA production - Homo sapiens (human)
Scavenging by Class H Receptors
Leishmaniasis - Homo sapiens (human)
Tuberculosis - Homo sapiens (human)
Glutathione metabolism - Homo sapiens (human)
Butanoate metabolism - Homo sapiens (human)
γ branching of actin filaments
Ub-specific processing proteases
Biological oxidations
Parkinson,s disease - Homo sapiens (human)
EPHB-mediated forward signaling
Attenuation phase
Post-translational protein modification
Pentose phosphate pathway - Homo sapiens (human)
Cooperation of PDCL (PHLP1) and TRiC/CCT in G-protein beta folding
Lysine degradation - Homo sapiens (human)
HSF1 activation
beta-Alanine metabolism - Homo sapiens (human)
Formation of annular gap junctions
Alzheimer,s disease - Homo sapiens (human)
Deubiquitination
Gap junction degradation
Glycogen synthesis
Nef Mediated CD4 Down-regulation
Beta oxidation of myristoyl-CoA to lauroyl-CoA
Formation of the active cofactor, UDP-glucuronate
Utilization of Ketone Bodies
EPH-Ephrin signaling
Gluconeogenesis
Glucose metabolism
Membrane Trafficking
Clathrin-mediated endocytosis
Citrate cycle (TCA cycle) - Homo sapiens (human)
Citric acid cycle (TCA cycle)
Protein processing in endoplasmic reticulum - Homo sapiens (human)
Beta oxidation of decanoyl-CoA to octanoyl-CoA-CoA
Beta oxidation of hexanoyl-CoA to butanoyl-CoA
Beta oxidation of lauroyl-CoA to decanoyl-CoA-CoA
Beta oxidation of octanoyl-CoA to hexanoyl-CoA
The citric acid (TCA) cycle and respiratory electron transport
Fatty acid elongation - Homo sapiens (human)
mitochondrial fatty acid beta-oxidation of saturated fatty acids
Metabolism of carbohydrates
Beta oxidation of palmitoyl-CoA to myristoyl-CoA
Glycolysis / Gluconeogenesis - Homo sapiens (human)
Fatty acid degradation - Homo sapiens (human)
Glycolysis
Legionellosis - Homo sapiens (human)
Pyruvate metabolism and Citric Acid (TCA) cycle
Amino sugar and nucleotide sugar metabolism - Homo sapiens (human)
UCH proteinases
Valine, leucine and isoleucine degradation - Homo sapiens (human)
corticosteroids and cardioprotection
Tryptophan metabolism - Homo sapiens (human)
Glyoxylate and dicarboxylate metabolism - Homo sapiens (human)
Recycling pathway of L1
Smooth Muscle Contraction
Retrograde neurotrophin signalling
Synthesis of bile acids and bile salts via 24-hydroxycholesterol
AUF1 (hnRNP D0) binds and destabilizes mRNA
Nef Mediated CD8 Down-regulation
Synthesis of bile acids and bile salts via 27-hydroxycholesterol
WNT5A-dependent internalization of FZD4
Shigellosis - Homo sapiens (human)
HSF1-dependent transactivation
Huntington,s disease - Homo sapiens (human)
Cardiac muscle contraction - Homo sapiens (human)
VLDL interactions
Mitochondrial Fatty Acid Beta-Oxidation
Advanced glycosylation endproduct receptor signaling
Cargo concentration in the ER
Endocrine and other factor-regulated calcium reabsorption - Homo sapiens (human)
COPII (Coat Protein 2) Mediated Vesicle Transport
Propanoate metabolism - Homo sapiens (human)
VLDLR internalisation and degradation
how does salmonella hijack a cell
Arginine and proline metabolism - Homo sapiens (human)
Cellular response to heat stress
N-glycan trimming in the ER and Calnexin/Calreticulin cycle
cystic fibrosis transmembrane conductance regulator (cftr) and beta 2 adrenergic receptor (b2ar) pathway
Detoxification of Reactive Oxygen Species
The role of GTSE1 in G2/M progression after G2 checkpoint
Starch and sucrose metabolism - Homo sapiens (human)
TP53 Regulates Metabolic Genes
Pyruvate metabolism - Homo sapiens (human)
Antigen Presentation: Folding, assembly and peptide loading of class I MHC
Cilium Assembly
Histidine metabolism - Homo sapiens (human)
Phase 1 - Functionalization of compounds
Synthesis of bile acids and bile salts via 7alpha-hydroxycholesterol
ahr signal transduction pathway
antisense pathway
Proximal tubule bicarbonate reclamation - Homo sapiens (human)
Respiratory electron transport, ATP synthesis by chemiosmotic coupling, and heat production by uncoupling proteins.
Ethanol oxidation
Gap junction trafficking
Lysine catabolism
eNOS activation
VEGFR2 mediated vascular permeability
Cargo recognition for clathrin-mediated endocytosis
Vasopressin-regulated water reabsorption - Homo sapiens (human)
Beta oxidation of butanoyl-CoA to acetyl-CoA
Leukocyte transendothelial migration - Homo sapiens (human)
Metabolism of lipids and lipoproteins
Epstein-Barr virus infection - Homo sapiens (human)
Gap junction trafficking and regulation
Golgi Cisternae Pericentriolar Stack Reorganization
Oxidative phosphorylation - Homo sapiens (human)
Regulation of mRNA stability by proteins that bind AU-rich elements
Non-integrin membrane-ECM interactions
Focal adhesion - Homo sapiens (human)
Platelet activation - Homo sapiens (human)
Intrinsic Pathway of Fibrin Clot Formation
Hematopoietic cell lineage - Homo sapiens (human)
Platelet Aggregation (Plug Formation)
Hemostasis
Platelet activation, signaling and aggregation
Formation of Fibrin Clot (Clotting Cascade)
Integrin alphaIIb beta3 signaling
ECM proteoglycans
ECM-receptor interaction - Homo sapiens (human)
Amoebiasis - Homo sapiens (human)
Metabolism
Vesicle-mediated transport
Phagosome - Homo sapiens (human)
proteasome complex
Binding and Uptake of Ligands by Scavenger Receptors
Platelet degranulation
Response to elevated platelet cytosolic Ca2+
Metabolism of proteins
Integrin cell surface interactions
Immune System
Extracellular matrix organization
Innate Immune System
Neutrophil degranulation
Pathways in cancer - Homo sapiens (human)
Spliceosome - Homo sapiens (human)
Salmonella infection - Homo sapiens (human)
Protein digestion and absorption - Homo sapiens (human)
Sema4D induced cell migration and growth-cone collapse
Assembly of collagen fibrils and other multimeric structures
Signaling by MET
Syndecan interactions
MET promotes cell motility
PI3K-Akt signaling pathway - Homo sapiens (human)
Regulation of actin cytoskeleton - Homo sapiens (human)
Sema4D in semaphorin signaling
GP1b-IX-V activation signalling
Molecules associated with elastic fibres
Laminin interactions
Platelet Adhesion to exposed collagen
Collagen chain trimerization
Elastic fibre formation
Arrhythmogenic right ventricular cardiomyopathy (ARVC) - Homo sapiens (human)
GPVI-mediated activation cascade
Cleavage of Growing Transcript in the Termination Region
Post-Elongation Processing of the Transcript
RNA Polymerase II Transcription Termination
mRNA Splicing
RHO GTPases activate KTN1
Post-chaperonin tubulin folding pathway
RHO GTPases activate PAKs
how progesterone initiates the oocyte maturation
MET activates PTK2 signaling
mRNA Splicing - Major Pathway
Cell junction organization
Cell-cell communication
Cell-extracellular matrix interactions
Influenza Virus Induced Apoptosis
Hypertrophic cardiomyopathy (HCM) - Homo sapiens (human)
mcalpain and friends in cell mobility
Ic epsilon receptor i signaling in mast cells
Processing of Capped Intron-Containing Pre-mRNA
Semaphorin interactions
stathmin and breast cancer resistance to antimicrotubule agents
Small cell lung cancer - Homo sapiens (human)
transcription factor creb and its extracellular signals
ERKS are inactivated
TGF-beta signaling pathway - Homo sapiens (human)
TGF-beta receptor signaling in EMT (epithelial to mesenchymal transition)
B cell receptor signaling pathway - Homo sapiens (human)
erk and pi-3 kinase are necessary for collagen binding in corneal epithelia
N-glycan trimming and elongation in the cis-Golgi
MAPK signaling pathway - Homo sapiens (human)
agrin in postsynaptic differentiation
mRNA Splicing - Minor Pathway
Protein repair
Regulation of signaling by CBL
Synthesis of Lipoxins (LX)
AGE-RAGE signaling pathway in diabetic complications - Homo sapiens (human)
role of mal in rho-mediated activation of srf
Bacterial invasion of epithelial cells - Homo sapiens (human)
role of pi3k subunit p85 in regulation of actin organization and cell migration
Chaperonin-mediated protein folding
COPI-mediated anterograde transport
Transport to the Golgi and subsequent modification
Collagen biosynthesis and modifying enzymes
Protein folding
Pathogenic Escherichia coli infection - Homo sapiens (human)
ER to Golgi Anterograde Transport
Prefoldin mediated transfer of substrate to CCT/TriC
Metabolism of amino acids and derivatives
Ribosome - Homo sapiens (human)
Selenoamino acid metabolism
Cap-dependent Translation Initiation
Eukaryotic Translation Initiation
Nonsense Mediated Decay (NMD) independent of the Exon Junction Complex (EJC)
Nonsense Mediated Decay (NMD) enhanced by the Exon Junction Complex (EJC)
Nonsense-Mediated Decay (NMD)
Peptide chain elongation
Selenocysteine synthesis
Formation of a pool of free 40S subunits
GTP hydrolysis and joining of the 60S ribosomal subunit
3, -UTR-mediated translational regulation
L13a-mediated translational silencing of Ceruloplasmin expression
SRP-dependent cotranslational protein targeting to membrane
Eukaryotic Translation Elongation
Eukaryotic Translation Termination
Translation
Formation of the ternary complex, and subsequently, the 43S complex
Ribosomal scanning and start codon recognition
Activation of the mRNA upon binding of the cap-binding complex and eIFs, and subsequent binding to 43S
Translation initiation complex formation
Cooperation of Prefoldin and TriC/CCT in actin and tubulin folding
Formation of tubulin folding intermediates by CCT/TriC
Asparagine N-linked glycosylation
Endocytosis - Homo sapiens (human)
Folding of actin by CCT/TriC
RHO GTPases Activate WASPs and WAVEs
RHO GTPase Effectors
Axon guidance
Golgi-to-ER retrograde transport
Dilated cardiomyopathy - Homo sapiens (human)
Collagen formation
Proteoglycans in cancer - Homo sapiens (human)

Normal
Fibrotic
Calcific

Supplemental Figure 9: CAVD Disease Stage Pathway Heatmap

Pathways that are significantly enriched ($q < 0.05$) in the non-diseased (ND, green), fibrotic (F, magenta), and calcific (C, cyan) stages, obtained from proteomics data (n=9 donors).

Supplemental Fig. 10

Calcific stage clusters highlighted

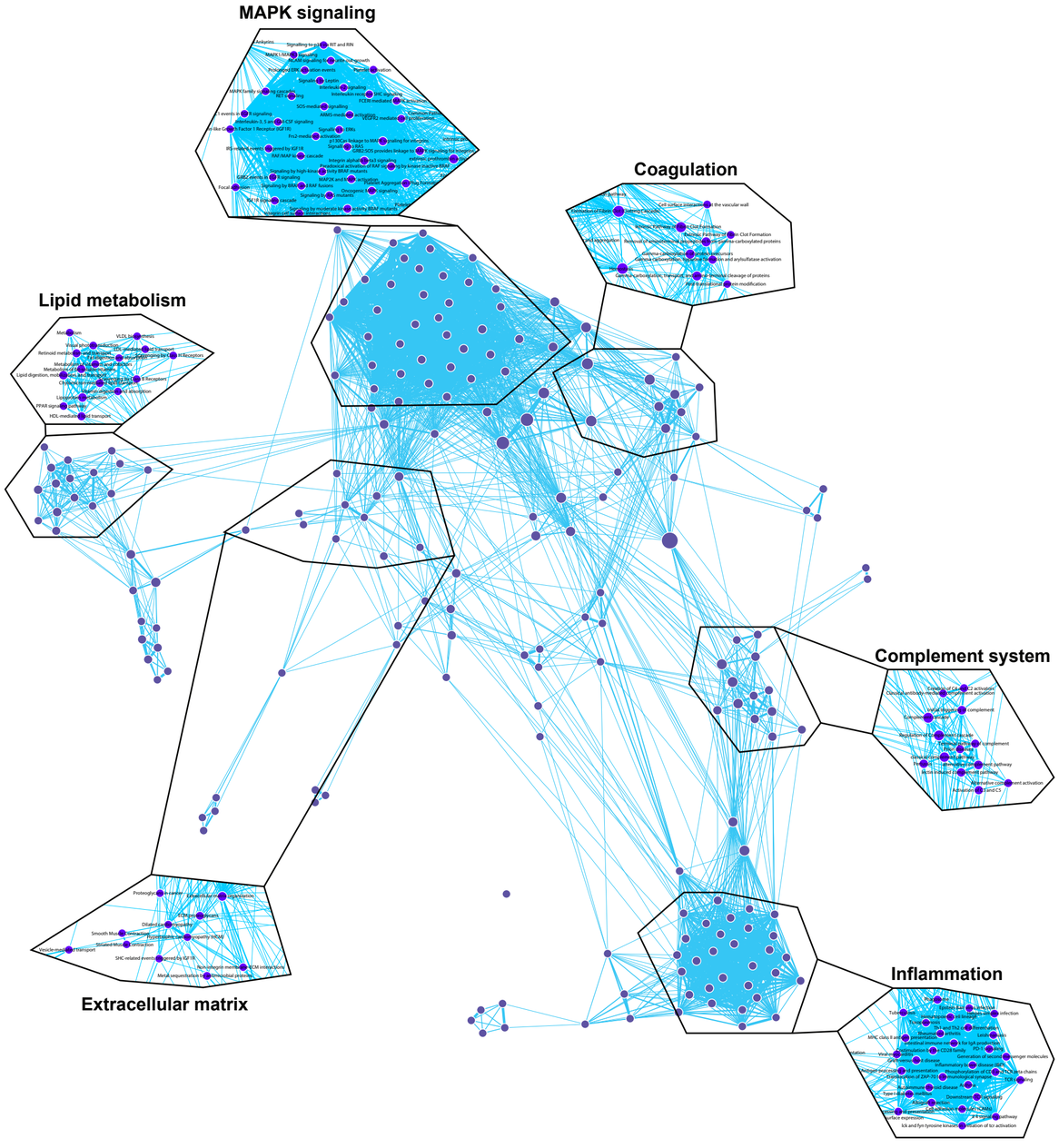

All calcific stage pathways

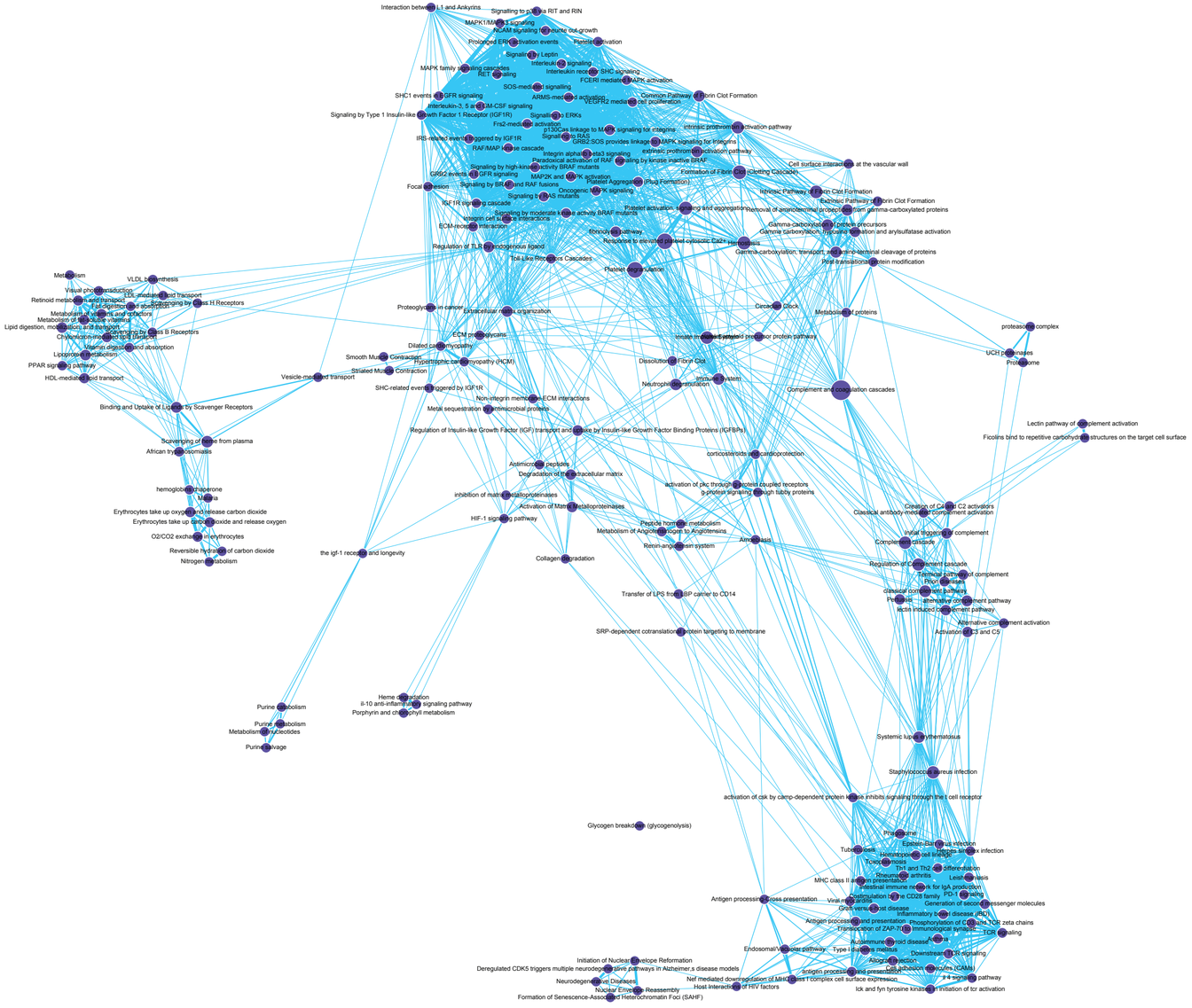

Supplemental Figure 10: Calcific Stage Pathway Network

The network of significantly enriched pathways of the calcific stage from proteomics data. The size of nodes indicates the significance of each pathway in –log(q-value) and the edge thickness represents the overlap between the genes of the two pathways they connect, measured in terms of the Jaccard index.

Supplemental Fig. 11

Early Phase of HIV Life Cycle
SEMA3A-Plexin repulsion signaling by inhibiting Integrin adhesion
pten dependent cell cycle arrest and apoptosis
Cap-dependent Translation Initiation
Eukaryotic Translation Initiation
Selenoamino acid metabolism
Platelet Adhesion to exposed collagen
b cell survival pathway
3, -UTR-mediated translational regulation
GTP hydrolysis and joining of the 60S ribosomal subunit
L13a-mediated translational silencing of Ceruloplasmin expression
Integration of provirus
Formation of a pool of free 40S subunits
Leukocyte transendothelial migration
Striated Muscle Contraction
Apoptotic cleavage of cellular proteins
Platelet activation
Axon guidance
Gene Expression
Nonsense Mediated Decay (NMD) enhanced by the Exon Junction Complex (EJC)
Nonsense-Mediated Decay (NMD)
Vascular smooth muscle contraction
rac1 cell motility signaling pathway
Depolymerisation of the Nuclear Lamina
The citric acid (TCA) cycle and respiratory electron transport
apoptotic dna-fragmentation and tissue homeostasis
Dilated cardiomyopathy
Cell junction organization
Semaphorin interactions
Cell-extracellular matrix interactions
Smooth Muscle Contraction
erk and pi-3 kinase are necessary for collagen binding in corneal epithelia
RHO GTPases activate PAKs
Regulation of actin cytoskeleton
integrin signaling pathway
Citric acid cycle (TCA cycle)
Cell-Cell communication
Muscle contraction
RHO GTPases Activate ROCKs
Apoptotic execution phase
rho cell motility signaling pathway
ucalpain and friends in cell spread
mRNA Splicing
Axon guidance
mRNA Splicing - Major Pathway
Localization of the PINCH-ILK-PARVIN complex to focal adhesions
Activation of DNA fragmentation factor
Apoptosis induced DNA fragmentation
Initiation of Nuclear Envelope Reformation
Nuclear Envelope Reassembly
Sema4D in semaphorin signaling
Signaling by Rho GTPases
Programmed Cell Death
Apoptosis
Formation of Senescence-Associated Heterochromatin Foci (SAHF)
RHO GTPase Effectors
RHO GTPases activate CIT
RHO GTPases activate PKNs
Spliceosome
Breakdown of the nuclear lamina
EPHA-mediated growth cone collapse
Tight junction
Sema4D induced cell migration and growth-cone collapse
agrin in postsynaptic differentiation
EPH-Ephrin signaling
Processing of Capped Intron-Containing Pre-mRNA
Pyruvate metabolism and Citric Acid (TCA) cycle
DNA Damage/Telomere Stress Induced Senescence
SRP-dependent cotranslational protein targeting to membrane
Salmonella infection
Citrate cycle (TCA cycle)
Translation
mcalpain and friends in cell motility
Bacterial invasion of epithelial cells
MET activates PTK2 signaling
Eukaryotic Translation Elongation
Adherens junction
antisense pathway
Shigellosis
CHL1 interactions
Nonsense Mediated Decay (NMD) independent of the Exon Junction Complex (EJC)
Eukaryotic Translation Termination
Selenocysteine synthesis
Glyoxylate and dicarboxylate metabolism
MET promotes cell motility
Peptide chain elongation
Regulation of cytoskeletal remodeling and cell spreading by IPP complex components
Nuclear Envelope Breakdown
caspase cascade in apoptosis
2-LTR circle formation
AUF1 (hnRNP D0) binds and destabilizes mRNA
Clearance of Nuclear Envelope Membranes from Chromatin
TFAP2A acts as a transcriptional repressor during retinoic acid induced cell differentiation
Activation of the mRNA upon binding of the cap-binding complex and eIFs, and subsequent binding to 43S
Ribosomal scanning and start codon recognition
Translation initiation complex formation
tnfr1 signaling pathway
L1CAM interactions
Pathogenic Escherichia coli infection
Deregulated CDK5 triggers multiple neurodegenerative pathways in Alzheimer,s disease models
Neurodegenerative Diseases
Other semaphorin interactions
Ribosome
hiv-1 nef: negative effector of fas and tnf
Formation of the ternary complex, and subsequently, the 43S complex
Viral myocarditis
prion pathway
Signaling by BRAF and RAF fusions
Nephrin interactions
Protein export
Oncogenic MAPK signaling
Signaling by MET
Basigin interactions
Arrhythmogenic right ventricular cardiomyopathy (ARVC)
Developmental Biology
Hypertrophic cardiomyopathy (HCM)
ECM proteoglycans
Proteoglycans in cancer
Laminin interactions
ECM-receptor interaction
Amoebiasis
Extracellular matrix organization
Focal adhesion
Non-integrin membrane-ECM interactions
Integrin cell surface interactions
Syndecan interactions
Hemostasis
Platelet activation, signaling and aggregation
Platelet degranulation
Response to elevated platelet cytosolic Ca2+
Metabolism of fat-soluble vitamins
Retinoid metabolism and transport
Elastic fibre formation
NCAM1 interactions
Systemic lupus erythematosus
Scavenging by Class A Receptors
alternative complement pathway
Collagen formation
Collagen chain trimerization
Collagen biosynthesis and modifying enzymes
Protein digestion and absorption
Terminal pathway of complement
classical complement pathway
PI3K-Akt signaling pathway
Prion diseases
lectin induced complement pathway
Molecules associated with elastic fibres
Assembly of collagen fibrils and other multimeric structures
Pertussis
Pancreatic secretion
A tetrasaccharide linker sequence is required for GAG synthesis
Keratan sulfate biosynthesis
AGE-RAGE signaling pathway in diabetic complications
Phagosome
Visual phototransduction
Glycosaminoglycan metabolism
Scavenging by Class H Receptors
Chylomicron-mediated lipid transport
VLDL biosynthesis
Malaria
Small cell lung cancer
Signaling by PDGF
Cross-presentation of particulate exogenous antigens (phagosomes)
Keratan sulfate/keratin metabolism
Lipoprotein metabolism
Gamma-carboxylation of protein precursors
Removal of aminoterminal propeptides from gamma-carboxylated proteins
Dermatan sulfate biosynthesis
Gamma-carboxylation, transport, and amino-terminal cleavage of proteins
regulators of bone mineralization
Synthesis of PC
Amine compound SLC transporters
Vesicle-mediated transport
Proximal tubule bicarbonate reclamation
VLDL interactions
Chondroitin sulfate/dermatan sulfate metabolism
Degradation of the extracellular matrix
Ion homeostasis
NCAM signaling for neurite out-growth
Heparan sulfate/heparin (HS-GAG) metabolism
Metabolism of vitamins and cofactors
Chondroitin sulfate biosynthesis
Ion transport by P-type ATPases
-arrestins in gpcr desensitization
Peroxisomal lipid metabolism
activation of camp-dependent protein kinase pka
role of -arrestins in the activation and targeting of map kinases
Glutathione conjugation
Pyruvate metabolism
Steroid hormones
Starch and sucrose metabolism
roles of arrestin dependent recruitment of src kinases in gpcr signaling
Ethanol oxidation
Hyaluronan metabolism
g-protein signaling through tubby proteins
ion channels and their functional role in vascular endothelium
Erythrocytes take up carbon dioxide and release oxygen
O2/CO2 exchange in erythrocytes
activation of pkc through g-protein coupled receptors
Dissolution of Fibrin Clot
Role of phospholipids in phagocytosis
Neutrophil degranulation
Histidine metabolism
Formation of Fibrin Clot (Clotting Cascade)
Intrinsic Pathway of Fibrin Clot Formation
Common Pathway of Fibrin Clot Formation
FCGR activation
Metabolism
Fcgamma receptor (FCGR) dependent phagocytosis
Glutathione metabolism
Regulation of actin dynamics for phagocytic cup formation
Alternative complement activation
Arginine and proline metabolism
Metal sequestration by antimicrobial proteins
corticosteroids and cardioprotection
beta-Alanine metabolism
Activation of C3 and C5
Pentose phosphate pathway (hexose monophosphate shunt)
Detoxification of Reactive Oxygen Species
Erythrocytes take up oxygen and release carbon dioxide
Pentose phosphate pathway
Hyaluronan uptake and degradation
Tryptophan metabolism
HDL-mediated lipid transport
Hormone-sensitive lipase (HSL)-mediated triacylglycerol hydrolysis
Glycogen breakdown (glycogenolysis)
Metabolism of Angiotensinogen to Angiotensins
Ascorbate and aldarate metabolism
Biological oxidations
PPAR signaling pathway
Renin-angiotensin system
Glycolysis / Gluconeogenesis
cystic fibrosis transmembrane conductance regulator (cftr) and beta 2 adrenergic receptor (b2ar) pathway
Lipid digestion, mobilization, and transport
Regulation of TLR by endogenous ligand
Initial triggering of complement
Classical antibody-mediated complement activation
Creation of C4 and C2 activators
Binding and Uptake of Ligands by Scavenger Receptors
Innate Immune System
Complement and coagulation cascades
Complement cascade
Immune System
Scavenging of heme from plasma
Regulation of Complement cascade
intrinsic prothrombin activation pathway
Cell surface interactions at the vascular wall
Staphylococcus aureus infection
African trypanosomiasis
Metabolism of carbohydrates

Fibrosa
Spongiosa
Ventricularis

Supplemental Figure 11: CAVD Leaflet Layer Pathway Heatmap

Pathways that are significantly enriched ($q < 0.05$) in the fibrosa (red), spongiosa (orange), and ventricularis (blue) layers, obtained from proteomics data (n=3 CAVD AV samples).

Supplemental Fig. 12

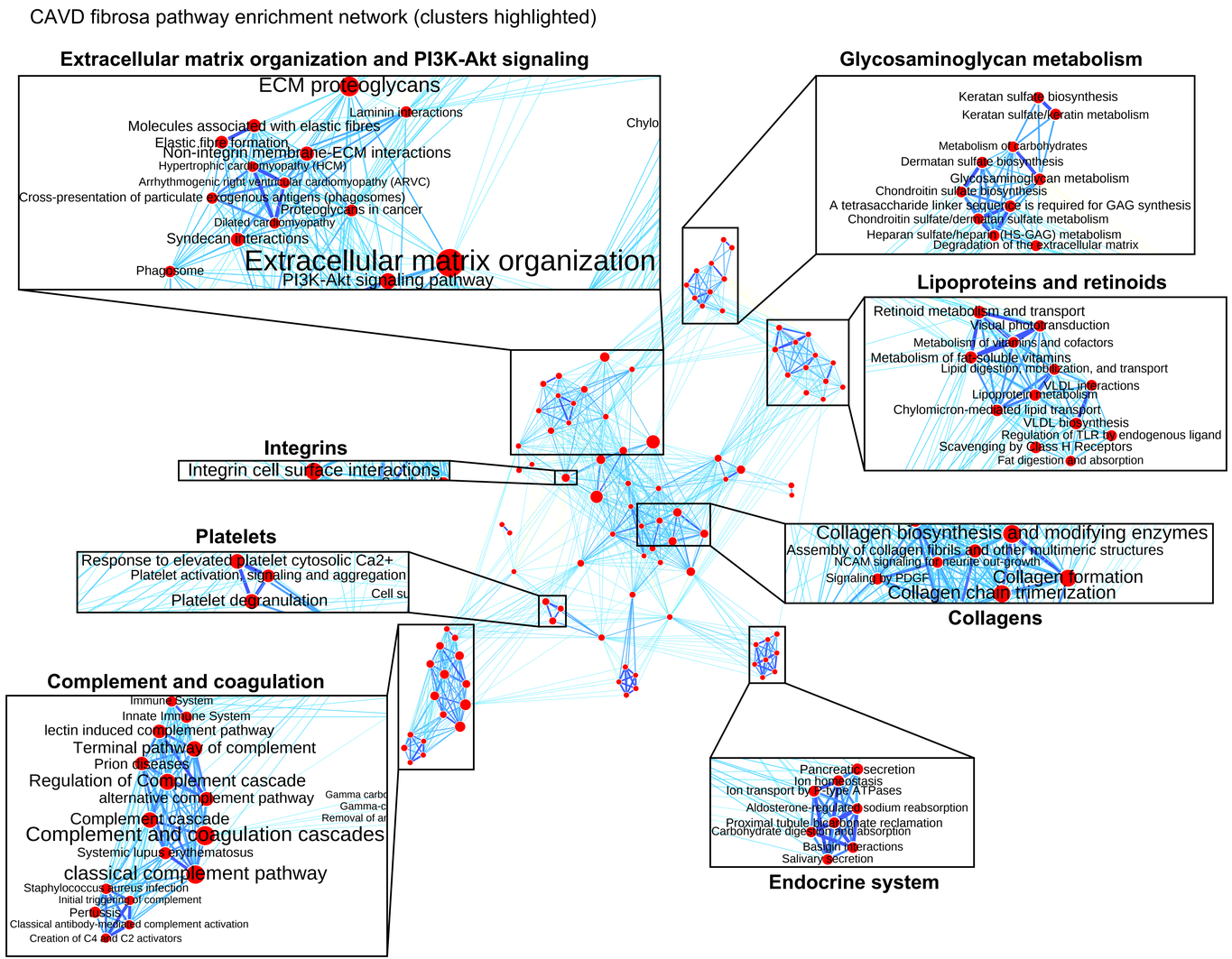

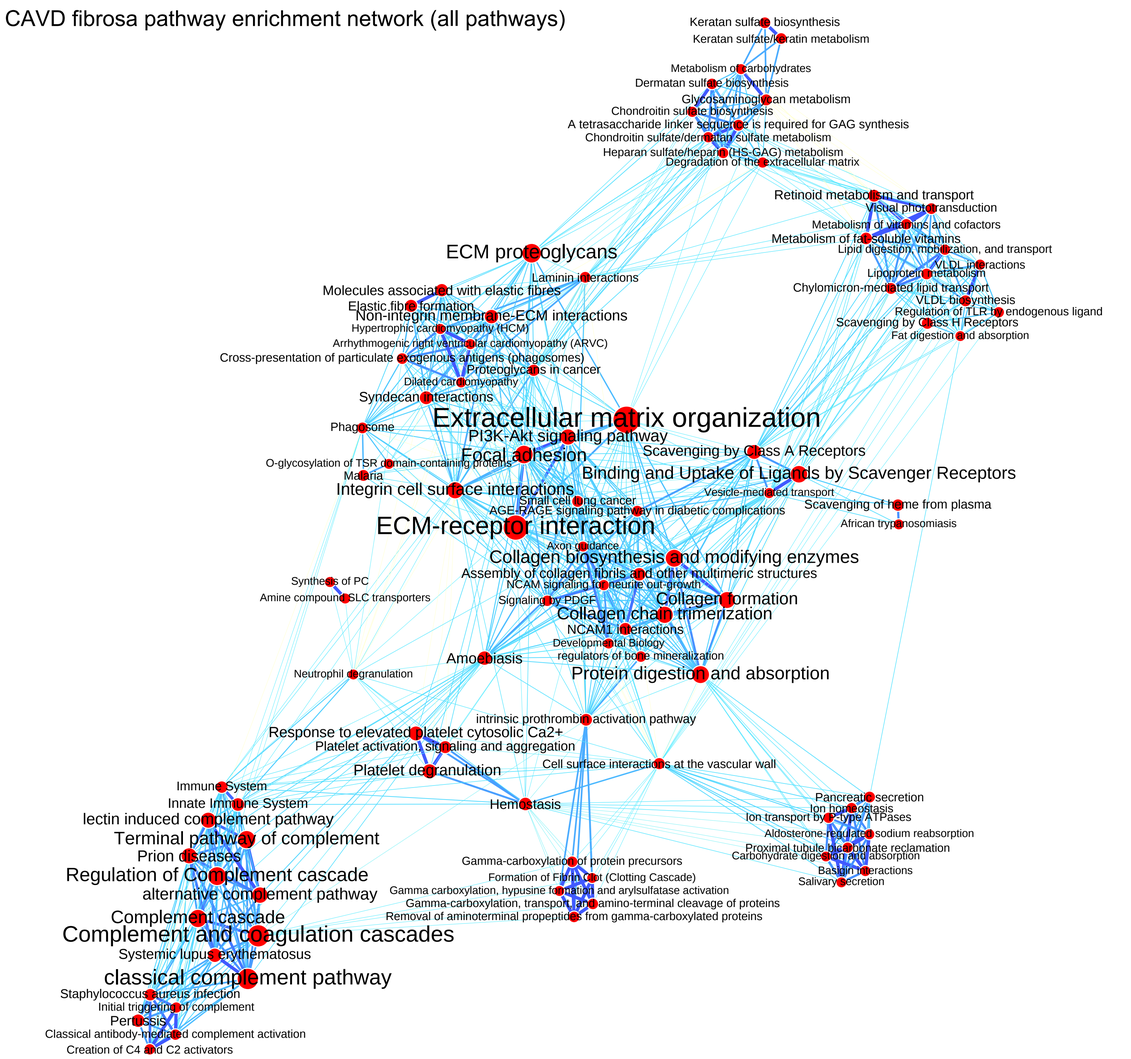

Supplemental Figure 12: CAVD Fibrosa Network

The network of significantly enriched pathways of the CAVD fibrosa layer from proteomics data. The size of nodes indicates the significance of each pathway in –log(q-value) and the edge thickness represents the overlap between the genes of the two pathways they connect, measured in terms of the Jaccard index.

Supplemental Fig. 13

Ventricularis VICs-enriched pathways

q-value	Pathway
0.001907	Binding and Uptake of Ligands by Scavenger Receptors
0.002426	Glycolysis / Gluconeogenesis
0.028974	Extracellular matrix organization

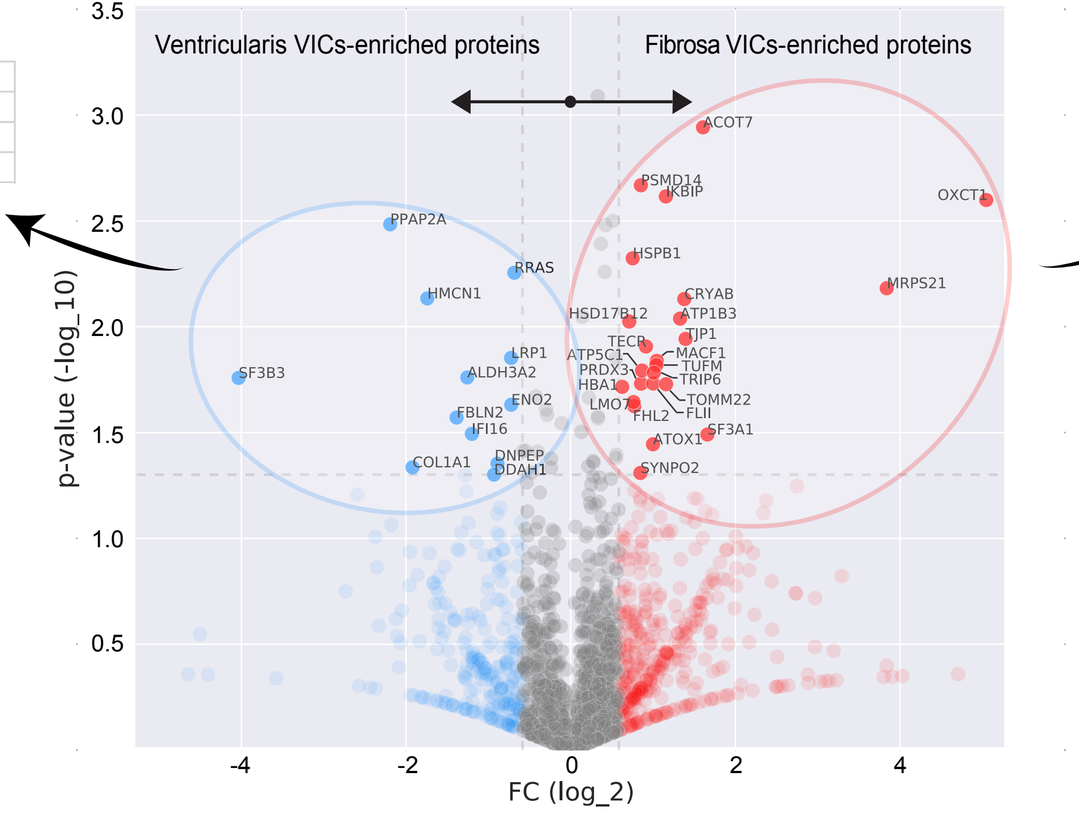

Fibrosa VICs-enriched pathways

q-value	Pathway
9.29E-05	Biosynthesis of unsaturated fatty acids
9.29E-05	Fatty acid elongation
0.000536	Fatty Acyl-CoA Biosynthesis
0.000536	Fatty acid, triacylglycerol, and ketone body metabolism
0.001346	Triglyceride Biosynthesis
0.003381	Synthesis of very long-chain fatty acyl-CoAs
0.009925	Mineral absorption
0.016409	Adherens junction
0.021498	Mitochondrial translation elongation
0.021962	Mitochondrial translation

Supplemental Figure 13: Fibrosa- and Ventricularis-derived VIC Enriched Proteins and Pathways (CAVD VICs)

Volcano plot for the Day 0 proteomics data. Blue and red markers indicate “layer-specific” proteins enriched in ventricularis and fibrosa, respectively, with a fold change cutoff of 1.5. The significant ($p<0.05$) layer-specific proteins are denoted with their names. Enriched pathways ($q<0.05$) of the “layer-specific” proteins are provided.

Supplemental Fig. 14

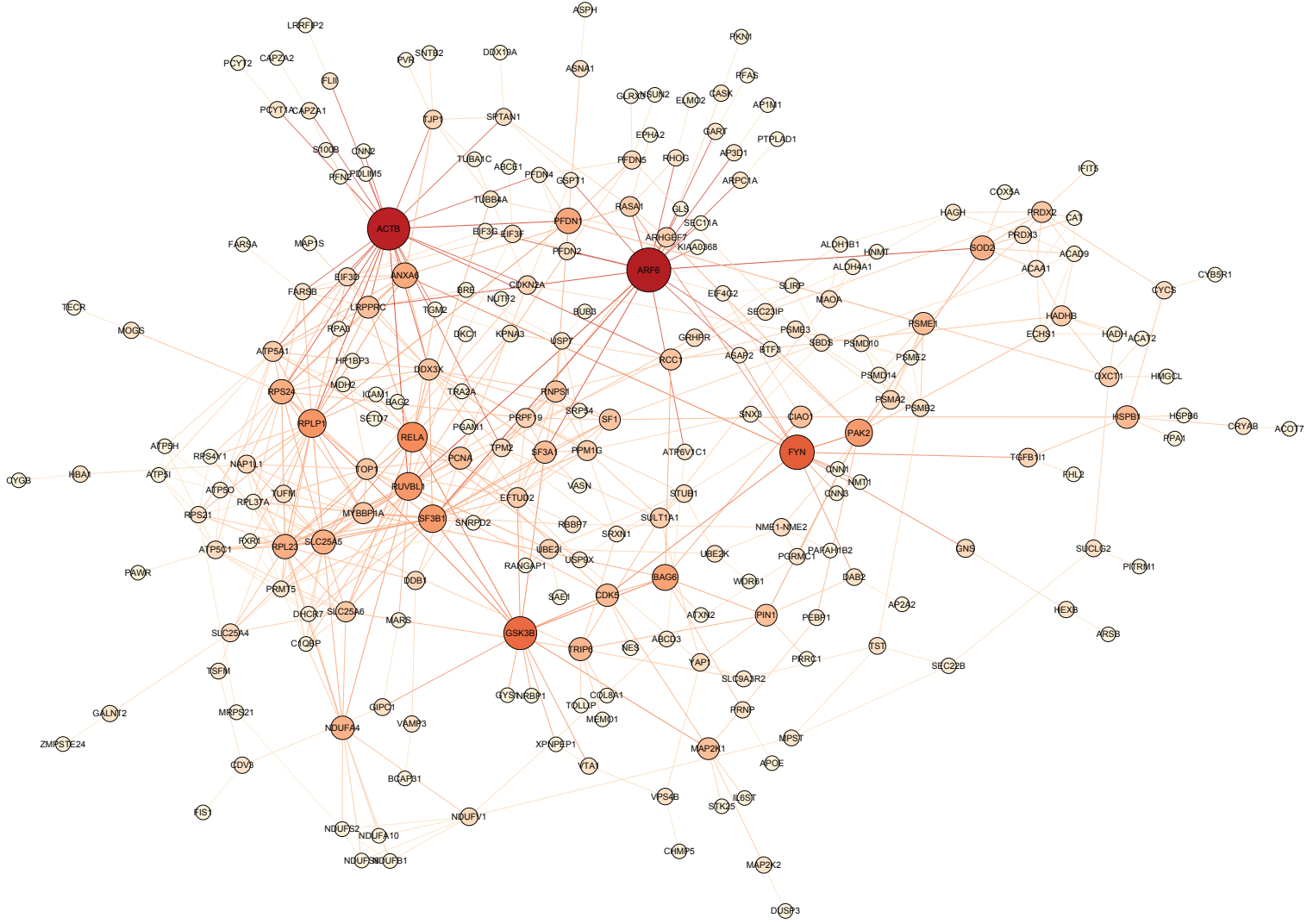

Protein	Betweenness
ARF6	0.16
ACTB	0.15
FYN	0.10
GSK3B	0.10
RELA	0.08
RPLP1	0.07
RUVBL1	0.07
SF3B1	0.07
PAK2	0.07
BAG6	0.06
PFDN1	0.06
ANXA6	0.06
RPS24	0.05
RPL23	0.05
SLC25A5	0.05
SOD2	0.05
NDUFA4	0.05
TRIP6	0.04
HSPB1	0.04
CDK5	0.04

Supplemental Figure 14: Fibrosa VIC Protein Network

The proteins overrepresented in the fibrosa layer with respect to the ventricularis layer (F/V FC>1.5) in the VIC cell proteomics, mapped onto the PPI network. Node size and color indicate betweenness centrality (a measure of how many shortest paths within the entire network pass through the node in question) with larger nodes with a darker shade of red having higher betweenness centrality.

Supplemental Fig. 15

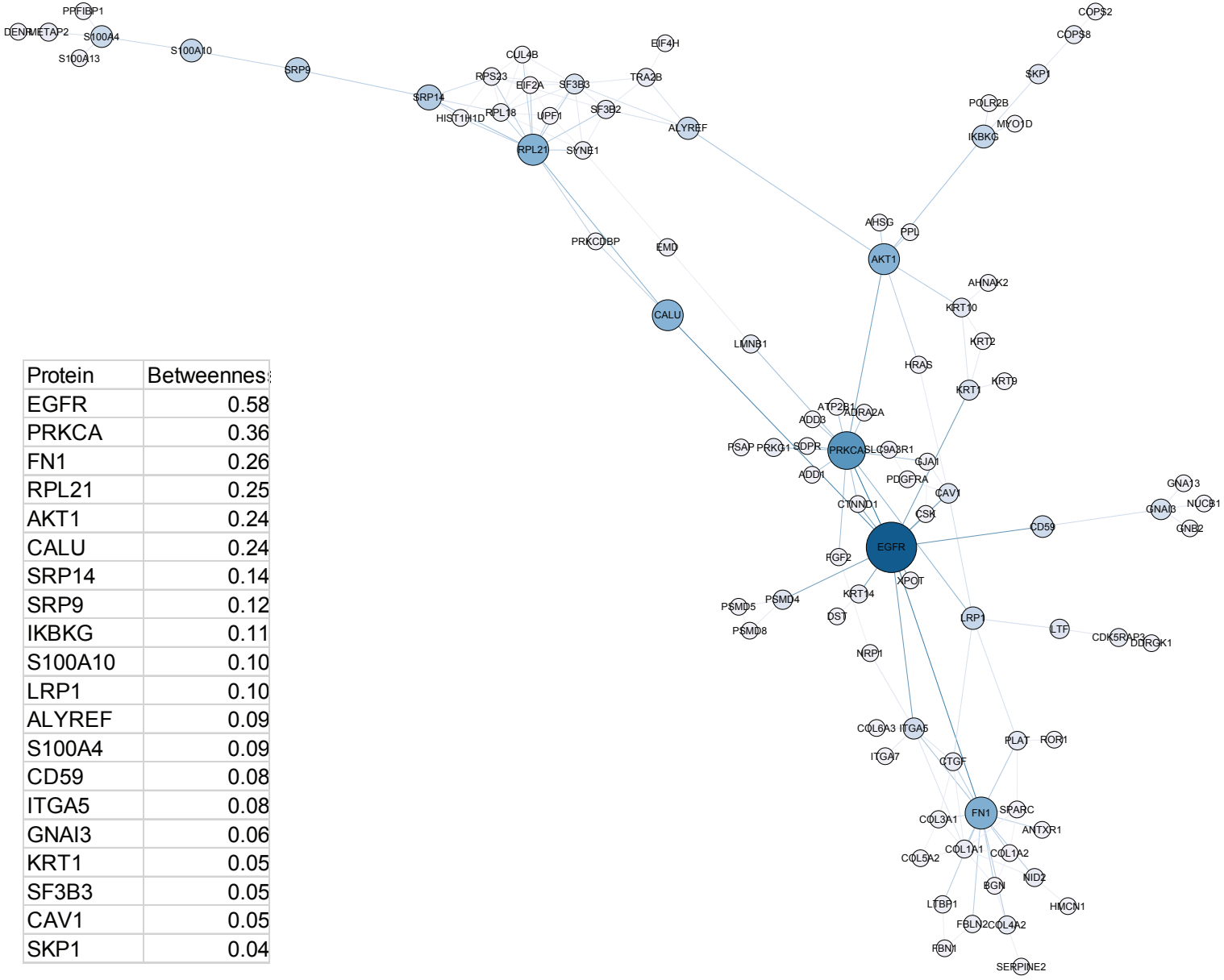

Protein	Betweenness
EGFR	0.58
PRKCA	0.36
FN1	0.26
RPL21	0.25
AKT1	0.24
CALU	0.24
SRP14	0.14
SRP9	0.12
IKBKG	0.11
S100A10	0.10
LRP1	0.10
ALYREF	0.09
S100A4	0.09
CD59	0.08
ITGA5	0.08
GNAI3	0.06
KRT1	0.05
SF3B3	0.05
CAV1	0.05
SKP1	0.04

Supplemental Figure 15: Ventricularis VIC Protein Network

The proteins over-represented in the ventricularis layer with respect to the fibrosa layer (F/V FC<1/1.5) in the VIC cell proteomics, mapped onto the PPI network. Node size and color indicate betweenness centrality with larger nodes with a darker shade of blue having higher betweenness centrality.

Supplemental Fig. 16

a

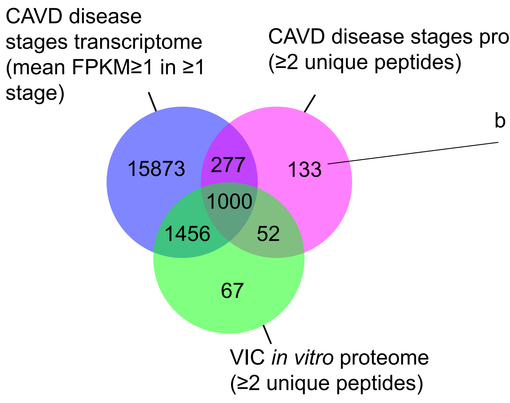

b

AFM
AMBP
APCS
APOA2
APOA4
APOA5
APOC3
APOC4-APOC2
APOH
APOM
BCHE
C2
C4B
C4BPA
C8A
C9
CA1
CD5L
CDH1
CFB
CFHR2
CFHR5
CLC
CPB2
CPN1
CPN2
CRP
DCD
DEFA1
DNPH1
ELANE
EPB42
EPX
F11
F12
F13B
F9
FCN2
FETUB
FGA
FGB
FGG
FGL1
GP1BA
GP5
GP9
GPLD1
GSTT2
GYPA
HABP2
HBD
HBG1
HGFAC
HLA-DPB1
HLA-DQB1
HLA-DRA
HLA-DRB1
HLA-DRB4
HRG
IGFALS
IGHA1
IGHA2
IGHG2
IGHG3
IGHG4
IGHM
IGKC
IGKV1-5
INHBE
ITGA2B
ITIH1
K7N7A8
KNG1
KRT6A
KRT6B
LPA
LRG1
MMP23A
MPO
ORM1
ORM2
P01597
P01598
P01610
P01611
P01612
P01621
P01623
P01701
P01703
P01714
P01743
P01763
P01764
P01766
P01768
P01779
P01781
P04208
P04220
P04433
P06310
P06316
P06331
P23083
P80748
PF4V1
PGLYRP2
PLG
PON1
PPBP
PRG3
PROC
PROZ
PZP
RNASE3
RTN4
SAA4
SBSPON
SEPT5
SERPINA10
SERPINA4
SERPINA6
SERPINA7
SERPINC1
SERPIND1
SHBG
SLC2A14
SLC4A1
SPP2
SPTA1
TNXB
TTR

c

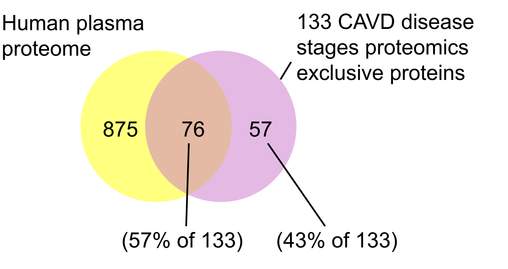

AFM
ORM1
ORM2
SERPINC1
APOA2
APOA4
APOA5
APOC3
APOM
LPA
APOH
C4BPA
CDH1
CA1
CPB2
CPN1
CPN2
CD5L
BCHE
F9
F11
F12
F13B
C2
C4B
C8A
C9
CFB
CFHR2
CFHR5
SERPINA6
CRP
DCD
FETUB
FGA
FGB
FGG
FGL1
FCN2
HBD
SERPIND1
HGFAC
HRG
HABP2
IGHA1
IGHA2
IGHG2
IGHG3
IGHG4
IGKC
IGKV1-5
IGHM
IGFALS
ITIH1
SERPINA4
KNG1
LRG1
PGLYRP2
GPLD1
PLG
PPBP
GP1BA
GP5
PZP
AMBP
SERPINA10
SPP2
SAA4
APCS
PON1
SHBG
TNXB
SERPINA7
TTR
PROC
PROZ

Supplemental Figure 16: Venn Diagram for CAVD Disease Stage Transcriptome, VIC and CAVD Disease-associated Stage Proteome

a. CAVD disease stage transcriptomics (FPKM ≥1 in at least one stage), CAVD disease stage proteomics (≥2 unique peptides), and the VIC *in vitro* proteome (≥2 unique peptides) and their commonly detected fractions

b. 133 proteins/transcripts were exclusively detected in the CAVD disease stage proteome, which are provided in a list.

c. Venn diagram of 133 proteins that were exclusively detected in the CAVD disease stage proteome and a human plasma proteome; the list provides the overlapping proteins

Supplemental Fig. 17

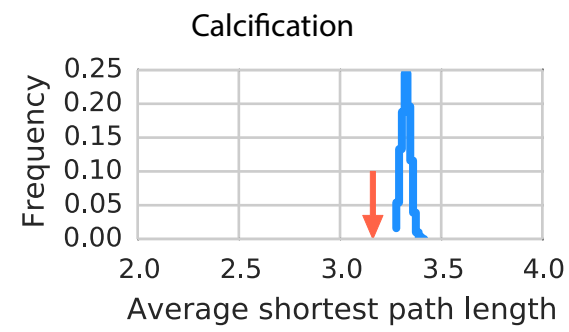

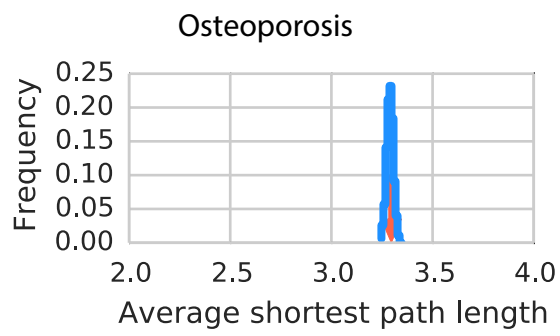

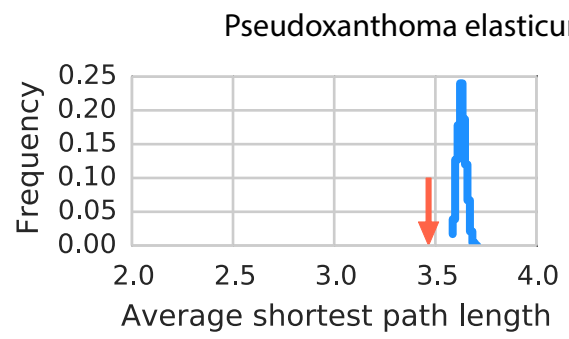

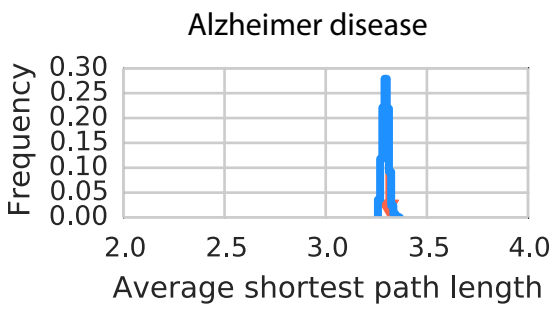

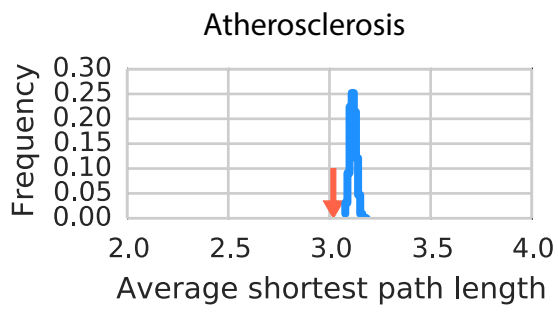

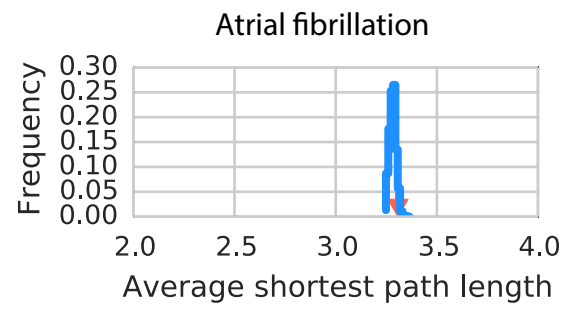

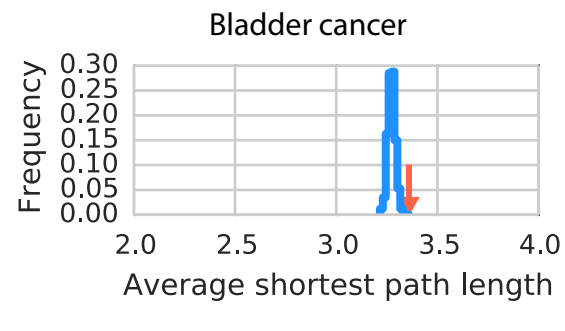

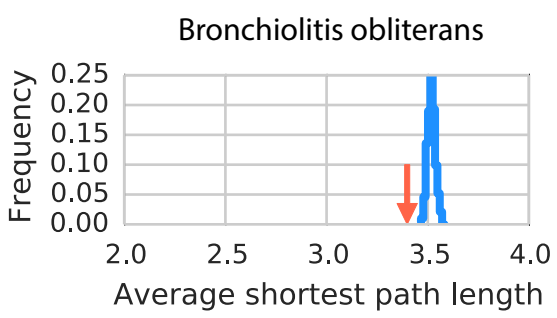

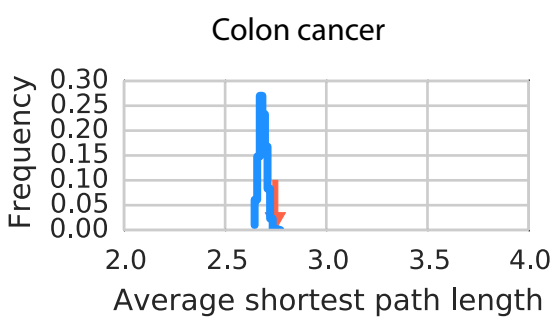

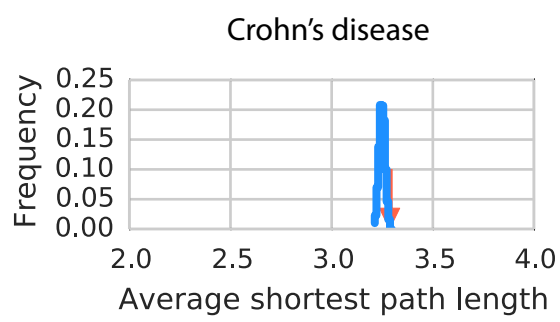

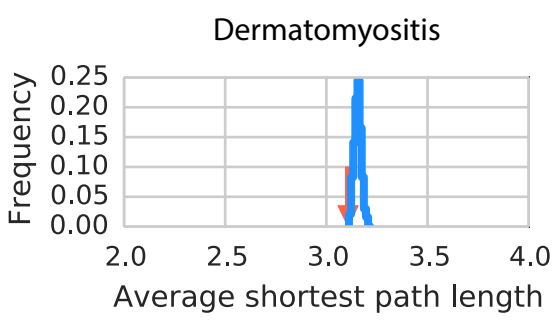

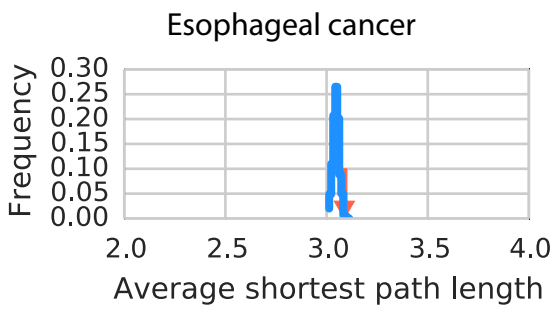

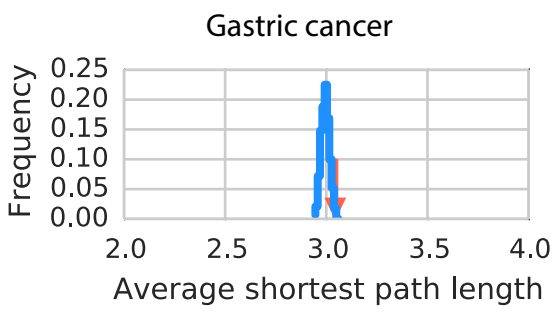

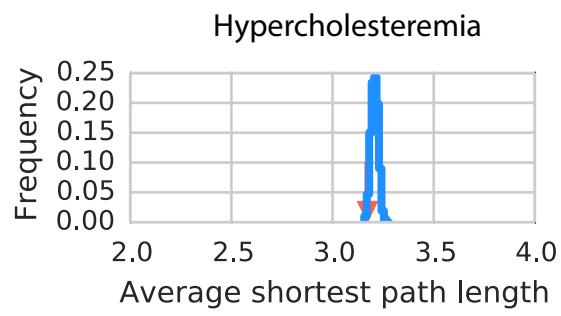

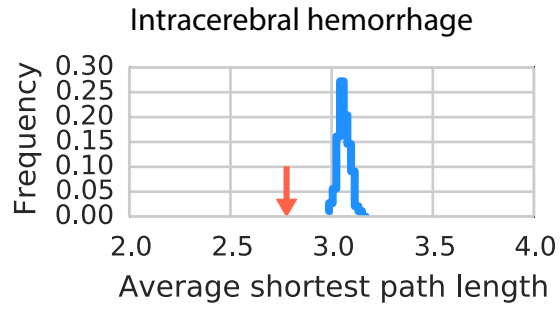

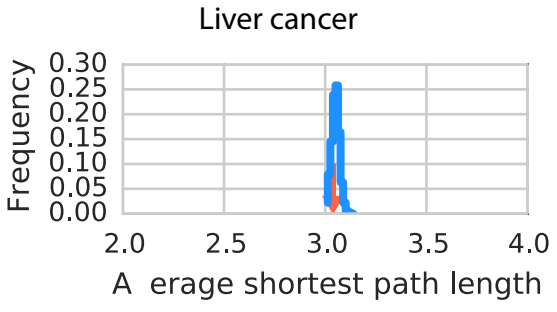

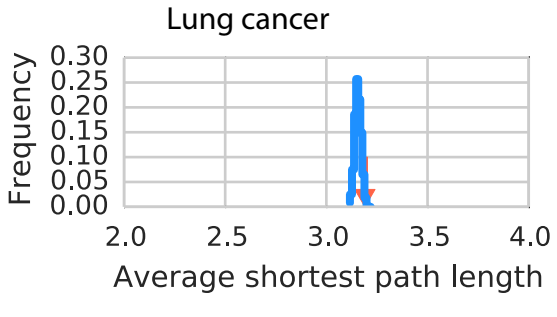

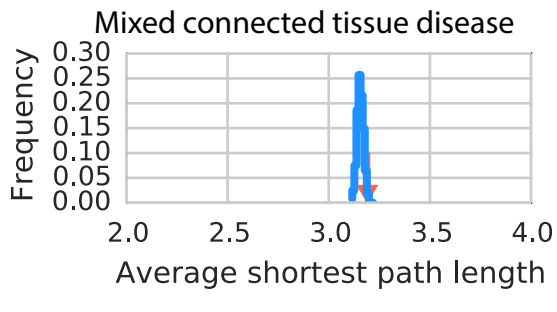

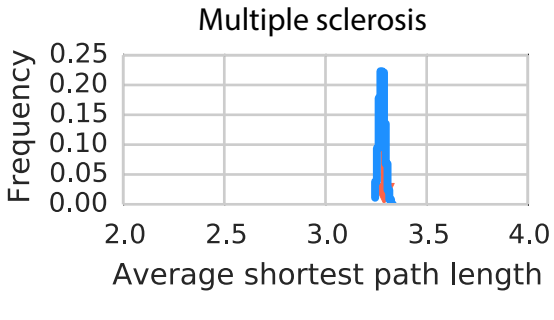

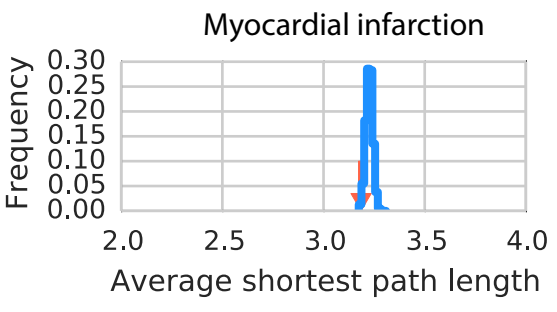

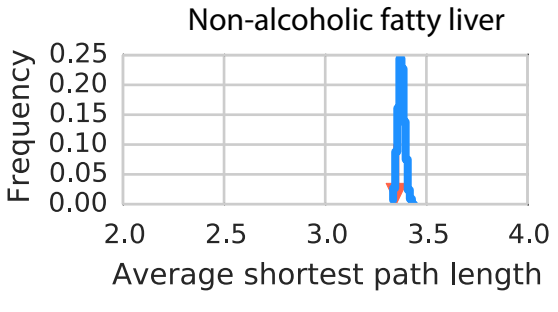

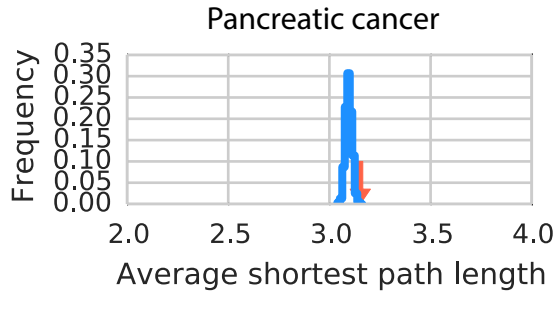

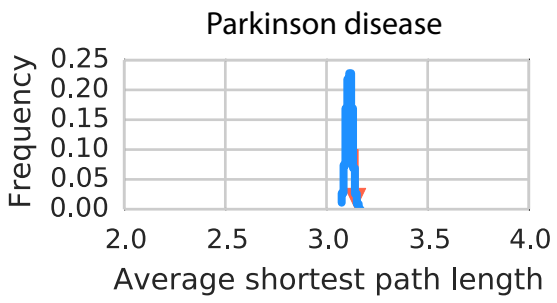

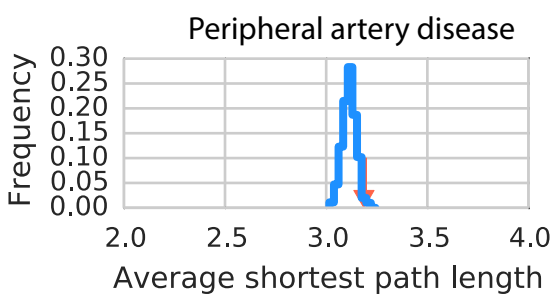

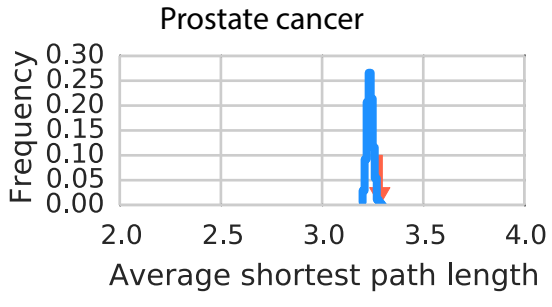

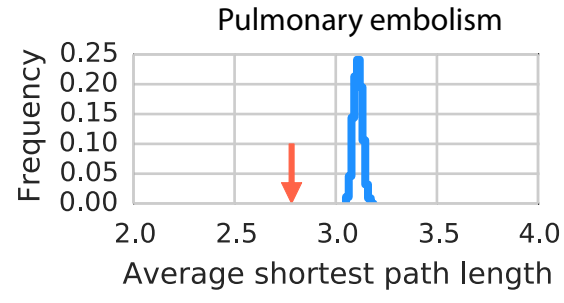

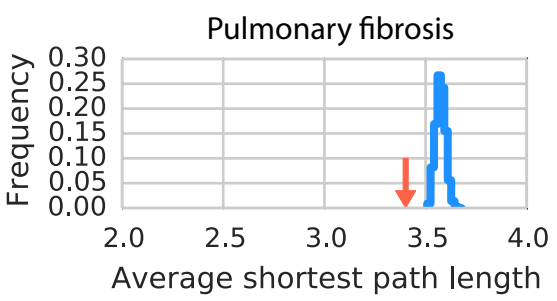

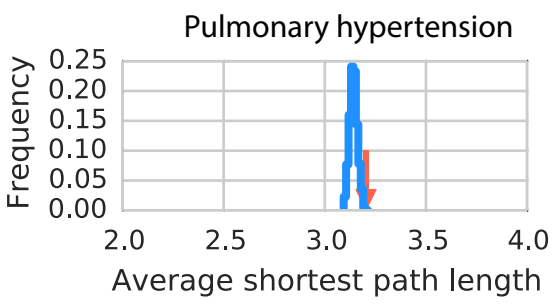

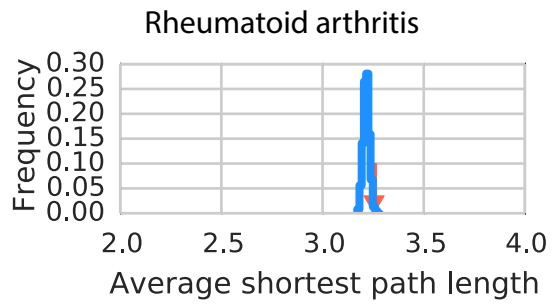

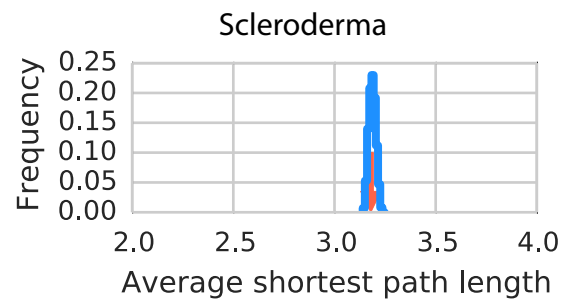

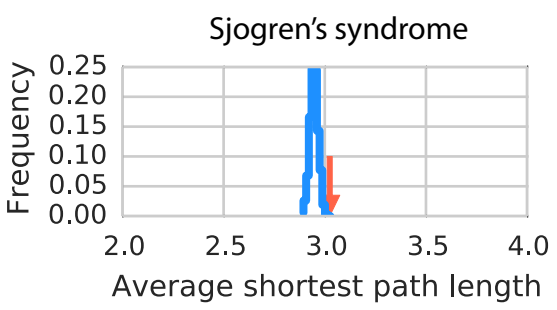

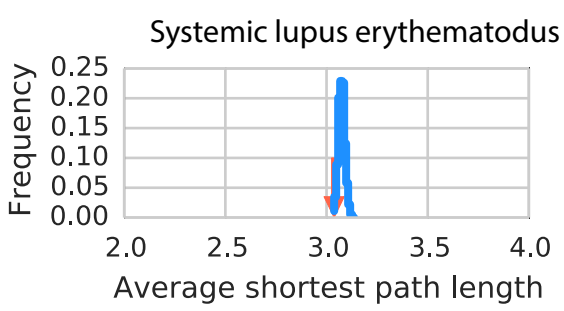

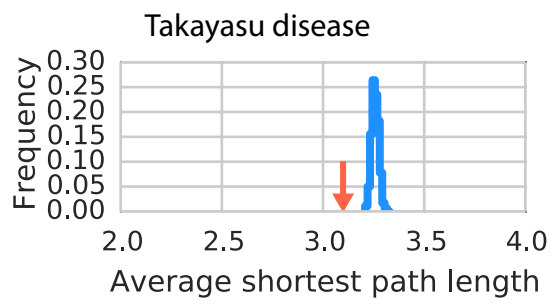

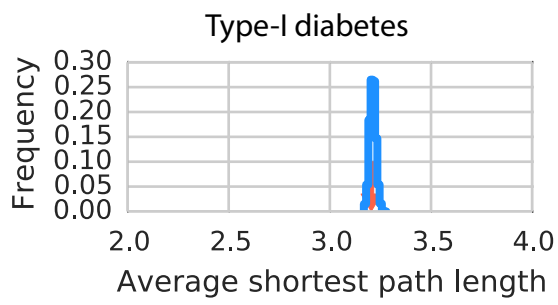

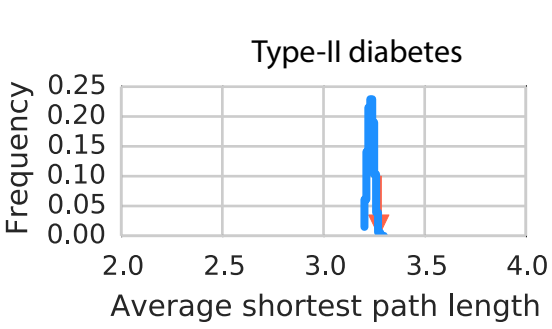

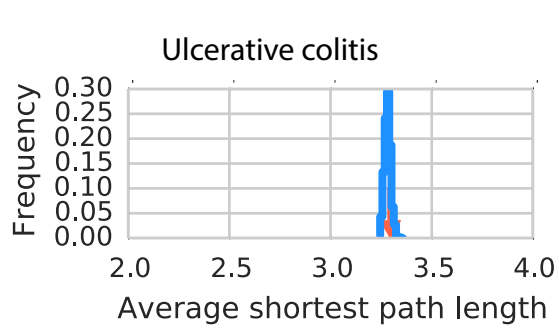

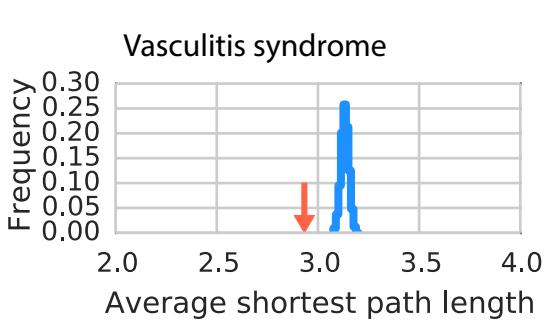

Supplemental Figure 17: Average Shortest Path Length Distributions between CAVD and Human Diseases

The average shortest path length between the calcific disease stage module and the respective disease genes are shown with the red arrow. The average shortest path lengths between the CAVD module and randomly selected genes (using degree-preserving randomization) of the same size as the disease gene set are shown with the blue distribution (for n=1,000 realizations).

Supplemental Fig. 18

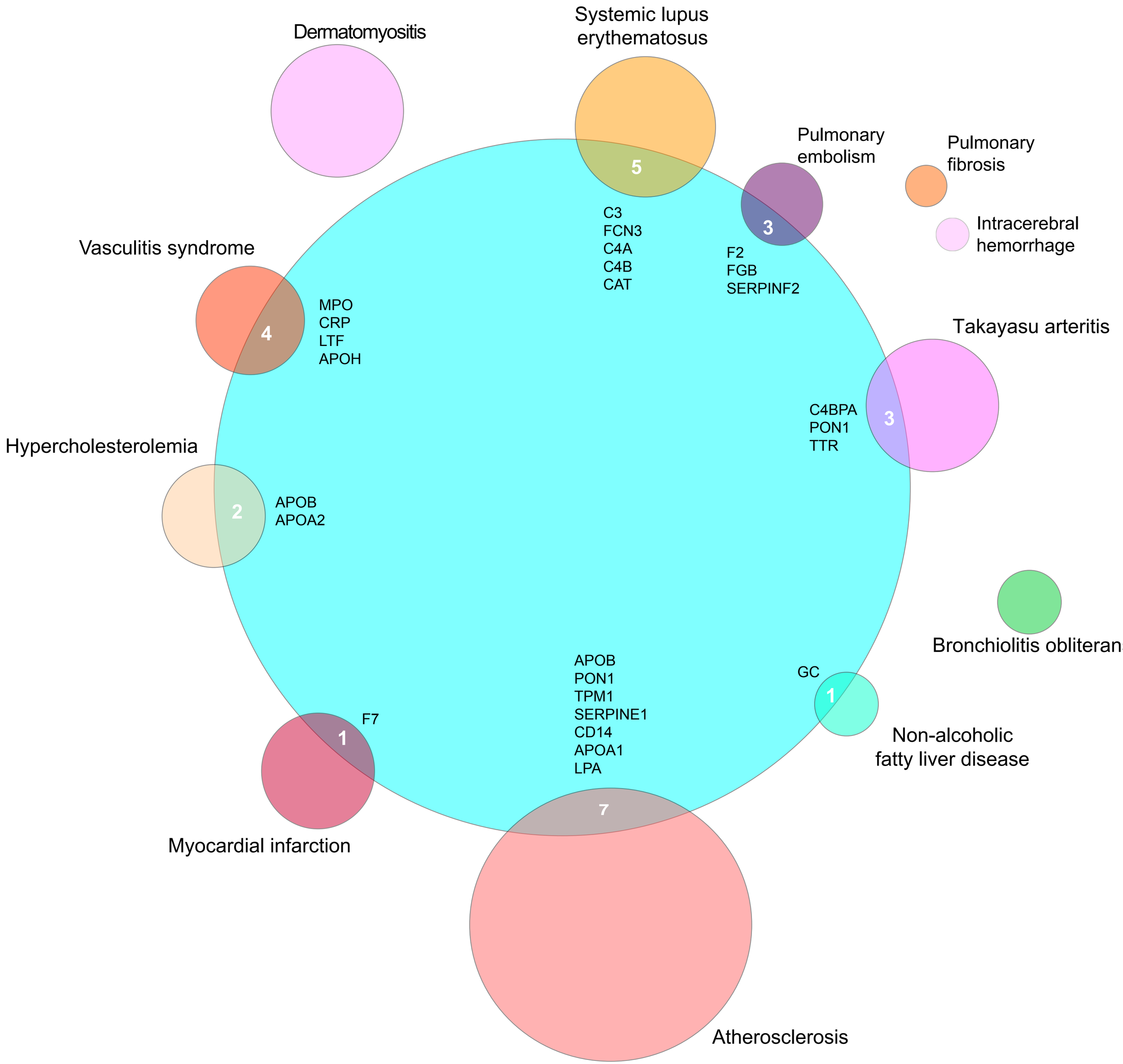

Supplemental Figure 18: Gene Overlap between the CAVD Module and Human Diseases

The direct gene overlap between the calcific disease stage module and the diseases shown in Fig. 6c. The numbers at the intersection of each pair of circles indicates the number of shared genes between the calcific disease stage proteome and the respective disease. The size of the circles indicates the size of the corresponding disease gene set.

1. Itou T, Maldonado N, Yamada I, Goettsch C, Matsumoto J, Aikawa M, Singh S, Aikawa E. Cystathionine γ-lyase accelerates osteoclast differentiation: Identification of a novel regulator of osteoclastogenesis by proteomic analysis. *Arterioscler Thromb Vasc Biol*. 2014;34:626-634.
2. Bastian M, Heymann S, Jacomy M. *Gephi: An open source software for exploring and manipulating networks*. 2009.
3. Käll L, Storey JD, MacCoss MJ, Noble WS. Assigning significance to peptides identified by tandem mass spectrometry using decoy databases. *J Proteome Res*. 2008;7:29-34.
4. Kirchner M, Renard BY, Kothe U, Pappin DJ, Hamprecht FA, Steen H, Steen JA. Computational protein profile similarity screening for quantitative mass spectrometry experiments. *Bioinformatics*. 2010;26:77-83.
5. Old WM, Meyer-Arendt K, Aveline-Wolf L, Pierce KG, Mendoza A, Sevinsky JR, Resing KA, Ahn NG. Comparison of label-free methods for quantifying human proteins by shotgun proteomics. *Molecular & Cellular Proteomics*. 2005;4:1487-1502.
6. Anderle M, Roy S, Lin H, Becker C, Joho K. Quantifying reproducibility for differential proteomics: Noise analysis for protein liquid chromatography-mass spectrometry of human serum. *Bioinformatics*. 2004;20:3575-3582.
7. Love MI, Huber W, Anders S. Moderated estimation of fold change and dispersion for rna-seq data with deseq2. *Genome Biol*. 2014;15:550.
8. Benjamini Y, Hochberg Y. Controlling the false discovery rate: A practical and powerful approach to multiple testing. *Journal of the Royal Statistical Society. Series B (Methodological)*. 1995;57:289-300.
9. Walt Svd, Colbert SC, Varoquaux G. The numpy array: A structure for efficient numerical computation. *Computing in Science & Engineering*. 2011;13:22-30.
10. Hunter JD. Matplotlib: A 2d graphics environment. *Computing in Science & Engineering*. 2007;9:90-95.
11. Kamburov A, Pentchev K, Galicka H, Wierling C, Lehrach H, Herwig R. Consensuspathdb: Toward a more complete picture of cell biology. *Nucleic Acids Res*. 2011;39:D712-717.
12. Chowdhury S, Sarkar RR. Comparison of human cell signaling pathway databases—evolution, drawbacks and challenges. *Database*. 2015;2015:bau126-bau126.
13. Liu C-C, Tseng Y-T, Li W, Wu C-Y, Mayzus I, Rzhetsky A, Sun F, Waterman M, Chen JJW, Chaudhary PM, Loscalzo J, Crandall E, Zhou XJ. Diseaseconnect: A comprehensive web server for mechanism-based disease–disease connections. *Nucleic Acids Research*. 2014;42:W137-W146.
14. Rappaport N, Nativ N, Stelzer G, Twik M, Guan-Golan Y, Iny Stein T, Bahir I, Belinky F, Morrey CP, Safran M, Lancet D. Malacards: An integrated compendium for diseases and their annotation. *Database*. 2013;2013:bat018-bat018.
15. Menche J, Sharma A, Kitsak M, Ghiassian SD, Vidal M, Loscalzo J, Barabasi AL. Disease networks. Uncovering disease-disease relationships through the incomplete interactome. *Science*. 2015;347:1257601.
16. Hagberg A, Schult D, Swart P. Exploring network structure, dynamics, and function using networkx. *SciPy 2008: Proceedings of the 7th Python in Science Conference*. 2008:11-15.